Universidad de Valladolid

ESCUELA DE INGENIERÍAS INDUSTRIALES

UNIVERSITY OF VALLADOLID

SCHOOL OF INDUSTRIAL ENGINEERINGS

Master's in Chemical Engineering

MASTER'S THESIS

Hydrogenation of selected carbohydrate molecules in the presence of solid foam catalysts in a stirred tank reactor

Author:

Araujo Barahona, German Rodrigo

Supervisors:

García Serna, Juan

University of Valladolid

Salmi, Tapio

Laboratory of Industrial Chemistry and Reaction Engineering
Åbo Akademi University

Valladolid, May 2021

Hydrogenation of selected carbohydrate molecules in the presence of solid foam catalysts in a stirred tank reactor

Master's Thesis

German Rodrigo Araujo Barahona

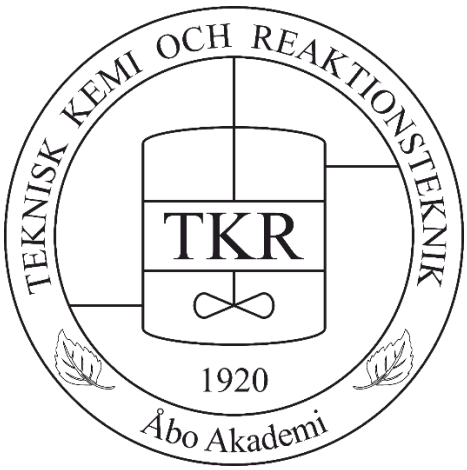

Johan Gadolin
Process Chemistry Centre

Laboratory of Industrial Chemistry and Reaction Engineering
Faculty of Science and Engineering/Chemical Engineering
Åbo Akademi University
Turku/Åbo, Finland, 2021

TFM REALIZADO EN PROGRAMA DE INTERCAMBIO

TÍTULO:	Hydrogenation of selected carbohydrate molecules in the presence of solid foam catalysts in a stirred tank reactor
ALUMNO:	German Rodrigo Araujo Barahona
FECHA:	17 de mayo de 2021
CENTRO:	Faculty of Science and Engineering
UNIVERSIDAD:	Åbo Akademi University
TUTOR:	Tapio Salmi

PREFACE

“While you live, shine. Have no grief at all; life exists only for a short while and time demands his due.”

- Seikilos epitaph.

These two years in the master's program have been a life-changing experience. I still remember that September 11, 2019, at the International Airport of El Salvador with my luggage full of dreams, my family saying goodbye, and a world of experiences waiting for me. None of this would have been possible without the support of many people.

First, I would like to express my gratitude to my master's coordinator, Professor Juan García Serna, for all the support from the very beginning, which made it possible for me to pursue my master's degree at the University of Valladolid, his enthusiasm and commitment to students are qualities that I have always admired about him. I would like to thank my supervisor at Åbo Akademi University, Professor Tapio Salmi, for the opportunity to work with him. Tapio is not only a great scientist but also a great person who shares his vast knowledge, kindness, and sense of humor with everyone around him. I feel privileged to have been able to learn from him in all these aspects.

The experimental work of this thesis would not have been possible without the help of Docent Kari Eränen, I am grateful not only for his exceptional ability to solve any problem in the lab, but also for all that I have learned about experimental work thanks to his patience and ingenuity. I would like to thank Professor Dmitry Yu. Murzin and Docent Narendra Kumar for their wise advice on catalyst preparation and characterization, a visit to their offices always brings new ideas and perspectives.

I would like to express my gratitude to Dr. Zuzana Vajglová for her guidance in the development of the incipient wetness impregnation method, that was definitely a turning point in this research. Thanks to Dr. Atte Aho for his help with HPLC and TPR measurements, thanks to Jay Pee for his help in the anodic oxidation experiments.

Thanks to all the good friends that I made in Finland for all the adventures and for making me feel at home: Christoph, Ole, Tom, Pontus, Adriana, Mark, Matias, Bernadette, Pasi, Mouad, Federica, and Luca. Thank you, Marcela, por estar a pesar de la distancia; thank you, Andrea and Hamza for being incredible friends; thank you, Olga for your friendship and good wishes; and thank you, Karen, for your friendship and advice.

I would like to thank the Latin America + Asia / University of Valladolid-Santander Bank Scholarship Program for providing the funds that allowed me to pursue my master’s studies, and the Erasmus Plus program for the financial support during my exchange in Finland.

Y, por último, pero no por eso menos importante, gracias a mi familia. Ustedes son mi todo y les debo todo lo que tengo; a mi madre Haydeé, a mi padre German, a mi hermana Lilian, a mis tíos Ruth y Carlos Humberto, muchas gracias por el apoyo incondicional y por siempre creer en mí.

Mil gracias, tack så mycket, kiitos paljon!

-German.

ABSTRACT

Keywords: hydrogenation, heterogeneous catalysis, structured catalysts, ruthenium, L-arabinose, D-galactose, binary sugar mixtures, sugar alcohols.

This research work was carried out at the Laboratory of Industrial Chemistry and Reaction Engineering (TKR) at Åbo Akademi University (Turku/Åbo, Finland) in collaboration with the University of Valladolid (Valladolid, Spain) under the supervision of Tapio Salmi (Professor of the Academy of Finland) and Juan García Serna (Full Professor at the University of Valladolid) as part of the Erasmus Plus exchange program.

The growing concern about the short and long-term consequences caused by climate change is driving humankind towards a more sustainable development, which requires adequate diversification of feedstock and industrial production processes. In this context, the use of lignocellulosic biomass as raw material for chemical industry is a promising option on which a lot of research effort has been focused in recent years, such as the production of sugar alcohols. These compounds can be obtained by catalytic hydrogenation of mono and disaccharides present in the cellulose and hemicelluloses fractions of biomass. Sugar alcohols have a wide range of applications e.g., in the alimentary industry as healthier sweeteners or in the pharmaceutical industry as excipients and anti-caries agents.

The research effort of this thesis was focused on the development of a novel solid foam catalyst based on ruthenium supported on carbon. This heterogeneous catalyst was used to perform kinetic experiments on the hydrogenation of L-arabinose and D-galactose at different temperatures (90˚C, 100˚C, and 120˚C) and hydrogen pressures (20 and 40 bar) to investigate the effect of these parameters on the hydrogenation rate. Furthermore, kinetic experiments were carried out with binary sugar mixtures at different D-galactose to L-arabinose molar ratios to study the interactions of these sugars during the reaction in the presence of the prepared catalyst.

The solid foam catalyst preparation comprised the following steps: cutting of the open-cell foam aluminum pieces, anodic oxidation pretreatment, carbon coating, acid pretreatment, ruthenium incorporation, and ex-situ reduction. The carbon coating method comprised the polymerization of furfuryl alcohol, followed by a pyrolysis process and activation with oxygen. The degree of crosslinking of polyfurfuryl alcohol was identified as a relevant parameter to obtain a carbon coating

with appropriate properties to act as catalyst support; thus, the polymerization conditions were optimized to obtain the desired catalyst properties.

Incorporation of ruthenium on the carbon-coated foam was done by two different methods, homogeneous deposition precipitation (HDP) and incipient wetness impregnation (IWI), using in both cases ruthenium(III) nitrosyl nitrate as the precursor solution. In the HDP method, the carbon content of the foams and the molar ratio of urea-to-ruthenium were the most relevant parameters to obtain an active catalyst. On the other hand, for the IWI method, the carbon content and the concentration of the precursor solution were identified as the most relevant parameters. Using IWI, it was possible to prepare an active catalyst with a ruthenium load of 1.1 wt. % for the conversion of the sugars to the corresponding sugar alcohol. This catalyst was used in the systematic kinetic experiments for both the individual sugars and sugar mixtures.

Several catalyst characterization techniques such as Scanning Electron Microscopy (SEM), Transmission Electron Microscopy (TEM), Temperature-Programmed Reduction (TPR), and Inductively Coupled Plasma Atomic Optical Emission Spectroscopy (ICP-OES) were used to interpret the behavior of the catalyst in terms of activity, durability and critical parameters for the catalyst preparation.

Extensive kinetic experiments were carried out in an isothermal laboratory-scale semibatch reactor to which gaseous hydrogen was constantly added. Two pieces of solid foam catalysts were placed at the endpoint of an agitating shaft and rotated at a constant speed during the experiments. From the individual kinetic experiments, high selectivities towards sugar alcohols, exceeding 98% were obtained for both sugars, in fact, the conversions were within the range of 60-98%, depending on the temperature. The temperature effect on the reaction rate was very strong, while the effect of the hydrogen pressure was rather minor. Regarding the sugar mixtures, in general, the L-arabinose presented a higher reaction rate, and an acceleration of the hydrogenation process was observed for both sugars as the ratio of D-galactose to L-arabinose increased, evidently as a result of competitive interaction on the catalyst surface.

A kinetic model based on a non-competitive adsorption mechanism between sugar molecules and hydrogen was tested with extensive experimental data by applying non-linear regression. A good description of the concentration profiles and the temperature effect on the reaction kinetics was achieved with the mathematical model. Furthermore, a detailed sensitivity analysis revealed that

the estimated parameters were very well defined and all of them had an important contribution to the model.

The obtained results demonstrate the feasibility of converting primary sugars from biomass such as L-arabinose and D-galactose and their mixtures into the corresponding sugar alcohols using ruthenium as the active metal on an active carbon support implemented in an open foam structure. A possible next step would be the use of this catalyst in continuous three-phase reactors that allow taking the advantage of the properties associated with structured catalysts, such as high flow rates, high external heat and mass transfer rates and low diffusion resistance in the active catalyst layer.

REFERAT

Nyckelord: hydrering, heterogen katalys, strukturerade katalysatorer, L-arabinos, D-galaktos, binära sockerblandningar, sockeralkoholer.

Detta arbete genomfördes vid Laboratoriet för teknisk kemi och reaktionsteknik vid Åbo Akademi, Finland i samarbete med Valladolid universitet, Spanien. Arbetet handleddes av akademiprofessor Tapio Salmi (Finlands Akademi och Åbo Akademi) och professor Juan García Serna (Valladolid universitet) inom ramen för Erasmus Plus –utbytesprogrammet.

Den växande medvetenheten om de kort- och långvariga konsekvenser som klimatförändringen orsakar driver mänsligheten mot en mer hållbar utveckling, vilket kräver en adekvat diversifiering av råvaror och industriella processer. I detta sammanhang är användningen av lignocellulosabaserad biomassa som råmaterial för kemisk industri ett lovande alternativ. Extensiv forskningsverksamhet har idkats kring detta tema under de senaste åren, t.ex. produktion av sockeralkoholer, som kan framställas via katalytisk hydrering av mono- och disackarider vilka finns tillgängliga i biomassans cellulosa- och hemicellulosafraktioner. Sockeralkoholer har många tillämpningar, t.ex. i livsmedelindustrin som hälsosamma sötningsmedel och i den farmaceutiska indusrin som fyllnadsmedel och anti-carieskomponenter.

Detta arbete fokuserades på utveckling av en fast skumkatalysator som baserar sig på ruteniumnanopartiklar på aktivt kol. Katalysatorn användes i kinetiska hydreringsexperiment av L-arabinos och D-galaktos vid olika temperaturer (90˚C, 100˚C och 120˚C) och vätetryck (20 och 40 bar). Experiment utfördes för att få fram dessa parametrars inverkan på hydreringshastigheten. Dessutom genomfördes kinetiska experiment med binära sockerblandningar med olika molära förhållanden av D-galaktos och L-arabinos för att studera växelverkan mellan sockerarterna under hydreringsprocessens gång.

Prepareringen av den fasta skumkatalysatorn bestod av följande steg: skärning av aluminiumstycken av fast skum, förbehandling av materialet med anodisk oxidation, beläggning av skummet med aktivt kol, förbehandling av skummet med syra, impregnering av materialet med rutenium samt ex situ –reduktion av katalysator-materialet. Beläggningsmetoden baserade sig på polymerisering av furfurylalkohol, pyrolys av polymeren samt aktivering av kolskiktet med syre. Graden av tvärbindning av polyfurfurylalkohol konstaterades vara en relevant parameter, då det gäller att åstadkomma en kolbeläggning med önskade egenskaper så att beläggningen kan fungera som

katalysatorbärare; därför optimerades polymerisationsbetingelserna för att erhålla de eftersträvade katalytiska egenskaperna.

Rutenium inkorporerades på kolbaserat skum med två olika metoder, homogen deponeringsfällning (HDP) samt porimpregnering (IWI). I båda fallen användes rutenium (III)nitrosylnitrat som prekursorlösning. I HDP-metoden var kolinnehållet i skummet och molförhållandet urea:rutenium de mest relevanta parametrarna då det gällde att åstadkomma en aktiv katalysator. För IWI-metoden konstaterades kolinnehållet och koncentrationen av prekursorlösningen vara de mest relevanta parametrarna. Genom användning av porimpregnering blev det möjligt att preparera en aktiv katalysator med en ruteniumhalt på 1.1 vikt-% för omvandling av sockerarter till motsvarande sockeralkoholer. Därför användes denna katalysatorvariant för kinetiska studier för både individuella sockerarter och blandningar av dem.

Flera katalysatorkarakteriseringsmetoder såsom svepelektronmikroskopi (SEM), transmissionselektronmikro-skopi (TEM), temperaturprogrammerad reduktion (TPR) och induktivt kopplad plasmaspektroskopi (ICP_OES) användes för att tolka och utreda katalysatorns aktivitet, hållbarhet och kritiska parametrar i själva katalysatorprepareringsprocessen.

Omfattande kinetiska experiment genomfördes i en isotermisk halvkontinuerlig reaktor i laboratorieskala. Reaktorn tillfördes en kontinuerlig ström av vätgas. Två stycken av fasta skumkatalysatorer placerades i ändan av en omrörare och katalysatorerna roterades med en konstant hastighet under experimentets gång. Höga selektiviteter av sockeralkoholer som överskred 98%, upptäcktes för båda sockerarterna, medan omsättnings-graden av sockerarten varierade mellan 60% och 98% i experimenten, beroende på den aktuella reaktions-temperaturen. Temperaturens inverkan på reaktionshastigheten var stark, medan vätetryckets inverkan på omsättningsgraden var relativt svag. I allmänhet hade L-arabinos en högre reaktionshastighet, men en acceleration av hydreringsreaktionen kunde observeras för båda sockerarterna då förhållandet D-galaktos:L-arabinos ökade, troligen p.g.a. konkurrerande växelverkan på katalysatorytan.

En kinetisk modell baserad på icke-konkurrerande adsorptionsmekanism mellan sockermolekyler och väte anpassades till de framtagna experimentella data med hjälp av icke-linjär regressionsanalys. Modellen gav en utmärkt beskrivning av de experimentella koncentrationsprofilerna och temperaturens inverkan på reaktionshastigheten. Utförliga känslighetsberäkningar visade att de estimerade kinetiska och adsorptions-parametrarna var statistiskt sätt väldefinierade och de hade ett väsentligt bidrag till den matematiska modellen.

De erhållna resultaten visar möjligheten att omsätta primära sockerarter som L-arabinos och D-galaktos samt binära blandningar av dem till de motsvarande sockeralkoholer på ruteniumnanopartiklar i aktiva kolskikt på aluminiumskum. En framtidsvision är att använda detta katalysator- och strukturkoncept i kontinuerliga kemiska reaktorer, vilka har obestridiga fördelar på tillämpning av strukturerade katalysatorer, t.ex. höga strömnings-hastigheter, höga mass- och värmeöverföringshastigheter samt en lågt internt diffusionsmotstånd i det porösa katalysatorskiktet.

RESUMEN

Palabras claves: hidrogenación, catálisis heterogénea, catalizadores estructurados, rutenio, L-arabinosa, D-galactosa, mezclas binarias de azúcares, alditoles.

El presente trabajo fue realizado en el laboratorio de Química Industrial e Ingeniería de la Reacción en Åbo Akademi University (Turku/Åbo, Finlandia) en colaboración con la Universidad de Valladolid (Valladolid, España) bajo la supervisión de Tapio Salmi (Profesor de la Academia de Finlandia) y Juan García Serna (Catedrático de la Universidad de Valladolid) en el marco del programa de intercambio Erasmus Plus.

La creciente preocupación por las consecuencias a corto y largo plazo generadas por el cambio climático está impulsando los esfuerzos de la humanidad hacia la adopción de un modelo de desarrollo más sostenible, lo que a su vez requiere una adecuada diversificación de las materias primas y los procesos de producción industriales. En este contexto el uso de biomasa lignocelulósica como materia prima para la industria química se presenta como una opción muy prometedora sobre la cual se han realizado numerosas investigaciones en los últimos años, como la producción catalítica de alditoles, derivados de las fracciones de celulosa y hemicelulosas de la biomasa. Estos compuestos poseen una variedad muy amplia de aplicaciones; desde la industria alimentaria donde son utilizados como edulcorantes de bajo contenido calórico hasta la industria farmacéutica como excipientes y agentes anti-caries.

Esta investigación estuvo centrada en el desarrollo de un novedoso catalizador de espuma sólida basado en rutenio soportado en carbono, con el cual se llevaron a cabo experimentos cinéticos de hidrogenación de los azúcares L-arabinosa y D-galactosa en diferentes condiciones de temperatura (90˚C, 100˚C y 120˚C) y presión de hidrógeno (20 y 40 bar), con la finalidad de dilucidar el efecto de dichos parámetros sobre la velocidad de reacción. Además, se realizaron experimentos cinéticos con mezclas binarias de azúcares a diferentes relaciones de D-galactosa a L-arabinosa con el objetivo de estudiar las interacciones de los dichos compuestos durante la reacción de hidrogenación en presencia del catalizador preparado.

La preparación del catalizador de espuma sólida comprendió las siguientes etapas: corte de las piezas de espuma de aluminio, pretratamiento por oxidación anódica, recubrimiento con carbono, pretratamiento ácido, incorporación de rutenio y reducción *ex-situ*. El método de recubrimiento de carbono se basó en la polimerización de alcohol furfurílico, seguido de un proceso de pirólisis y

activación con oxígeno. El grado de entrecruzamiento del alcohol polifurfurílico fue una variable muy relevante para obtener un recubrimiento de carbono con buenas propiedades para actuar como soporte de catalizador, en este sentido, las condiciones de polimerización se optimizaron con la finalidad de obtener dichas propiedades.

Para la incorporación de rutenio en las espumas recubiertas con carbono se emplearon dos métodos: Precipitación-deposición homogénea (PDH) e impregnación a humedad incipiente (IHI), usando en ambos casos nitrato de nitrosil rutenio(III) como solución precursora. En el método PDH, el contenido de carbono de las espumas y la relación molar de urea a rutenio fueron identificados como las variables más importantes para obtener un catalizador activo. Por otra parte, en el caso del método IHI, lo fueron el contenido de carbono y la concentración de la solución precursora. Utilizando este último fue posible preparar un catalizador activo (contenido de rutenio 1.1 %) para la conversión de los azúcares en sus correspondientes alditoles, y, por ende, dicho catalizador fue utilizado en el estudio cinético sistemático tanto de azúcares individuales como de sus mezclas.

Diversas técnicas de caracterización como microscopia electrónica de barrido, microscopia de transmisión electrónica, reducción a temperatura programada y espectroscopia de emisión óptica de plasma acoplado inductivamente fueron utilizadas para interpretar el comportamiento del catalizador en cuanto a actividad, desactivación y variables críticas para su preparación.

Los experimentos cinéticos se llevaron a cabo en un reactor semi discontinuo en modo isotérmico, en el cual el hidrógeno gaseoso era constantemente alimentado, dos piezas de catalizador de espuma sólida fueron colocadas en el extremo del eje de agitación y girados a una velocidad constante durante los experimentos. De los experimentos cinéticos de azúcares individuales se obtuvieron selectividades hacia alditoles por encima del 98% para ambos azúcares, mientras que las conversiones estuvieron en el rango de 60-98%, dependiendo de la temperatura. Se observó un efecto fuerte de la temperatura sobre la velocidad de reacción, mientras que el efecto de la presión de hidrógeno fue mucho menos pronunciado. En cuanto a las mezclas binarias de azúcares, en general la L-arabinosa presentó una velocidad superior, además se observó una aceleración de la reacción de hidrogenación en ambos azúcares a medida se aumentaba la cantidad de D-galactosa en las mezclas como resultado de interacciones competitivas entre los azúcares.

Se ajustó a los datos experimentales un modelo cinético mediante regresión no lineal, el modelo estuvo basado en un mecanismo de adsorción no competitivo entre las moléculas de azúcar y el hidrógeno. Se logró una muy buena descripción de los perfiles de concentración y el efecto de la

temperatura. Además, un análisis de sensibilidad detallado reveló que los parámetros estimados estaban bien definidos y tenían una contribución importante al modelo.

Para concluir, se puede afirmar que este trabajo demuestra la viabilidad de convertir azúcares primarios de biomasa como lo son la L-arabinosa y la D-galactosa y sus mezclas en los correspondientes alditoles utilizando rutenio como metal activo sobre un soporte de carbón en una estructura de espuma sólida. Un posible siguiente paso sería el uso de este catalizador en reactores trifásicos continuos que permitan aprovechar las propiedades asociadas a los catalizadores estructurados; altas tasas de transferencia de masa y calor externo y baja resistencia a la difusión en la capa de catalizador.

TABLE OF CONTENTS

INDEX OF FIGURES

INDEX OF TABLES

NOTATION

Nomenclature

A'_s	Lumped pre-exponential factor.
a	Slope in HPLC calibration curves
A_{HPLC}	Area in HPLC graphs
$C_{*'H}$	Hydrogen concentration in the active sites *'.
C_{*s}	Sugar concentration in the active sites *.
C'_0	Total concentration in the active sites *'.
C_0	Total concentration in the active sites *.
C_A	Concentration of L-arabinose in the liquid phase.
C_{AOH}	Concentration of L-arabitol in the liquid phase.
C_{cacli}	Estimated concentration of the component i.
C_{expi}	Experimental concentration of the component i.
C_G	Concentration of D-galactose in the liquid phase.
C_{GOH}	Concentration of D-galactitol in the liquid phase.
C_H	Atomic hydrogen concentration in the liquid phase.
C_{mean}	Mean concentration.
C_S	Sugar concentration in the liquid phase.
E_s	Activation energy of the sugar s.
K_A	Adsorption constant for L-arabinose.
K_G	Adsorption constant for D-galactose.
K_H	Adsorption constant for hydrogen.
k_s	Reaction rate constant of the surface reaction between hydrogen and sugars.
k'_s	Merged reaction parameter.
k''_s	Merged reaction parameter at constant hydrogen concentration for sugar s.
k_{si}	Adsorption constant for component i.
m_{cat}	Mass of catalyst.
Q	Objective function.
R^2	Coefficient of determination.
r_i	Reaction rate of component i.

r_s	Reaction rate of sugar s.
T	Temperature.
V_L	Reaction volume.
α	Relative reactivity.
κ'_A	Merged parameter of L-arabinose in sugar mixture modeling at constant hydrogen concentration.
κ'_G	Merged parameter of D-galactose in sugar mixture modeling at constant hydrogen concentration.
κ_A	Merged parameter of L-arabinose in sugar mixture modeling.
κ_G	Merged parameter of D-galactose in sugar mixture modeling.
ρ_B	Bulk density.

Abbreviations

A	L-Arabinose.
A_{OH}	L-Arabitol.
EDX	Energy dispersive X-ray analysis.
FA	Furfuryl alcohol.
G	D-Galactose.
G_{OH}	D-Galactitol.
H	Hydrogen.
HDP	Homogenous deposition precipitation.
ICP-OES	Inductively coupled plasma atomic emission spectroscopy.
IWI	Incipient wetness impregnation.
PFA	Polyfurfuryl alcohol.
S	Sugar.
SEM	Scanning electron microscope.
S_{OH}	Sugar alcohol.
SSR	Sum of the square residues.
TEM	Transmission electron microscopy.
TPR	Temperature-programed reduction.

1. INTRODUCTION

1.1. The Biorefinery Concept

The growing concern about the short and long-term environmental, social, and economic consequences caused by climate change is driving humankind towards a more sustainable development [1, 2]. In this context, at the time, 189 countries have signed The United Nations Paris Agreement, which aims to limit global warming from 2.0°C to 1.5 °C [3].The actions required to accomplish the Paris Agreement goals represent enormous scientific, logistic, and political challenges. Despite the advances in terms of technology and the implementation of renewable energy sources such as solar, wind, and biomass, a successful and smooth transition to a carbon-neutral economy requires a proper diversification of the feedstock and production processes [4, 5].

Therefore, the use of biomass appears to be a highly promising alternative to tackle the upcoming challenges of the chemical industry through the adoption of a new and sustainable biorefinery concept [6]. The biorefinery is a novel platform based on the conversion of biomass from different sources into high-value products, with the aim of increasing the economic potential by integrating various technologies that allow the use of the by-products generated in different transformation processes [7, 8]. The barriers to implementing this concept are mainly related to factors such as the geographic biomass availability, the chemical diversity of biomass, the economic viability compared to traditional refinery products, and the cultivable land usage, such in case of first-generation biofuels [6, 9].

The so-called second-generation biorefinery is oriented to the utilization of lignocellulosic biomass created from agriculture, forestry, and the alimentary industry, generating chemical compounds from residues [9]. This approach has outstanding advantages such as the wide availability of lignocellulosic materials, which represent 75% of the renewable biomass [10] and the absence of competition for cultivable soil. However, the transformation processes are complex due to the chemically diversified nature of its constituents: cellulose, hemicellulose, lignin, and extractives [5, 11].

Lignocellulosic biomass is composed of 40-50 wt. % of cellulose (glucose-based polymer linked by β-1, 4-glycosidic bonds), 16-33 wt. % of hemicelluloses (heteropolymers containing various monomers

of different sugars, such as arabinose, galactose, glucose, mannose, and xylose), and 15-30 wt. % of lignin (complex cross-linked polymer with coniferyl, coumaryl, and sinapyl alcohols as monomeric units). Thus, the elaboration of fuels and chemicals from these materials requires applying thermal, chemical, catalytic, or biological methods to obtain its constituents [12].

From extraction processes combined with chemical treatments, for example, acid hydrolysis, simpler carbohydrates are obtained, such as mono and disaccharides. In this sense, several conversion routes have been proposed to use these compounds as platforms for chemical production. A prime example is glucose as a building block from cellulose and starch, which after a reduction process can be transformed into its respective sugar alcohol, sorbitol, and afterwards, in polyesters, polyamides, and polyurethanes [5].

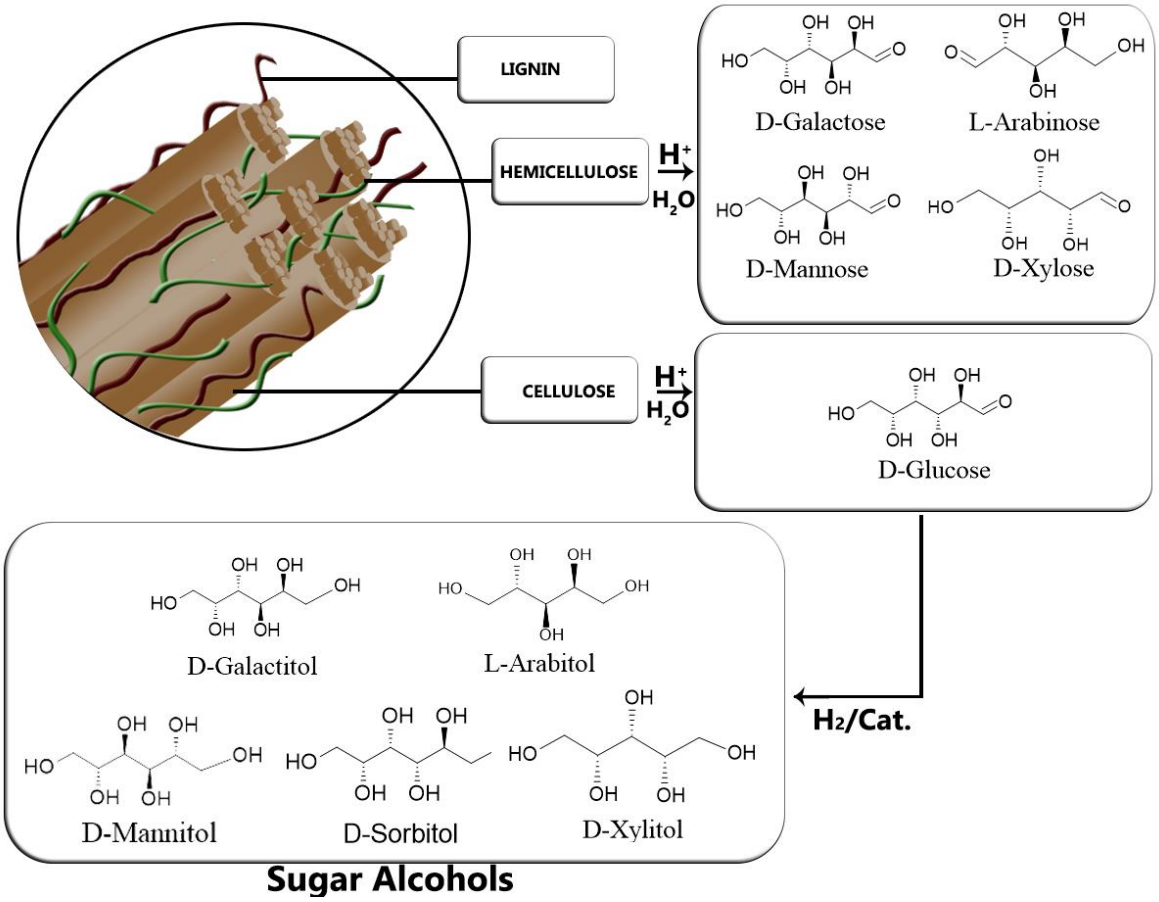

Figure 1.1. Sugar alcohols from lignocellulosic biomass.

Sugar alcohols are versatile substances with a wide range of applications that have aroused interest in recent years due to their potential to act as precursors for complex molecules and to produce renewable hydrogen or alkanes via aqueous-phase reforming [13].

1.2. Sugar Alcohols

1.2.1. Applications and Sources

Sugar alcohols are polyols with the general formula $H_2(CH_2O)_{n+1}$, which are formed by the reduction of the carbonyl group present in the sugar molecules employing either chemical reagents (e.g. sodium borohydride) or molecular hydrogen in contact with a homogenous or heterogeneous catalyst [4, 5, 14]. The route based on the use of heterogenous catalysts is preferred from an environmental point of view since it avoids the formation of stoichiometric co-products and facilitates the separation processes [5, 11].

Sugar alcohols find their applications in the alimentary, pharmaceutical, and cosmetics industries. The global market size of the sugar alcohols was 3.61 billion USD in 2019 and is projected to reach 6.79 billion USD by 2027, exhibiting an increasing rate of 7.75% within 2020-2027 [15]. Their main applications rely on the alimentary industry as healthier alternatives for sucrose due to their sweet taste and low caloric content, especially in the case of xylitol [16]. Sugar alcohols are also widely used in the production of hand sanitizers, which have had a remarkable demand increase since 2020 [15]. It is noteworthy that some studies have shown that sugar alcohols exhibit significant health-promoter effects, such as anti-carries and antioxidant activity [17, 18].

Currently, the production of the most important sugar alcohols on the market, sorbitol and mannitol, depends on agricultural resources, such as cassava, corn, and wheat [11]; alternatively, hydrolysis processes have been sought to produce them using cellulose [11, 19–21]. On the other hand, the production of sugars from hemicelluloses has gained much attention because the extraction is an easier task compared to the extraction of cellulose and it requires milder operation conditions; the use of acids, water, steam, or combinations at a moderate temperature range (150-190˚C) generally yields to a selective solubilization of hemicelluloses totally or partially hydrolyzed to oligomeric and monomeric sugars [16, 22, 23].

Hemicelluloses are present in different biomass sources, e.g., softwood and hardwood, pulping liquors from paper industry, plant gums, agricultural wastes, such as sugar cane bagasse, sugar beet pulp, rice straw, carrot pulp, among others [20–24]. Being mannans, xylans, arabinans and galactans the major units of hemicellulose present in nature, from which sugar monomers like xylose, mannose, rhamnose, arabinose and galactose can be derived [22].

L-arabinose and D-galactose were the objects of this study. These rare sugars can be produced from arabinogalactan, which appears in large quantities in larch species such as *Larix sibirica*. Arabinogalactan consists of β-D-galactopyranose as the backbone with D-galactopyranose and L-arabinofuranose side chains (Figure 1.2). The average molar ratio of galactose to arabinose is about 6:1, the molar mass is in the range of 20,000–100,000 g mol^{-1} [24] and the average degree of polymerization (DP) is around 130–200 [25].

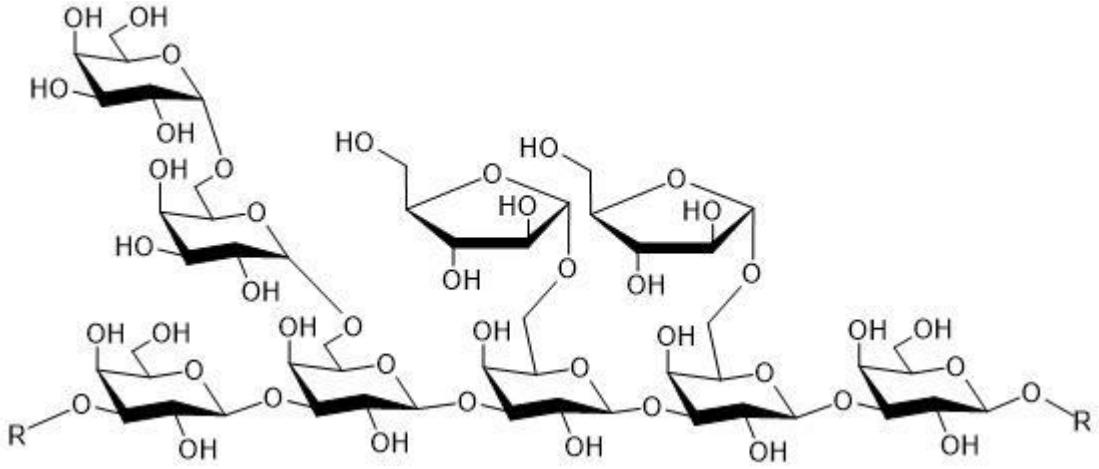

Figure 1.2. Structure of arabinogalactan.

1.2.2. Catalytic Production of Sugar Alcohols

Conventional sugar hydrogenation processes use semi-batch reactors operating isothermally (80-150˚C) in the presence of a finely dispersed solid catalyst, in most cases based on sponge nickel (Raney nickel) [26]. Hydrogen is constantly added to maintain pressure at 10-180 bar. The reaction is usually carried out with an aqueous sugar solution; however, other solvents such as ethanol can be used to improve the hydrogen solubility. Overall, under optimum conditions, high conversions (exceeding 95%) and selectivities towards sugar alcohols are obtained, except for some cases such as the hydrogenation of fructose to mannitol, with a product selectivity ranging from 60 to 70% [5, 27].

Nickel-based catalysts are relatively inexpensive and as above-mentioned, have good activity and selectivity. However, some serious pitfalls are evident, for instance, leaching of nickel during the process, leading to the formation of harmful by-products and catalyst deactivation, hence the purification costs increase. To surmount these problems, the use of ruthenium catalysts has been ambitioned, since it does not dissolve under typical hydrogenation conditions and exhibits the highest activity of the conventional catalytic metals (the activity order for glucose hydrogenation: Ru>Ni>Rh>Pd) [5, 26].

Ruthenium catalysts have been intensely studied in recent years for sugar hydrogenation using different supports such as carbon, alumina (Al_2O_3), silica (SiO_2), titanium dioxide (TiO_2), magnesium oxide (MgO), and hyper-cross-linked polystyrene. Ru/C catalysts have displayed a particular good performance and stability [28, 29]. Moreover, many efforts have been made to develop efficient carbon-supported catalysts [30–34] that would allow a stable continuous production of sugar alcohols with a special emphasis on structured catalysts, given their advantages over slurry technology.

1.3. Sugar Hydrogenation: Reaction Mechanism

Regarding the kinetic model of sugar hydrogenation, a reaction mechanism has been suggested in previous references according to which the reactants (sugars and hydrogen) are adsorbed on the active sites of the catalyst. Afterwards, the adsorbed sugar molecules react with hydrogen on the surface of the catalyst to form the correspondent products, which are finally desorbed [28, 34–38]. Generally, it is inferred that the reaction between the adsorbed sugar species and the adsorbed hydrogen is the rate-determining step, while the adsorption of the reactants and the desorption of products are rapid [28, 34–38].

Other aspects concerning a plausible mechanism are still a matter of debate, such as the mode of the hydrogen adsorption i.e., in molecular or dissociated form. Moreover, the simultaneous adsorption of sugar and hydrogen, species of very different sizes, raises the question of whether the adsorption is of competitive or non-competitive nature [39].

Competitive and non-competitive adsorption models have been proposed and implemented in the literature to describe the hydrogenation of several sugar molecules [5, 28, 35, 39]. Although given the huge size differences between sugar molecules and hydrogen, it is reasonable to imagine a

completely non-competitive adsorption, this approach is only an approximation from a physical point of view [38].

In this sense, an alternative semi-competitive mechanism has been proposed by Mikkola et al. [40] and Salmi et al. [39]. The idea behind this concept is that the larger molecules (sugar molecules) are adsorbed in the primary sites of the catalyst surface, leaving some accessible interstitial sites for small species such as hydrogen (whether in atomic or molecular form). The semi-competitive adsorption concept is illustrated in Figure 1.3, assuming a dissociated adsorption of hydrogen.

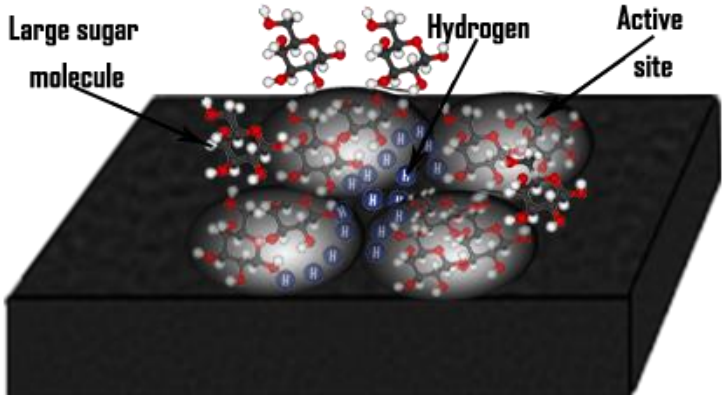

Figure 1.3. Illustration of the semi-competitive sugar/hydrogen adsorption concept (hydrogen is adsorbed in dissociated form).

1.4. Solid Foam Catalysts

Structured catalysts consist of regular tridimensional structures made of ceramics (Al_2O_3, cordierite, and SiC), metals (Al, Ni, Cu, Co, or alloy, i.e., stainless steel, Inconel, FeCrAl, NiCrAl, FeNiCrAl) or carbon over which a catalytic material is dispersed [41–44]. Among the possible configurations used for structured catalysts are monoliths, corrugated open crossflow packings, corrugated closed crossflow packings, knitted packing, fibers, as well as solid foams [45].

These materials have some common features that make them very attractive to be used in chemical reactors, such as a high void fraction, lower pressure drop compared to conventional packed beds of pellets and low flow resistance [44, 46]. These properties have made of structured catalysts extremely successful in some commercial applications, particularly in case of honeycomb monoliths catalysts, used in the cleaning of automotive exhaust gases [42].

Despite this success in a limited number of applications, the use of monolith catalysts is still rather limited in the chemical industries, because structured catalyst tend to have a lower load of the active phase compared to a bed of a catalyst particles, and in case of ceramic monoliths, low mass and heat transfer rates, which is an issue of particular importance for chemical processes [44, 46].

Moreover, metallic open-cell foam catalysts have been proposed as an alternative, since they offer higher mass and heat transfer coefficients compared to ceramic monoliths and lower pressure drop than packed bed [46]. Open-cell foams are tridimensional cellular materials made of interconnected solid struts, which enclose cavities (the cells), communicating by windows (the pores), as illustrated in Figure 1.4. The foam structures provide a disruptive and tortuous flow path and hence an exceptional mixing as well as good heat transfer properties [47].

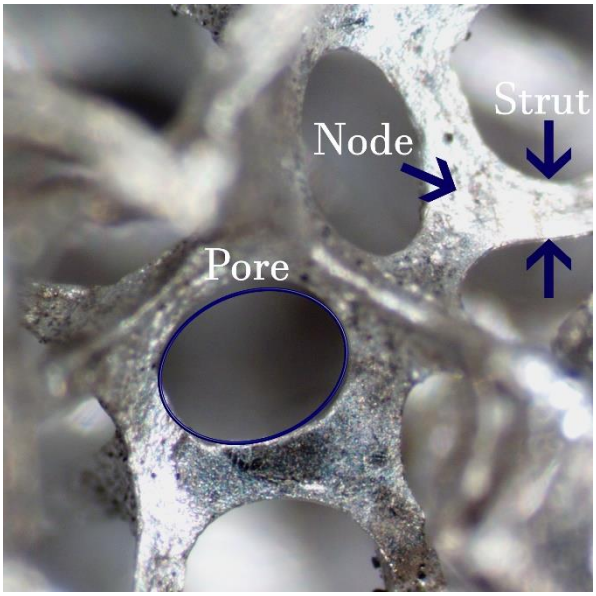

Figure 1.4. Optical microscope photograph of an open-cell metallic foam.

However, the absence of micropores in the metallic foams implies a low surface area available for the active phase deposition, but this gap can be bridged by coating the foams with appropriate substances that increase the area to take up the catalytic material [48]. Some authors has investigated the use of furfuryl alcohol (FA) as a carbon coating precursor for structured catalysts [32–34, 49–51]. The use of FA has multiple advantages such as a high carbon yield (around 50%) [51] and reactivity to form resinous carbon compounds. Besides, FA is obtained from the catalytic conversion of lignocellulosic materials, which makes it a promising sustainable reagent [52].

Carbon coating with polyfurfuryl alcohol comprises the following steps: A controlled polymerization of furfuryl alcohol, immersion of the piece to coat, control of amount and shape of the polymerized mixture on the surface of the piece, curing (crosslinking), pyrolysis of the formed polymer, activation, and functionalization [32, 49, 50, 53].

Although the exact mechanism and structure of all the FA polymerization products are still partially unknown, it is widely accepted that the predominant product of furfuryl alcohol polymerization under acidic conditions is constituted by a linear aliphatic structure of repeating units of polyfurfuryl alcohol linked by methylene bridges [46] as illustrated in Figure 1.5. On the other hand, the curing degree of the polyfurfuryl alcohol is highly dependent on the polymerization conditions i.e., temperature and acid amount, thus minimal variations of these conditions can lead to a wide range of possible products [54].

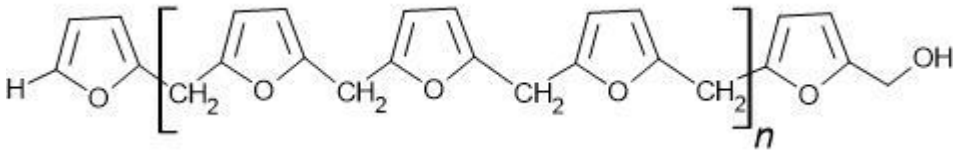

Figure 1.5. Linear Polyfurfuryl alcohol structure (PFA).

A carbon coating method for metallic open-cell foams was developed by Lali et al. [32] and replicated by Najarnezhadmashhadi et al. [34]. The authors used furfuryl alcohol as the carbon yielding binder, oxalic acid as the polymerization catalyst, and water as the pore former. The foams were rotated at a constant speed fixed to a stirrer, which prevented the clogging of the pores and allowed a smooth growth of the polymer layer on the struts of the foams [32]. The method was applied in this work to prepare carbon-coated aluminum foams.

1.5. Ruthenium Incorporation Methods

The fundamentals of the two methods applied in this work for ruthenium incorporation are briefly reviewed below.

1.5.1. Homogenous Deposition Precipitation (HDP)

A relatively easy method of adding an active phase on supported catalysts is the homogeneous deposition precipitation (HDP). In the HDP, the nucleation of the active metal species on the catalyst support is induced by changing the pH of the precursor solution to create low-solubility compounds

e.g., hydroxides. The gradual change of pH is carried out by adding a precipitant agent, such as urea [55]. When heated up above to 70˚C, urea decomposes, releasing OH^- ions [56].

$$CO(NH_2)_2 \xrightarrow{+H_2O} 2NH_4^+ + CO_2 + 2OH^-$$

Ru(III) nitrosyl nitrate has been identified as a suitable Ru precursor solution due to its ability to generate well-dispersed small-sized nanoparticles [57]. The released OH^- ions hydrolyzes metal salts by interacting with the precursor solution forming metal hydroxides. Thakur et al. [57] reported the following reaction network for the cation hydrolysis and precipitation reactions using Ru(III) nitrosyl nitrate as precursor solution.

$$Ru(NO)(NO_3)_3 \xrightarrow{+H_2O} [Ru(HO_2)_6]^{3+}$$

$$[Ru(HO_2)_6]^{3+} + OH^- \leftrightarrow [Ru(OH)(HO_2)_5]^{2+} + HO_2$$

$$[Ru(OH)(HO_2)_5]^{2+} + OH^- \leftrightarrow [Ru(OH)_2(HO_2)_4]^{+} + HO_2$$

$$[Ru(OH)_2(HO_2)_4]^{+} + OH^- \leftrightarrow Ru(OH)_3 \downarrow + 4HO_2$$

The interactions between the $[Ru(OH)_n]^{n-1}$ species of the precursor solution and the carbon support are relevant for the adequate performance of the HDP. Thus, acid functionalization of carbon is needed to generate carboxylic groups that allow anchoring the Ru-containing compounds on the active carbon support. Further the HDP, the hydroxide species are reduced to metallic Ru^0 under a hydrogen flow. Temperature-programmed reduction (TPR) measurements reported in literature for $Ru(NO)(NO_3)_3$ and carbon supports confirm 450-500˚C as a suitable temperature range for the reduction [30, 58].

1.5.2. Incipient Wetness Impregnation (IWI)

Methods based on impregnation and drying are frequent in catalyst preparation due to their simple execution and low waste generation. The impregnation techniques are based on the filling of the pores of the catalyst support. Incipient wetness impregnation (IWI) or dry impregnation is a method whereby the support is wetted, drop by drop, with a volume of a precursor solution containing the active metal, until filling the pores while the material keeps a dry character at a macroscopic scale, and after a time, the excess of solvent is removed by evaporation [55, 59].

Common precursors include inorganic salts e.g., nitrates, chlorides, sulfates, and organometallic complexes. Water is the most common solvent because of the high solubility of many precursors in

it. The uptake of the support occurs by capillary pressure differences. In hydrophobic supports such as carbon, the capillary pressure difference becomes negative; hence, the presence of oxygen surface groups (as in the case of HDP) is relevant to enhance the precursor adsorption. In structured catalysts, obtaining a good metal particle dispersion through this method is challenging because of the geometric complexity of these materials [45, 49].

1.6. Research Strategy

The goal of the present research work was to develop a novel open-cell solid foam Ru/C catalyst to study the catalyst activity and the reaction kinetics of the hydrogenation of L-arabinose and D-galactose and their mixtures to sugar alcohols. To achieve this objective, the following tasks were carried out:

- Development of an effective and reproducible carbon-coating method of aluminum foams based on the polymerization of furfuryl alcohol.
- Incorporation of a suitable amount of ruthenium on the carbon-coated foams and evaluation of the optimal condition of the incorporation method.
- Performance of kinetic hydrogenation experiments with L-arabinose and D-galactose to explore the product selectivity, reactant conversion, and influence of the pressure and temperature on the reaction rate and product distribution.
- Conduction of kinetic experiments with sugar mixtures to investigate the interaction of the sugars during the hydrogenation reaction.
- Fitting the experimental data to a plausible kinetic model.
- Application of catalyst characterization techniques that contribute to the clarification of the results.

2. EXPERIMENTAL

2.1 Catalyst Preparation

The catalyst preparation consisted of six general steps: Cutting of the open-cell aluminum foam pieces, anodic oxidation pretreatment, carbon coating, acid pretreatment, ruthenium incorporation (through homogenous deposition precipitation (HDP) or incipient wetness impregnation (IWI)), and *ex-situ* reduction. An overview of the catalyst preparation process is shown in Figure 2.1.

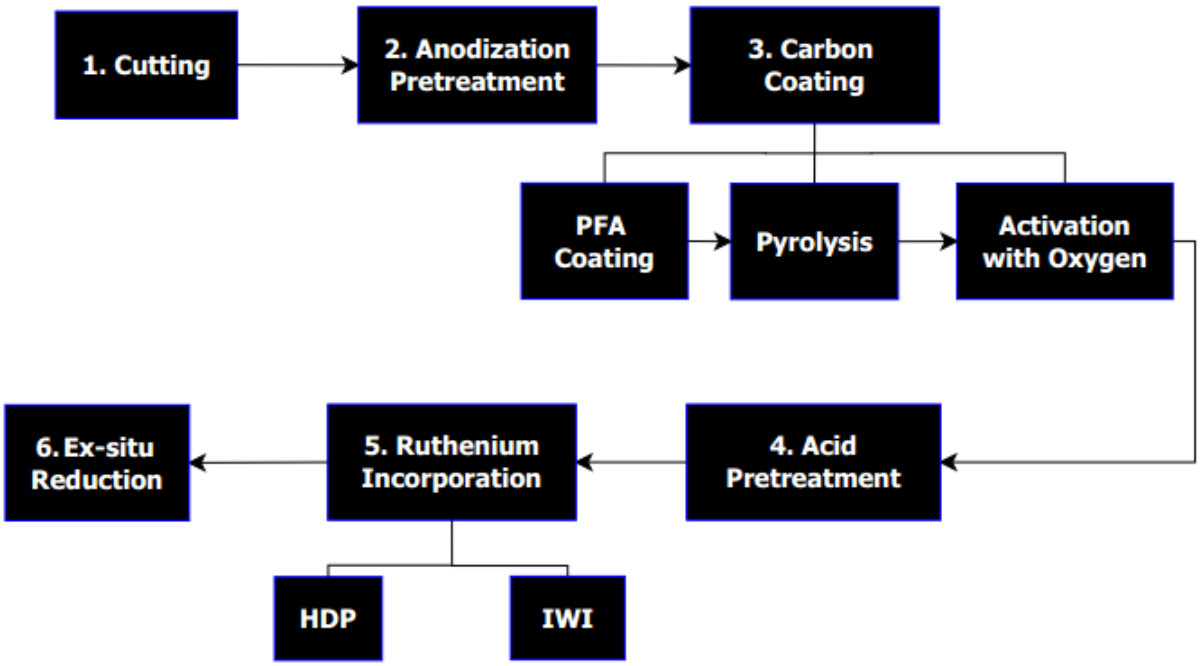

Figure 2.1. Overview of the solid foam catalyst preparation process.

Ten catalyst batches were elaborated, in which different preparation parameters were tested and several characterization techniques were applied to obtain an efficient catalyst for the kinetic study of the hydrogenation of sugars. Table 2.1 shows the general information of the catalysts.

Table 2.1. Batch codes and general information of the prepared catalysts.

Batch Code	Foam Code	Initial Mass (Al foam) [g]	Anodic Oxidation Pretreatment	Ruthenium Incorporation Method
C1-HDP1	C1-HDP1-F1 C1-HDP1-F1	0.4679 0.4934	No	HDP
C2-HDP1	C1-HDP2-F1 C1-HDP2-F2	0.7970 0.8679	No	HDP
C3-HDP2	C3-HDP2-F1 C3-HDP2-F2 C3-HDP2-F3	0.5420 0.4963 0.4753	No	HDP
C4-HDP3	C4-HDP3-F1 C4-HDP3-F2	0.4640 0.4620	No	HDP
C5-HDP4	C5-HDP4-F1 C5-HDP4-F2 C5-HDP4-F3	0.5951 0.5863 0.5872	No	HDP
C6-IWI1	C6-IWI1-F1 C6-IWI1-F2 C6-IWI1-F3	0.5901 0.5773 0.6000	No	IWI
C7-IWI1	C7-IWI2-F1 C7-IWI2-F2	0.4935 0.5495	No	IWI
C8-IWI2	C8-IWI3-F1 C8-IWI3-F2	0.5544 0.5481	No	IWI
C9-AO-IWI2	C9-IWI3-F1 C9-IWI3-F2	0.3674 0.3763	Yes	IWI
C10-AO-IWI2-R300	C10-IWI3-F1 C10-IWI3-F2 C10-IWI3-F3	0.4799 0.4464 0.5251	Yes	IWI

2.1.1. Cutting

Cylindrical pieces with dimensions of 33 mm length and 11 mm diameter were cut from a pure aluminum foam sheet with a pore density of 40 PPI (Goodfellow Cambridge Ltd) using a diamond hole saw bit (Figure 2.2). The cut foams were sonicated for 15 min in deionized water and for 15 min in acetone, then oven-dried for 2 hours at 70˚C, and overnight at room temperature.

Figure 2.2. Cutting of aluminum foams.

2.1.2. Anodic Oxidation Pretreatment

In order to enhance the carbon adhesion to the foams, the surface of some Al supports was pretreated as follows: One cleaned foam with the above-mentioned dimensions was attached to a thin platinum flat strip using PTFE tape, then connected to the anode (working anode) of a power supply (Autolab PGSTAT100N) with a rectangular 4cmx9cm aluminum plate (the immersed area was of 18 cm^2) connected to the cathode (counter electrode). Both were immersed in the electrolyte solution keeping 2.5 cm distance.

The electrolyte solution consisted of 100 mL of 1.6 M sulfuric acid (Sigma-Aldrich; 96%), 60 g/L of aluminum sulfate hexadecahydrate (Fluka; 98%) were also added to control the dissolution of aluminum during the anodization process [60, 61]. The temperature was set to 40˚C using a thermostat (Grant GR150 GP200) by circulating oil in the jacketed vessel containing the solution. A magnetic stirrer at the bottom of the vessel was utilized to homogenize the temperature.

A constant electrical current of 2 A was circulated through the system during 1 h and the voltage was monitored with the General-Purpose Electrochemical System (GPES) version 4.1 software. Thereafter, the foam was taken out from the acid and washed by dipping in deionized water. The same solution was used to anodize three different foam pieces. The obtained foams were oven-dried at 70˚C for 30 minutes and afterwards, calcined at 600 °C for 4h. Figure 2.3 shows the setup of the anodic oxidation procedure.

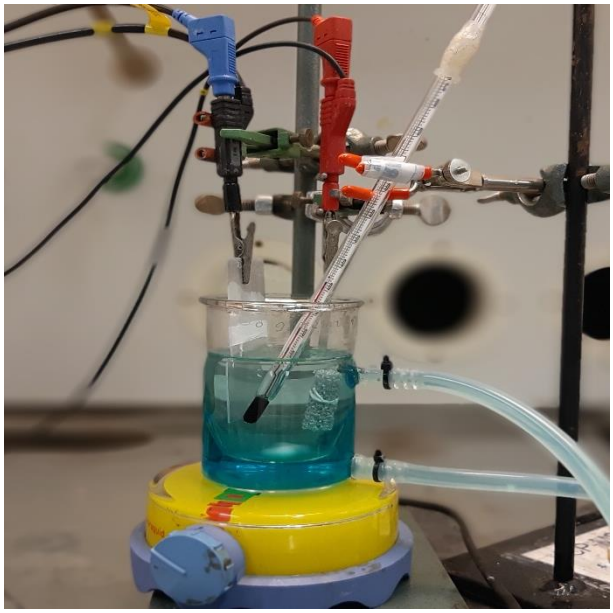

Figure 2.3. Experimental arrangement of the anodic oxidation process.

The required electrical current (2 A) was estimated using the geometrical surface area information and the optimal current density reported by Lali et al. (2015) [61]. On the other hand, the time and the electrolyte concentration were chosen by carrying out experiments and evaluating qualitatively the physical stability and homogeneity of the obtained oxide layers.

2.1.3. Carbon Coating

The carbon-coated foam batches consisted of two or three pieces, which were attached to a crossed blade stirrer shaft using thin stainless-steel wires and introduced in a 300 mL metallic vessel provided with an electric band heater (Ogden Mighty-Tuff MT-03015-0424). Thereafter, 136.2 g of furfuryl alcohol (Sigma Aldrich; 98 wt.%), 0.42 g of oxalic acid dihydrate (Sigma Aldrich; 99.5 wt.%), and 16.7 g of distilled water were poured into the vessel.

The heating rate of the electrical band was adjusted at 2 $K \cdot min^{-1}$ from room temperature (about 20˚C) to 120˚C using a temperature process controller (The CAL 9500P). A Heidolph RZR 2021 mechanical stirrer was utilized to rotate the foams during the polymerization process; two different stirring speeds were tested (200 rpm and 700 rpm).

The mixture under the above-described conditions kept between 20˚C and 110˚C within 55-60 min. When it reached 110˚C, the water evaporation began, the viscosity and temperature increased sharply due to the reaction heat, therefore, the automatic heating was turned off and the temperature was adjusted manually to reach 120˚C within 45-60 min in such a way that the water

slowly vaporized. Once the polymerization process was finished, the excess of PFA was removed by centrifuging the foams at 1000 rpm for 5 min. The experimental setup of the PFA coating procedure is shown in Figure 2.4.

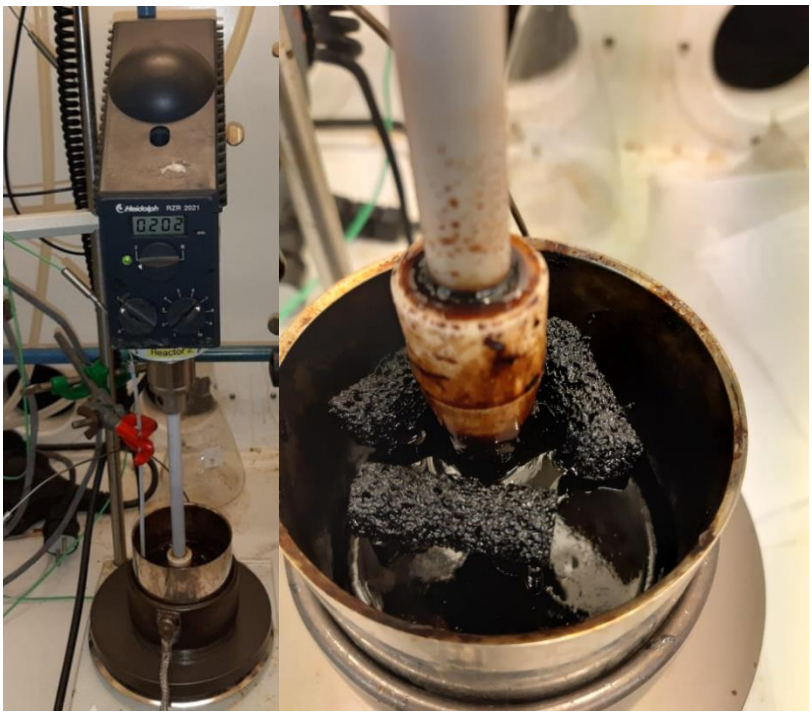

Figure 2.4. Experimental setup for PFA coating.

The PFA coated foams were pyrolyzed in a furnace (Carbolite CTF 12/100/900) heating at 5 $K \cdot min^{-1}$ up to 550 °C and held for 5 h in a nitrogen stream with a flow rate of 1 $L \cdot h^{-1}$. Subsequently, the carbon coating was activated in an oxygen stream of 2 $L \cdot h^{-1}$, heating from room temperature at 5 $K \cdot min^{-1}$ up to 380°C and held for 2h. The experimental conditions and the obtained carbon loads are presented in Table 3.2.

2.1.4. Ruthenium Incorporation

The carbon-coated foams were pretreated in a 3 wt.% nitric acid (Sigma-Alrich;70 wt.%) solution for 2 h. The acid-pretreated foams were then washed in deionized water, oven-dried at 70˚C for 2h and overnight at room temperature. The ruthenium incorporation was carried out testing two different methods: homogeneous deposition precipitation (HDP) and incipient wetness impregnation (IWI).

Homogenous Deposition Precipitation (HDPE)

The used homogeneous deposition precipitation procedure was modified from the method proposed by Lali et al.[32] and Najarnezhadmashhadi et al. [34] by suitably tuning the experimental conditions to obtain a proper pH evolution and a catalyst with a feasible Ru content.

A volume of 500 mL of Ru precursor solution with a nominal load as specified in Table 2.3 for each catalyst was prepared by diluting in deionized water an adequate amount of Ru(III) nitrosyl nitrate (Sigma-Alrich; 1,4 wt.% Ru, diluted in nitric acid).

Two carbon-coated and acid-treated foam pieces were placed inside a vessel containing the Ru precursor solution; a pH meter (InoLab 7310) was also introduced to monitor the pH during the entire process. The vessel was immersed in an oil bath under a hot plate (Velp Scientific). Two magnetic stirrers (one in the solution and one in the oil bath) were utilized to keep the concentration and the temperature homogeneous, and a stream of nitrogen was bubbled through the precursor solution to avoid the accumulation of carbon dioxide [30].

The system was heated until a constant temperature of 80˚C was reached, after which urea (Sigma-Alrich; 99 wt.%) was added to get a molar ratio of urea-to-Ru as is specified in Table 2.2. for each catalyst batch. The experimental arrangement is shown in Figure 2.5.

Figure 2.5. Experimental setup for HDP.

Table 2.2. Ruthenium incorporation conditions.

Batch Code	Foam Code	Final Mass of Carbon [g]	Ru Deposition Method	Ru Nominal Load Based on Carbon [%]	Urea-to-Ru Molar Ratio (for HDP)	*Ex-situ* Reduction Conditions
C1-HDP1	C1-HDP1-F1	0.0635	HDP	170%	5	450˚C for 2h
	C1-HDP1-F1	0.0618				
C2-HDP1	C1-HDP2-F1	0.1212	HDP	100%	5	450˚C for 2h
	C1-HDP2-F2	0.0935				
C3-HDP2	C3-HDP2-F1	0.3472	HDP	10%	20	450˚C for 2h
	C3-HDP2-F2	0.3259				
	C3-HDP2-F3	0.3075				
C4-HDP3	C3-HDP3-F1	0.0705	HDP	5%	1:20 at t=0min and 1:20 at t=400min	450˚C for 2h
	C3-HDP3-F2	0.0799				
C5-HDP4	C5-HDP4-F1	0.3342	HDP	30%	40	450˚C for 2h
	C5-HDP4-F2	0.3746				
	C5-HDP4-F3	0.3576				
C6-IWI1	C6-IWI1-F1	0.0043	IWI	24%	-	450˚C for 2h
	C6-IWI1-F2	0.0040				
	C6-IWI1-F3	0.0024				
C7-IWI1	C7-IWI2-F1	0.0384	IWI	24%	-	450˚C for 2h
	C7-IWI2-F2	0.0311				
C8-IWI2	C8-IWI3-F1	0.2989	IWI	4%	-	450˚C for 2h
	C8-IWI3-F2	0.3504				
C9-AO-IWI2	C9-IWI3-F1	0.3042	IWI	6%	-	450˚C for 2h
	C9-IWI3-F2	0.3063				
C10-AO-IWI2-R300	C10-AO-IWI2-R300-F1	0.5128	IWI	4%	-	300˚C for 5h
	C10-AO-IWI2-R300-F2	0.5371				
	C10-AO-IWI2-R300-F3	0.5879				

Incipient Wetness Impregnation (IWI)

Two concentrations of Ru(III) nitrosyl nitrate (diluted in nitric acid solution; Sigma-Aldrich) were tested for the incorporation of ruthenium in the foam catalyst: a 1.4 wt.% Ru solution for catalysts C6-IWI1 and C7-IWI1, and a 0.6 wt.% Ru solution for catalysts C8-IWI2, C9-AO-IWI2 and C10-AO-IWI2-R300.

The precursor solution was dripped to distribute it as homogeneously as possible on the surface of the carbon-coated foams using an adequate number of impregnation steps (avoiding overflowing)

until reaching the nominal load of each batch as reported in Table 2.2. For catalysts labeled as IWI1 the amount of precursor solution per step was approximately 0.10 g and 0.25 g for catalysts labeled as IWI2. After each impregnation step, the foams were dried in an oven at 110 ° C for 24 h.

2.1.5. *Ex-Situ* Catalyst Reduction

The *ex-situ* reduction of the catalysts was carried out in a furnace (Carbolite CTF 12/100/900), using 1 $L \cdot h^{-1}$ of hydrogen stream under the conditions of time and temperature described in Table 2.2. The reduction temperature of 450˚C is based on previous works that reported Ru/C catalysts prepared through the HDP method, in which ruthenium hydroxide and ruthenium oxide species are expected to be formed [30, 58]. On the other hand, the temperature of 300 ˚C is based of TPR measurements gauged in this work with catalyst C10-AO-IWI3-R300.

2.2. Kinetic Experiments

The kinetic experiments were carried out in a 0.3 L laboratory-scale semi-batch reactor (Parr 4561) provided with baffles, a sampling line with a sintered filter (7 µm), a heating jacket, a temperature and stirring rate controller (Parr 4843), a cooling coil, a pressure display module (Parr 4843) and a bubbling chamber. Two foam catalyst pieces were mounted at the endpoint of the mechanical agitating shaft to work as the stirrer during the experiments (Figure 2.6).

Preliminary experiments were conducted in a 1:1 molar ratio solution of L-arabinose (Sigma-Aldrich; 99 wt. %) to D-galactose (Across Organics; 99 wt. %) with a concentration of 0.13 M at 20 bar and 120˚C to test the prepared catalysts.

A set of individual kinetic experiments were performed with L-arabinose and D-galactose at three different temperatures (90°C, 100°C, and 120°C) and two hydrogen pressures (20 and 40 bar) in the presence of the catalyst C8-IWI3, using an initial sugar concentration of 0.13 M.

To study the interaction of the sugars during the hydrogenation reaction, a series of experiments were conducted using binary mixtures of D-galactose and L-arabinose in the presence of the catalyst C10-AO-IWI3-R300. The reaction conditions were 120°C and 20 bar, varying the molar ratio of D-galactose to L-arabinose (ratios: 0.5, 1, and 5).

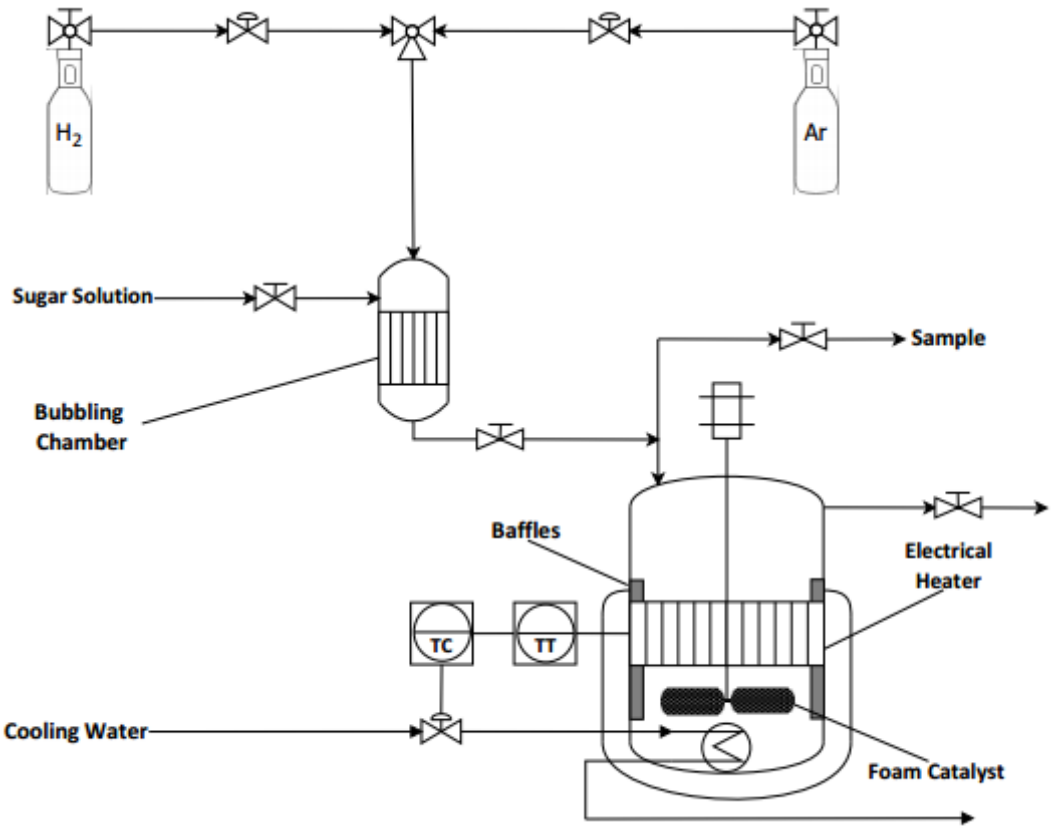

Figure 2.6. Overview of the setup for sugar hydrogenation experiments.

Prior to the kinetic experiments, the reactor was purged with argon and hydrogen, the foam catalyst was *in-situ* reduced for 2 hours at 5 bar pressure of hydrogen and 120˚C. Once the catalyst was reduced, 130 mL of sugar solution were pumped to the bubbling chamber and purged with argon, afterwards, with hydrogen during 15 min each, then the temperature was set to the required one, the hydrogen pressure adjusted, and the hydrogen-saturated solution injected to the reactor; hence the experiments started under the desired conditions of temperature and hydrogen pressure. A stirring rate of 600 rpm was utilized for all the experiments. Samples were withdrawn from the reactor to measure the concentration of reactants and products.

The concentration analysis of the sugars and sugar alcohols was conducted using a High-Performance Liquid Chromatograph (HITACHI Chromaster HPLC) equipped with a refractive index (RI) detector (HITACHI 5450 RI Detector). A Biorad HPX-87C carbohydrate column was used with 1.2 mM $CaSO_4$ solution (0.5 mL·min^{-1} flow rate) as the mobile phase, the temperature of the oven was 70˚C and an injection volume of 10 µL was utilized. The calibration data are shown in Appendix I.

2.3. Catalyst Characterization

2.3.1. Scanning Electron Microscopy (SEM)

Scanning Electron Microscopy (Zeiss Leo Gemini 1530) was used to study the morphology of the anodized aluminum foam, the carbon layer morphology and distribution of the carbon-coated catalyst foams prepared in different conditions.

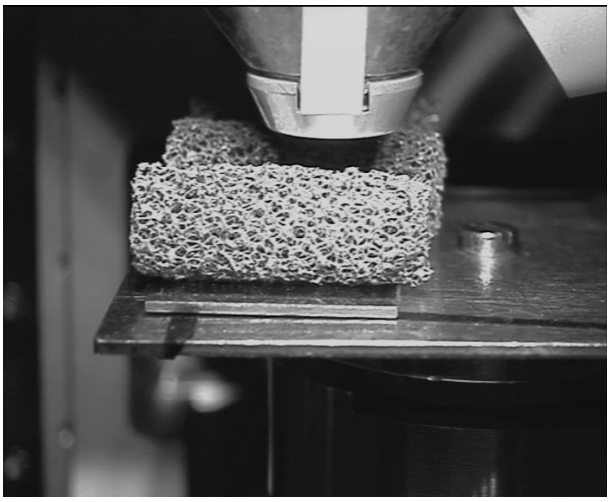

Figure 2.7. SEM analysis of foam catalysts.

2.3.2. Energy dispersive X-ray analysis (EDX)

Elemental analysis of the Al foams before and after the anodic oxidation process and the ruthenium content of the coated foams was evaluated by Energy dispersive X-ray analysis (LEO Gemini 1530 with a Thermo Scientific Ultradry Silicon Drift Detector).

2.3.3. Transmission Electron Microscopy (TEM)

Transmission Electron Microscopy (JEM 1400 Plus Transmission Electron Microscope) was used to measure the Ru particle size distribution of the catalyst prepared with different incorporation methods, and to compare the particle size of fresh and deactivated catalysts. Electron microphotographs of three random points per sample were obtained, and Image J software was utilized to measure 300 particles per micrograph.

2.3.4. Temperature-Programmed Reduction (TPR)

Temperature-Programmed Reduction (Micrometrics AutoChem 2910) measurements were carried out to study the catalysts prepared by incipient wetness impregnation (C8-IWI3 and C10-AO-IWI3-

R300). TPR experiments were conducted from 30 ˚C up to 700˚C following a temperature ramp of 10˚C·min^{-1} in a stream of hydrogen and argon (20% hydrogen in argon).

2.3.5. Inductively Coupled Plasma Atomic Emission Spectroscopy (ICP-OES)

The ruthenium content of the catalysts used for the kinetic experiments was gauged by ICP-OES (Perkin Elmer, Optima 5300 DV). The carbon coating (0.1 g) of the catalyst samples was digested using a mixture of acids (3 mL of sulfuric acid (Sigma-Aldrich; 96% wt.) + 3 mL of nitric acid (Sigma-Aldrich; 65%)) in a microwave oven prior to the analysis.

3. RESULTS AND DISCUSSION

3.1. Catalyst Preparation Results

Figure 3.1. shows the open-cell foam catalyst thought its different preparation stages. The shrinkage of the piece after the heat treatment stages is noticeable.

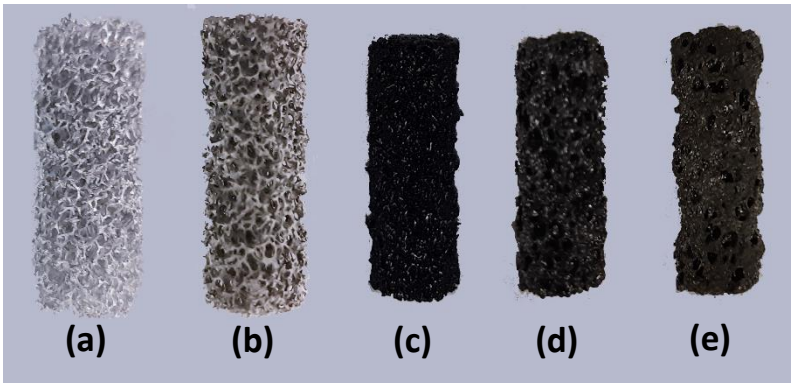

Figure 3.1.Changes in the open-cell foam catalyst through its different preparation stages: (a) Al untreated foam, (b) anodized Al foam, (c) foam coated with PFA, (d) pyrolyzed/oxygen treated carbon-coated foam, (e) carbon-coated, Ru impregnated and reduced catalyst.

3.1.1. Anodic Oxidation Results

An anodic oxidation pretreatment was performed to generate surface roughness on some Al foam samples in order to improve the carbon cohesion in the coating step. The noble properties of the used platinum strip allowed the total immersion of the foam piece and good contact throughout the process. The recorded voltage displayed a typical behavior [62, 63] for all the treated pieces; the potential increased at the beginning until it reached a maximum and then decreased to a constant value of around 3 V (Figure 3.2).

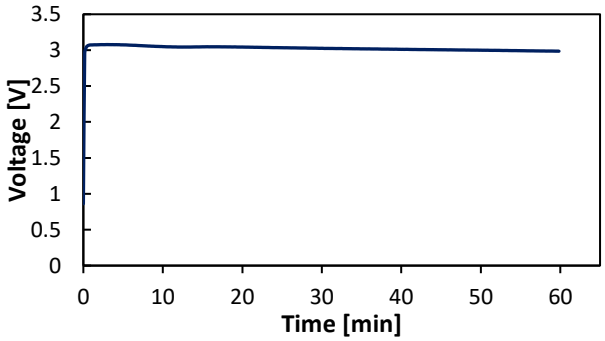

Figure 3.2. Potential variation during aluminum foam anodic oxidation at constant current.

After anodic oxidation, the glossy silver color of the untreated Al foam pieces changed to a gray mate color, indicating a well-distributed oxide layer (Figure 3.3).

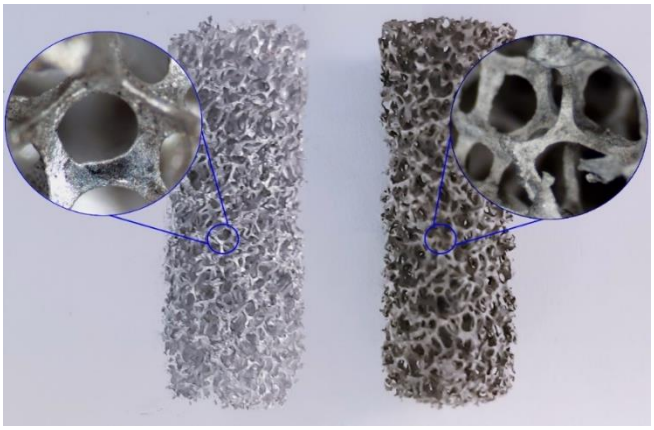

Figure 3.3. Visual change on the surface of the Al foams. Untreated foam (left) and anodized foam (right).

Figure 3.4 shows the SEM images of the surface texture of the untreated sample, anodized sample, and anodized and calcined sample at different magnifications. As revealed by the figure, the surface went from having a mainly smooth texture to be covered by fiber-shaped features in the case of the anodized sample, and by a semi-regular hexagonal nanopores (with an average size of 220 nm) in the case of the anodized and calcined sample. This pores hexagonal arrange is typical of anodic aluminum oxide [9, 10, 11], which has been highlighted for its suitability to work as a catalyst support [65].

On the other hand, the differences between the micrographs before and after the calcination demonstrate the need for such a treatment to obtain a more uniform pore pattern and to eliminate surface sub-holes [27]. This effect is ascribed to the diffusion of the ambient oxygen and the aluminum from the substrate through the existing aluminum oxide layer, which combine to form additional alumina [65], suggested also by the remarkable increase of the oxygen content after the calcination step (see Table 3.1).

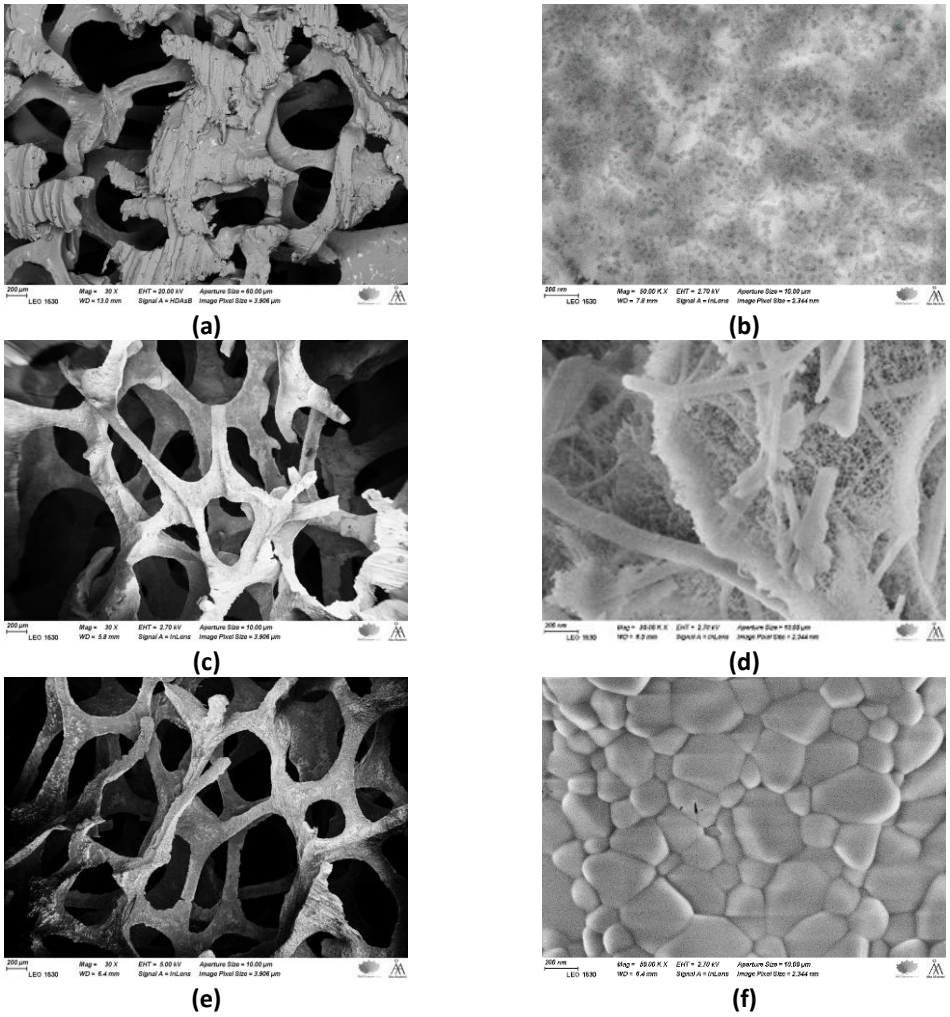

Figure 3.4. SEM micrographs of the oxide texture generated in catalyst C8-AO-IWI3-R300. (a) Untreated foam (30X), (b) untreated foam (50 kX), (c) anodized foam (30X), (d) anodized foam (50 kX), (e) anodized and calcined foam (30K X), (f) anodized and calcined foam (50 kX).

Table 3.1. Elemental Analysis (EDX) of aluminum foam during the different anodic oxidation stages (sample: C8-AO-IWI2-R300).

Stage	Al [wt. %]	O [wt. %]	Fe [wt. %]	S [wt. %]	Si [wt. %]	Mg [wt.%]
Untreated Foam	99.33	-	-	-	0.67	-
Anodized Foam	66.59	28.72	0.12	2.20	2.08	0.29
Anodized/Calcined Foam	41.63	46.20	0.44	6.04	1.79	3.89

3.1.2. Carbon Coating

The carbon coating of the aluminum foams was carried out by a controlled polymerization of furfuryl alcohol over their surface, followed by a pyrolysis step, and carbon activation in an oxygen stream. As can be observed in Table 3.2, the residence time between room temperature and 110˚C influenced the resulting carbon load, which is consistent with previous observations about this type of coating process [4, 3].

Table 3.2. Carbon-coating conditions of the prepared catalyst supports.

Batch Code	Foam Code	Initial Mass [g]	Rotation Speed [rpm]	Time [min]		PFA Loaded [%]	Carbon After Pyrolysis [wt. %]	Carbon After Oxidation [wt. %]	Final Mass of Carbon [g]
				20˚C-110˚C	20˚C-110˚C				
C1-HDP1	C1-HDP1-F1	0.4679	700	58	29	38%	16%	12%	0.0635
	C1-HDP1-F1	0.4934				37%	15%	11%	0.0618
C2-HDP1	C1-HDP2-F1	0.7970	700	60	41	37%	15%	13%	0.1212
	C1-HDP2-F2	0.8679				30%	12%	10%	0.0935
C3-HDP2	C3-HDP2-F1	0.542	200	55	45	65%	45%	39%	0.3472
	C3-HDP2-F2	0.4963				65%	45%	40%	0.3259
	C3-HDP2-F3	0.4753				66%	46%	39%	0.3075
C4-HDP3	C4-HDP3-F1	0.4640	700	60	34	38%	17%	14%	0.0705
	C4-HDP3-F2	0.462				39%	17%	15%	0.0799
C5-HDP4	C5-HDP4-F1	0.5951	200	55	44	77%	57%	36%	0.3342
	C5-HDP4-F2	0.5863				70%	60%	39%	0.3746
	C5-HDP4-F3	0.5872				79%	59%	38%	0.3576
C6-IWI1	C6-IWI1-F1	0.5901	700	55	45	27%	12%	8%	0.0527
	C6-IWI1-F2	0.5773				28%	12%	8%	0.0497
	C6-IWI1-F3	0.6000				26%	11%	6%	0.0387
C7-IWI2	C7-IWI2-F1	0.4935	700	55	40	47%	25%	24%	0.1581
	C7-IWI2-F2	0.5495				46%	24%	22%	0.1535
C8-IWI3	C8-IWI3-F1	0.5544	200	60	50	77%	56%	51%	0.5831
	C8-IWI3-F2	0.5481				79%	59%	56%	0.6837
C9-IWI3	C9-IWI3-F1	0.3674	200	60	50	67%	46%	45%	0.3042
	C9-IWI3-F2	0.3763				66%	45%	45%	0.3063
C10-AO-IWI2-R300	C10-AO-IWI2-R300-F1	0.4799	200	60	50	69%	54%	52%	0.5128
	C10-AO-IWI2-R300-F2	0.4464				72%	56%	55%	0.5371
	C10-AO-IWI2-R300-F3	0.5251				71%	54%	53%	0.5879

Under the experimental conditions of this work, two types of polymeric coatings were obtained. The first one was a foamy and dark-colored material formed when there was a sudden increase in temperature and water vaporization after reaching 110 ˚C, while in the absence of these effects, the result was a golden-colored and less viscous polymer (Figure 3.5).

In general, the carbon made from the dark foamy polymer exhibited better properties to be used as catalyst support: higher surface area, more homogeneous coverage, and better resistance to acids.

Figure 3.5. Obtained PFA coating: (a) foamy dark polymer obtained when sudden rising of temperature takes place, (b) golden polymer obtained when not sudden rising of the temperature takes place.

Despite that the exact reaction mechanism and products obtained in the polymerization of furfuryl alcohol remain uncertain [12, 13, 14], it is widely accepted that under acid conditions, the main product is a linear aliphatic structure of repeating units of polyfurfuryl alcohol linked by methylene bridges, produced by the condensation of the OH groups [14, 15]. Then, as the branching and cross-linking of the linear PFA take place, the mixture becomes darker and more viscous, and the water vaporizes due to the exothermic character of these phase reactions, creating cavities on the polymer, which enables it to become a good active carbon precursor [68].

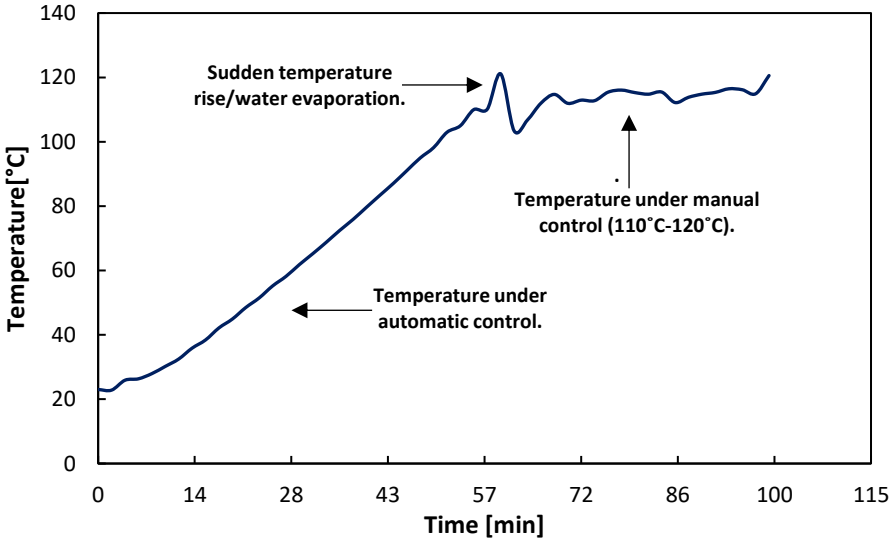

Figure 3.6. Temperature pattern during PFA coating when a foamy dark PFA coverage is obtained (catalyst C8-IWI3).

As Figure 3.7 shows, the carbon coating obtained from the less crosslinked PFA looks inhomogeneous and has a considerable amount of uncovered areas compared to the carbon from the foamy PFA. Additionally, the anodized foams presented a carbon coating with fewer cracks and improved cohesion due to the roughness of their surface.

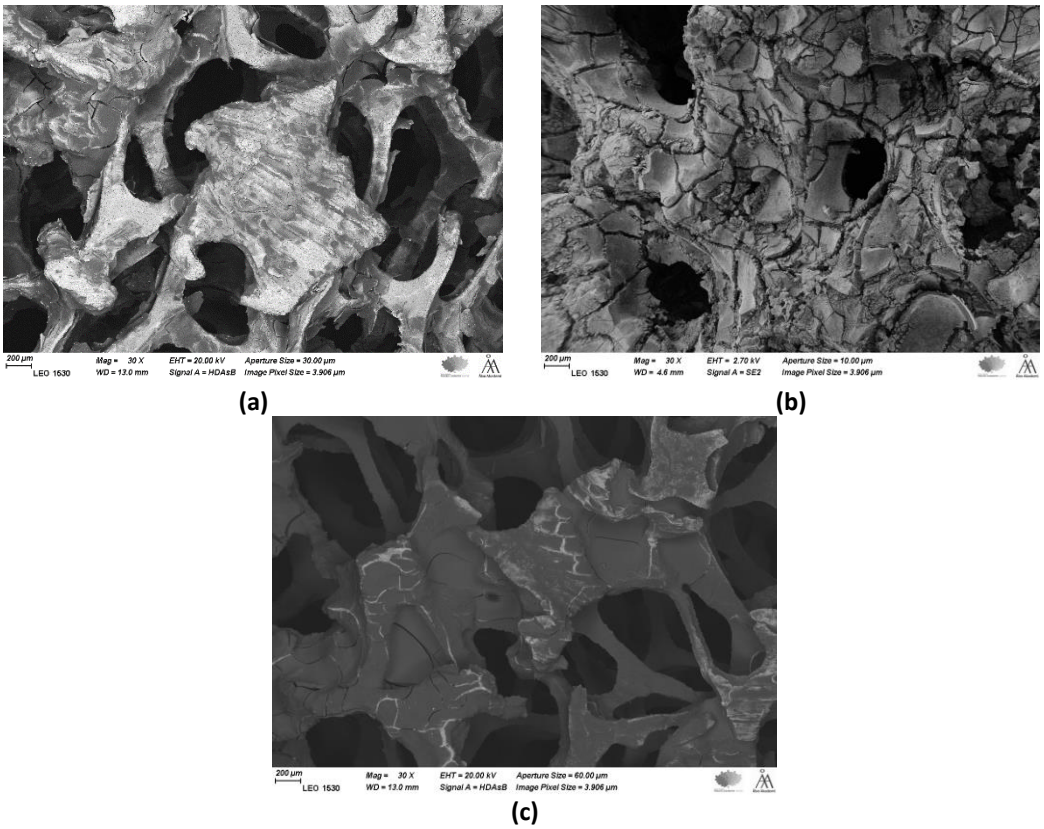

Figure 3.7. Surface structure of a carbon-coated foam substrate: (a) C2-HDP2 (12 wt.% carbon), obtained from golden-colored PFA, (b) C7-IWI2 (50 wt.% carbon), obtained from foamy dark PFA, (c) C10-AO-IWI2-R300 (50 wt.% carbon), preanodized and obtained from foamy dark PFA.

Another significant parameter identified was the rotation speed. The ruthenium incorporation experiments indicated that a carbon content above 40 wt.% was required to get enough active metal on the support. Thus, a rotation speed of 200 rpm was used, resulting in higher carbon loads at similar polymerization conditions (see Table 3.2).

3.1.3. Ruthenium Incorporation

Homogenous Deposition Precipitation Results

The homogeneous deposition precipitation technique has been reported in the literature as a suitable method to incorporate ruthenium on carbonaceous supports [3, 4, 17] using Ru(III) nitrosyl nitrate as precursor solution due to the feasibility of this reagent to generate small-sized nanoparticles [57]. In the HDP, a precipitant agent, such as urea, in this case, decomposes and releases OH^- ions that interact with the precursor solution, precipitating $Ru(OH)_3$ as the pH smoothy increases to a constant value of 7.

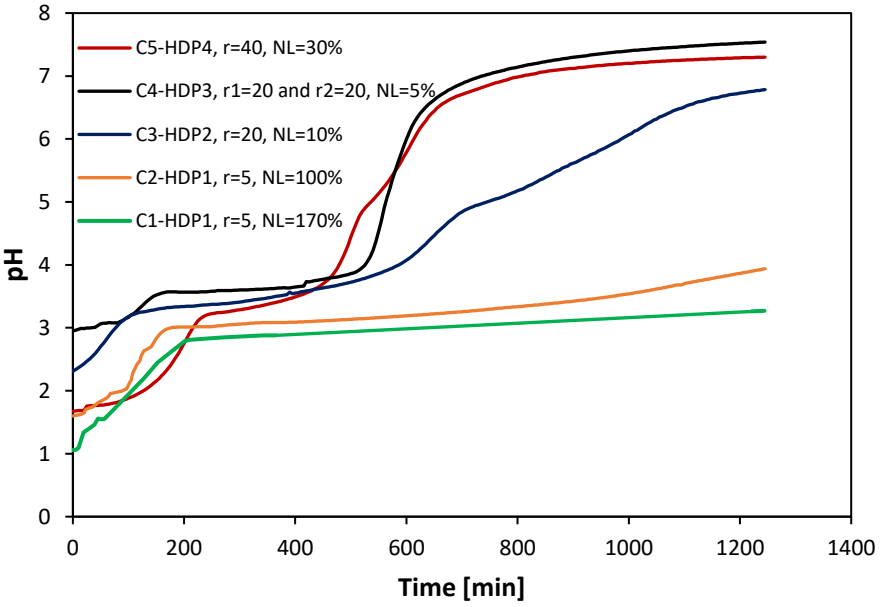

Figure 3.8. Evolution of pH during HDP at different conditions of Ru nominal load based on carbon (NL) and urea-to-Ru molar ratio (r).

The presence of aluminum in the support and nitric acid in the precursor solution represented additional difficulties for the incorporation of an adequate amount of active metal through this method. Different Ru nominal loads, urea-to-Ru molar ratios, and carbon loads on the support were investigated.

It can be seen in Figure 3.8 that the solution goes through a first plateau of pH attributable to the neutralization of nitric acid, since this behavior is not observed in HDP using only $Ru(NO)(NO_3)_3$ [3,17]. If the amount of added urea is not enough to neutralize the acid, the deposition process is not completed in 24 h, hence the prolonged exposure to acidic conditions causes a damage to the Al support, and in some cases, the precipitation of the ruthenium on the aluminum substrate (Figure 3.9).

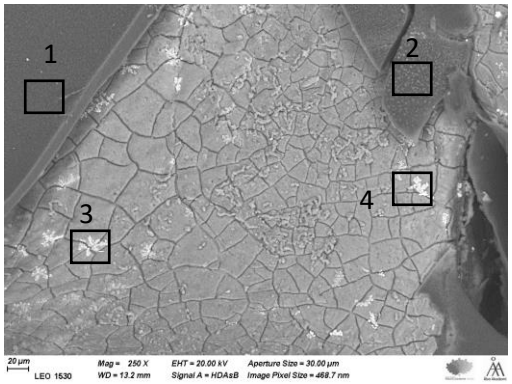

Point	Ru [wt. %]	C [wt. %]	Al [wt. %]	O [wt. %]
1	-	59.58	1.53	37.90
2	-	58.31	1.85	32.92
3	12.69	4.70	28.28	49.51
4	12.54	5.83	29.58	29.58

Figure 3.9. SEM image and elemental analysis (by EDX) of catalyst C3-HDP2 displaying cracks on the aluminum support and incorporation of Ru on the aluminum phase.

Considering the above-mentioned results, the catalyst C5-HDP4 was elaborated utilizing the found optimal conditions: a urea-to-Ru molar ratio of 40, coated foams with a high carbon content (~ 40 wt. %), and a nominal load of 30 wt.% Ru based on carbon. The result was a catalyst considerably more active, with a Ru load of 0.5 wt. % and a small particle size distribution (~80% of the particles smaller than 4 nm), yielding an average size of 3.3 nm (Figure 3.10).

Incipient Wetness Impregnation

Incipient wetness impregnation was used to incorporate Ru on the surface of the carbon-coated foams as an alternative method to HDP aiming to increase the active metal content of the catalyst. Two concentrations of Ru(III) nitrosyl nitrate were tested: 1.4 wt.% Ru. and 0.6 wt.% Ru, the amount of precursor solution per step was established as the maximum liquid volume that could be uptaken by the support without overflowing.

Two fundamental aspects for the preparation of this type of catalyst were confirmed as a result of the IWI tests; the carbon obtained from the foamy PFA (see Section 3.1.2) exhibited superior adsorption of the precursor solution compared to the carbon from the golden-colored PFA, and the

presence of nitric acid in the precursor solution represents a risk for the aluminum structure if the carbon load is insufficent.

Therefore, the most active catalysts (C8-IWI3 and C10-IWI3) obtained in this work were elaborated using supports with a high carbon content (~50%), a precursor solution with a concentration of 0.6 wt.% Ru, and a nominal load of 4 wt. % Ru based on carbon, yielding a 1.1 wt.% of Ru content with an average nanoparticle size of 3.7 nm, and 70% of the particles smaller than 4 nm (Figure 3.11).

3.1.4. Preliminar Catalyst Tests

The catalysts prepared by the optimal conditions of both HDP and IWI were tested for the hydrogenation of a 1:1 molar ratio of D-galactose to L-arabionse solution with a concentration of 0.13 M under the conditions discribed in Section 2.2. Table 3.3 shows a comparison between the prepared catalysts.

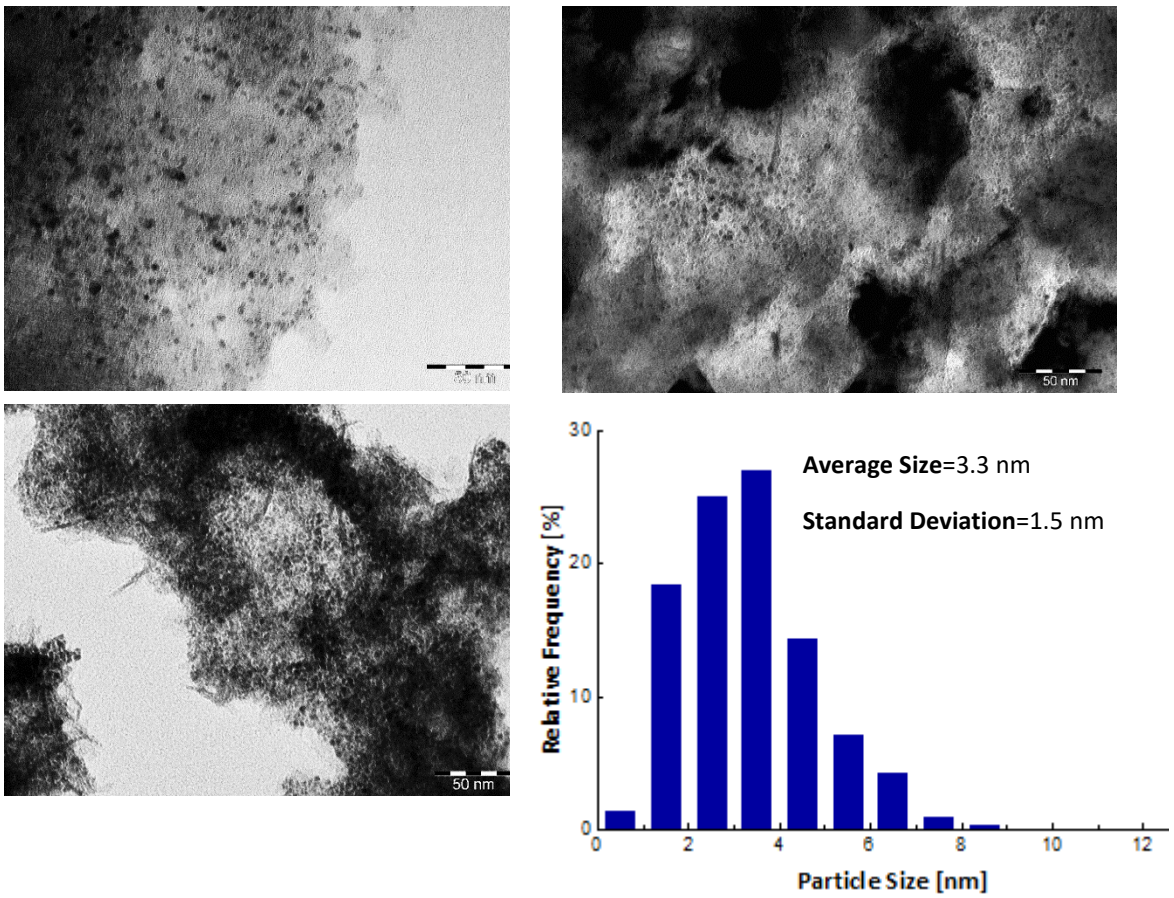

Figure 3.10. TEM images of catalyst C5-HDP4 and particle size distribution.

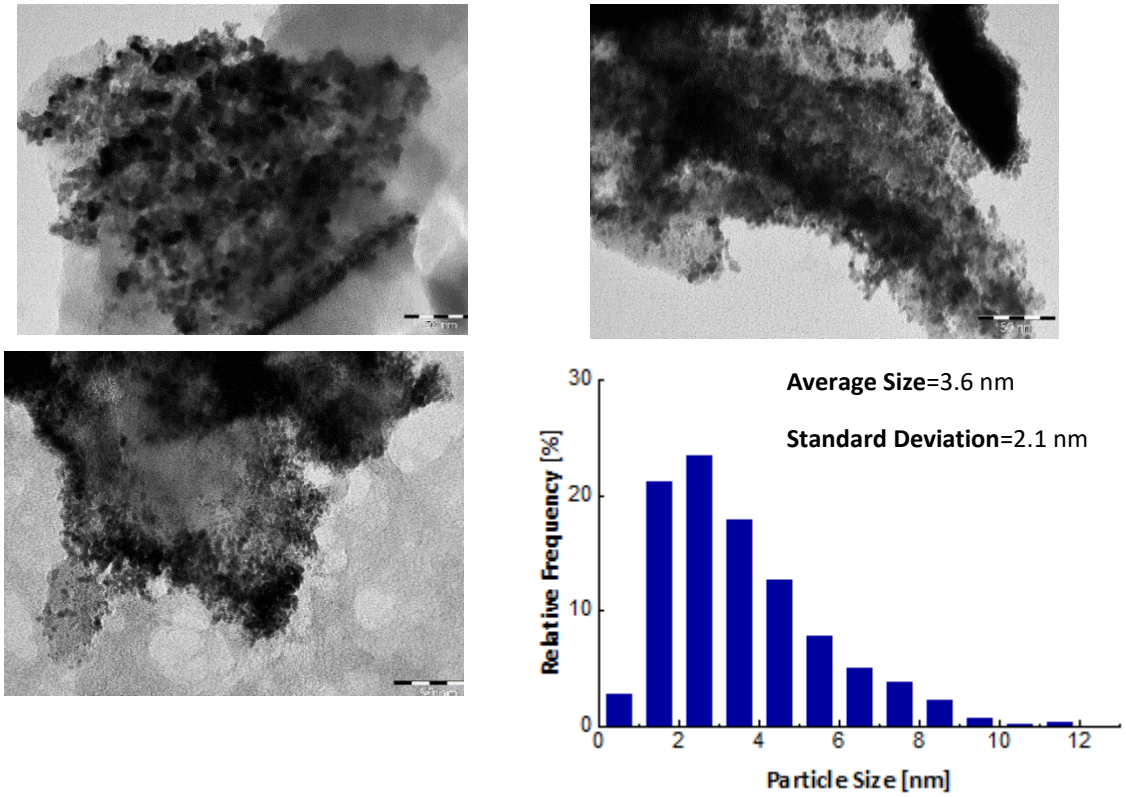

Figure 3.11. TEM images of catalyst C10-OA-IWI3-R300 and particle size distribution.

Considering the high activity of catalyst C8-IWI3, this was selected to perform the kinetic study of the individual sugars, and catalyst C10-OA-IWI3-R300, made utilizing the same carbon coating and Ru incorporation conditions, was used in the kinetic study of the sugar mixtures.

Table 3.3. Comparison of the physical properties and reactivity of the prepared catalyst

Catalyst	Total Carbon Mass (two foams) [g]	Ru load [wt. %]	Arabinose conversion in 4h [%]	Galactose conversion in 4h [%]	Average Ru particle size [nm]
C4-HDP3	0.1504	0.23	2%	4%	3.3
C5-HDP4	0.7322	0.52	54%	27.4%	3.3
C8-IWI3	1.2668	1.12	98%	97%	3.7

3.1.5. Effect of the Reduction Conditions and Deactivation

As mentioned in Section 2.1.5., catalyst C8-IWI3, used for the hydrogenation of individual sugars, was *ex-situ* reduced in a hydrogen stream (1 L·h^{-1}) at 450˚C for 2h. An induction period (~ 1 h) was observed when using this catalyst in the first two experiments (Figure 3.12), and it displayed an increase of activity in the subsequent experiments until reaching a considerably stable behavior in the fourth experiment; after approximately 32 h of use (including *in-situ* reduction time).

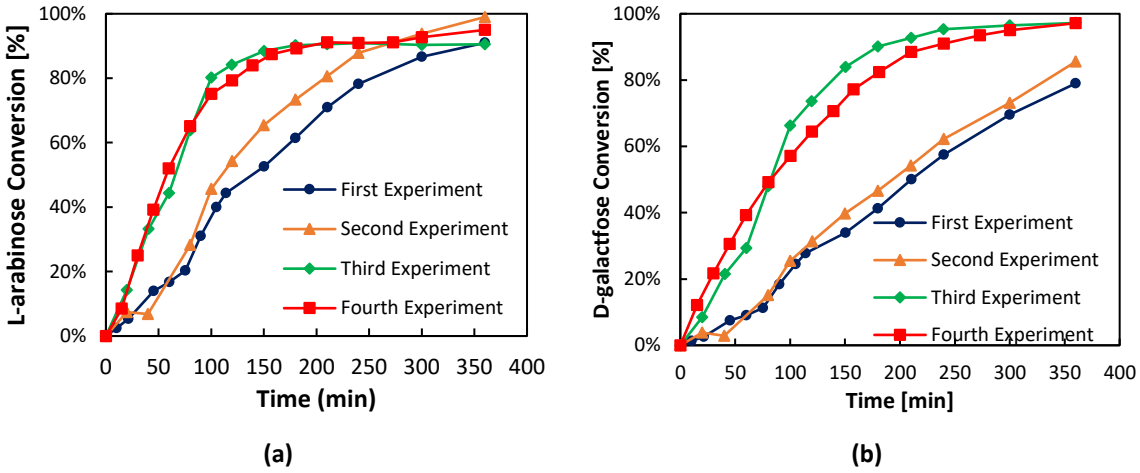

Figure 3.12. Induction behavior of Catalyst C8-IW3 during hydrogenation of 1:1 D-galactose to L-arabinose 0.13 M solution at 120˚C and 20 bar. (a) L-arabinose conversion vs time, (b) D-galactose conversion vs time.

Induction periods are relatively frequent in ruthenium catalysts, especially for liquid phase reactions [69–72], and are generally explained in terms of surface oxides, which are reduced during the time of reaction, forming more active metallic Ru^0.

Temperature-programmed reduction measurements displayed in Figure 3.13 were conducted with catalyst C10-AO-IW3-R300 to establish more adequate reduction conditions, thus avoiding induction periods. A single hydrogen consumption peak appeared at 245˚C, attributable to the reduction of ruthenium oxides [73, 74]. Therefore, the new reduction temperature was set at 300˚C and the reduction time was increased to 5 h (temperature ramp = 3˚C·min^{-1}) for catalyst C10-AO-IWI3-R300, in which no induction periods were observed.

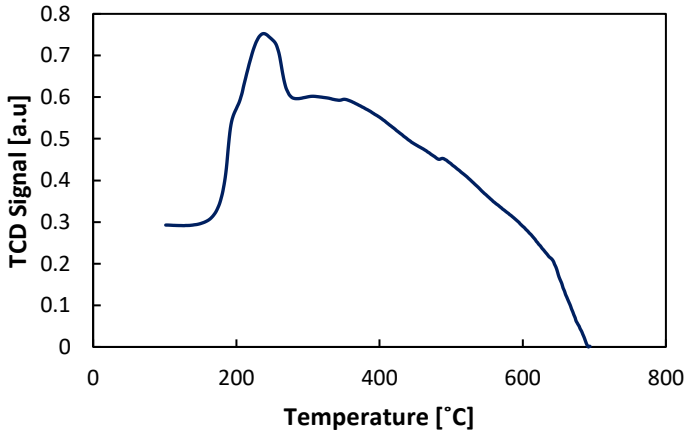

Figure 3.13. Hydrogen-TPR profiles of catalyst C10-IWI-R300 (before *ex-situ* reduction).

On the other hand, after 96 h of use, catalyst C8-IWI3 presented a considerable deactivation for the hydrogenation of both L-arabinose and D-galactose (Figure 3.14). TPR and TEM measurements were performed to investigate the possible causes of deactivation.

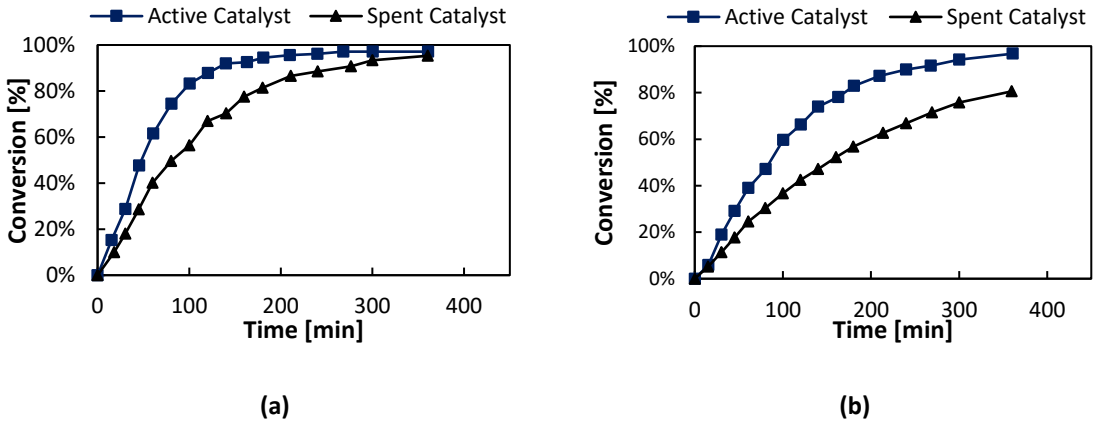

Figure 3.14. Deactivation of catalyst C8-IW3 during hydrogenation of (a) L-arabinose, (b) D-galactose at 120˚C and 20 bar.

Figure 3.15 shows the TEM micrograph of the spent catalyst. A substantial agglomeration of particles took place, resulting in the increase of the average size, from 3.6 nm to 5.2 nm. Some authors have reported agglomeration Ru nanoparticles after hydrogenation reactions of sugars [75, 76] and other chemicals [56].

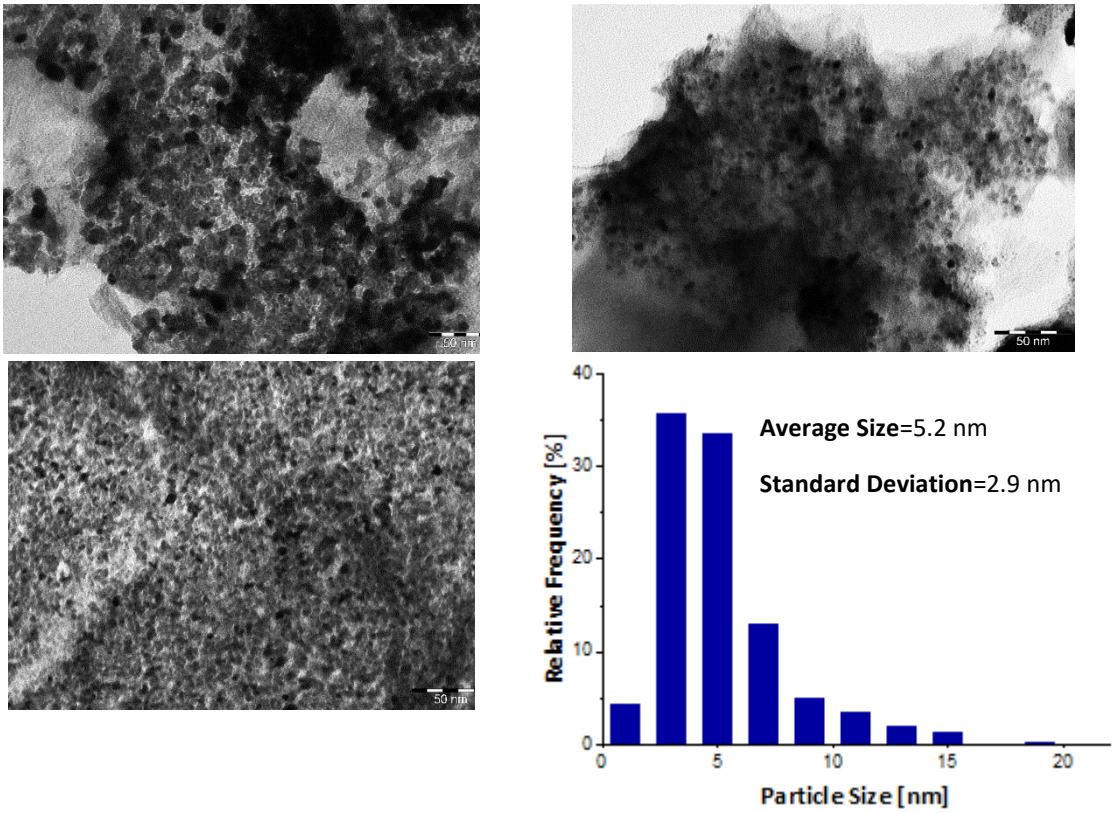

Figure 3.15.TEM images of catalyst C8-IWI3 after 100 h of use and particle size distribution.

Other studies have suggested the formation of $Ru(OH)_x$ species during liquid phase reactions in the presence of water [30, 58]. Nevertheless, TPR measurements carried out with the spent catalyst did not shown any significant hydrogen consumption peak within the temperature range of 400-500˚C associated with the reduction of these species [32, 56, 58].

Furthermore, Simakova et al. [29] found that the rates of hydrogenation of L-arabinose and D-galactose on Ru/C catalysts are highly influenced by the metal cluster size, with a maximum turnover frequency at 3 nm (approximately the particle size of the fresh catalyst), and that decays rapidly as the size increases, indicating that the increased particle size in our catalyst is the main cause of deactivation.

Although more research is needed to establish certainly the causes of the deactivation of this kind of catalyst, which also would allow developing suitable regeneration methods. In general, the prepared catalyst exhibited a good selectivity, activity, and stability similar [77] and even superior to other Ru/C catalysts described in the literature [75].

3.2. Kinetics Results

3.2.1. Individual Sugar Results

Selectivity and Conversion

Individual sugar hydrogenation experiments were performed at 20 bar and different temperatures (90, 100, 20˚C) on the prepared Ru/C foam catalyst. The overall selectivity towards sugar alcohols was higher than 98% in all the cases, whilst the conversion ranged 60-98% depending on the temperature. L-arabinose presented higher reactivity, as can be seen in Table 3.4.

Table 3.4 Selectivity and conversion of L-arabinose and D-Galactose after 6 h of reaction at 20 bar and different temperature (individual sugar hydrogenation).

Temperature	D-galactose		L-arabinose	
	Conversion (%)	Selectivity (%)	Conversion (%)	Selectivity (%)
90	60	100	85	99
100	73	99	97	99
120	97	98	98	98

The yield of by-products was negligible (1-5%) in all the experiments and dependent on the operation conditions; higher pressures and higher temperatures resulted in the formation more by-products, which could be detected by inspecting the chromatograms.

Temperature and Pressure Influence

Temperature showed a significant influence on the reaction rate for both sugars, as can be seen in Figure 3.16. The effect of temperature was successfully described by Arrhenius's law, the estimated values for the apparent activation energy of L-arabinose and D-galactose were 44 kJ·mol^{-1} and 51 kJ·mol^{-1}, respectively (see section 4.1.2).

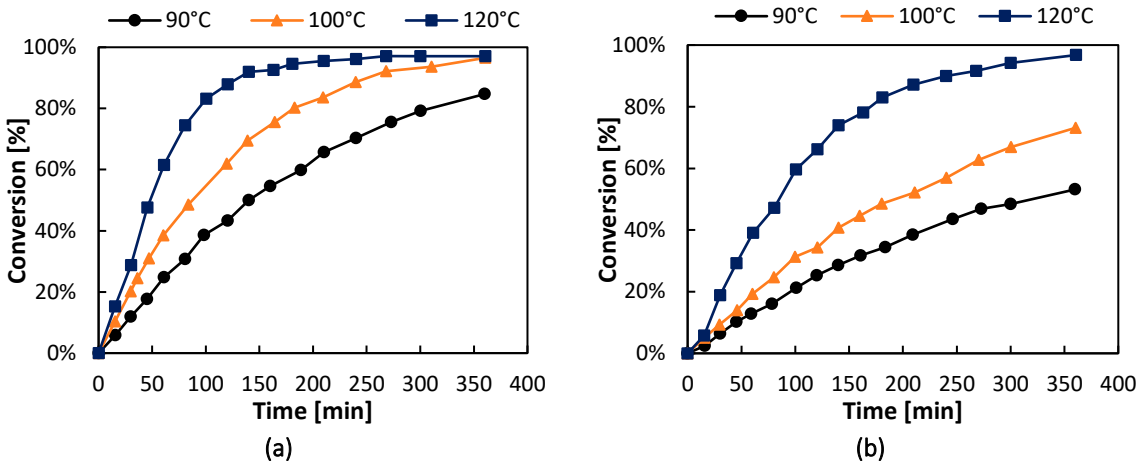

Figure 3.16. Effect of temperature on the hydrogenation rates at 20 bar for (a) L-arabinose, (b) D-galactose.

On the other hand, the hydrogen pressure effect was rather minor, as can be seen in Figure 3.17. Although weak, the pressure influence at other temperatures could not be studied due to the appearance of deactivation in the catalyst, as mentioned in Section 3.1.5.

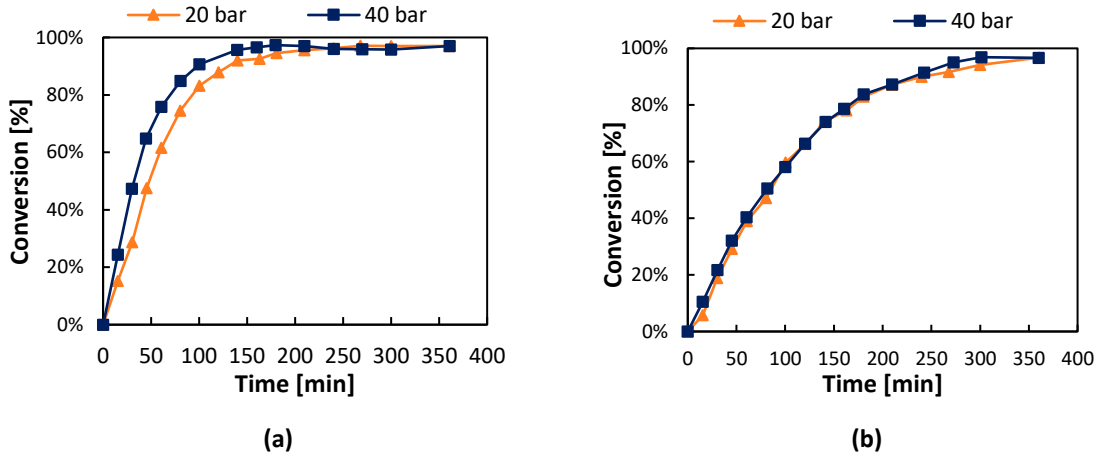

Figure 3.17. Effect of pressure on the hydrogenation rates at 120˚C for (a) L-arabinose, (b) D-galactose.

These results are consistent with the observations reported by Sifontes et al. [35], who carried out several sugar hydrogenation experiments in the presence a Ru/C powder catalyst, finding that temperature has a strong effect on the reaction rate, while pressure has a minimal effect, with the extreme case of D-galactose that exhibited almost invariant behavior with respect to hydrogen pressure.

3.2.2. Sugar Mixtures Results

To study the interaction of the sugars during the hydrogenation reaction, a series of experiments were conducted using mixtures at 120°C and 20 bar, varying the molar ratio of D-galactose to L-arabinose (ratios: 0.5, 1 and 5).

As in individual sugar experiments, high conversions (85-99%) and selectivities (95-99%) were obtained and the yield of by-products were almost undetectable after 6 h of reaction.

Regarding to the effect of the molar ratio, D-galactose exhibited an increase in the reaction rate as the ratio of D-galactose in the mixture was higher, which it is an expected result that can be ascribed to the presence of other sugar competing for the same active sites on the catalyst.

However, L-arabinose displayed an acceleration in the reaction rate with the increase of the D-galactose ratio, as can be seen in Figure 3.13. Although counterintuitive, this effect has been observed in competitive catalytic reactions, where the addition of a component (D-galactose, in this cas) leads to the increase of the reaction rate [78]. This observation was also obtained by Sifontes et. al. [36] for D-galactose/L-arabinose mixtures, so overall, the increase in the concentration of L-arabinose retards the hydrogenation rate of both sugars competing for hydrogen.

Noteworthy, these results demonstrate the possibility of carrying out the direct hydrogenation of sugar mixtures , such as those obtained from the hydrolysis of arabinogalactan (hemicellulose), resulting in a mixture with an approximate molar ratio of 6:1 D-galactose to L- arabinose [79].

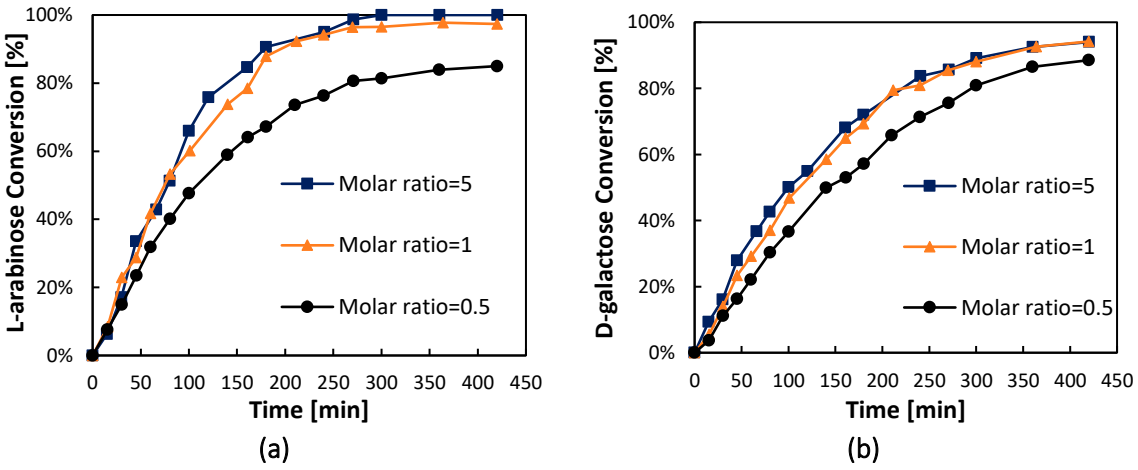

Figure 3.18. Effect of the D-galactose to L-arabinose molar ratio on the hydrogenation rates at 120˚ of (a) L-arabinose, (b) D-galactose.

4. KINETIC MODELING

4.1. Individual Sugars Modeling

4.1.1. Model Hypotheses

The kinetic experiments were conducted in an isothermal semi-batch reactor with a fixed mass of catalyst, where hydrogen was continuously added in such a way that the pressure and the concentration of the dissolved hydrogen can be assumed constant, and the energy balance can be dismissed.

The reactions were inferred to be in the kinetic regime, in the absence of mass transfer limitation due to the high stirring speed used. On other hand, since the change of the liquid volume during the reaction is minor, the volume of the reaction medium was considered constant.

Regarding the kinetic mechanism, sugar hydrogenation is known to be an irreversible reaction in practice [28, 34–38], and given the negligible amount of by-products observed in the experimental data (see Section 3.2.1), the reactions were assumed to proceed towards the exclusive formation of sugar alcohols.

Although another reaction mechanisms have been proposed for the hydrogenation of sugars (See Section 1.3), for the sake of simplicity, a non-competitive adsorption model was used, dissociative adsorption of hydrogen was considered, but maintaining its molecular identity in the sense that two atoms of hydrogen react with the adsorbed sugar.

Since the adsorption affinity of sugar alcohols has been shown to be lower than that of the corresponding sugar monomers [35], the adsorption of the reaction products was neglected. The catalyst surface was assumed ideal so that the Langmuir model was applied and the surface reaction between the adsorbed sugar species and the adsorbed hydrogen was presumed as the rate-determining step in the catalytic process.

4.1.2. Derivation of the Rate Expressions for the Kinetic Model

In accordance with the hypothesis described in the previous section, the reactions took place in a constant liquid volume (V_L) with a fixed mass of catalyst (m_{Cat}) in the reactor vessel. Therefore, the mole balance for the implied chemical species in the liquid phase can be expressed by equation 4.1, where C_i denotes the concentration of the component i.

$$\frac{dC_i}{dt} = r_i \cdot \frac{m_{Cat}}{V_L} \quad (4.1)$$

The hydrogenation reactions proceeded by consuming the sugar (S) to form the corresponding sugar alcohol (S_{OH}), then the mole balances for the participating species are given by equations 4.2 and 4.3, where the bulk density $\rho_B = \frac{m_{Cat}}{V_L}$, and r_S is the reaction rate per mass of catalyst.

$$\frac{dC_S}{dt} = -r_S \cdot \rho_B \quad (4.2)$$

$$\frac{dC_{S_{OH}}}{dt} = r_S \cdot \rho_B \quad (4.3)$$

The non-competitive kinetic mechanism of sugar hydrogenation is shown in Figure 4.1. An active site for sugar adsorption is represented by *, whilst *' denotes a site for hydrogen adsorption.

$$S + * \overset{K_S}{\leftrightarrow} S*$$

$$H_2 + 2*' \overset{K_H}{\leftrightarrow} 2H*'$$

$$S* + 2H*' \overset{k_{Si}}{\rightarrow} S_{OH} + * + *'$$

Figure 4.1. Reaction mechanism for hydrogenation of individual sugars.

Therefore, the adsorption quasi-equilibria for the sugar molecules and hydrogen are defined by equations 4.4. and 4.5, respectively.

$$C_{*S} = K_S \cdot C_S \cdot C_* \quad (4.4)$$

$$C_{*'H} = \sqrt{K_H \cdot C_H} \cdot C_{*'} \quad (4.5)$$

The site balances for sugar and hydrogen adsorption are written as

$$C_{*S} + C_* = C_0 \quad (4.6)$$

$$C_{*'H} + C_{*'} = C'_0 \quad (4.7)$$

Where C_0 and C'_0 denote the total concentration of the adsorption sites available for sugar and hydrogen, respectively. After substituting equilibria expressions (equations 4.4.and 4.5) in the site balances (equations 4.6 and 4.7), the concentrations of vacant sites are

$$C_* = \frac{C_0}{1 + K_S \cdot C_S} \quad (4.8)$$

$$C_{*'} = \frac{C'_0}{1 + \sqrt{K_H \cdot C_H}} \quad (4.9)$$

Considering that the surface reaction between the adsorbed sugar molecules and the hydrogen is the rate-determining step, the rate equation can be written as it follows

$$r_S = k_S \cdot C_{*S} \cdot C_{*'H}{}^2 \tag{4.10}$$

Substituting equations 4.8 and 4.9 in equation 4.10 yields

$$r_S = \frac{k_S \cdot K_S \cdot K_H \cdot C_0 \cdot C'_0{}^2 \cdot C_S \cdot C_H}{(1+K_S \cdot C_S) \cdot \left(1+\sqrt{K_H \cdot C_H}\right)^2} \tag{4.11}$$

A merged parameter is defined as

$$k'_s = k_S \cdot K_S \cdot K_H \cdot C_0 \cdot C'_0{}^2 \tag{4.12}$$

And the reaction rate equation becomes

$$r_S = \frac{k'_s \cdot C_S \cdot C_H}{(1+K_S \cdot C_S) \cdot \left(1+\sqrt{K_H \cdot C_H}\right)^2} \tag{4.13}$$

Furthermore, since the hydrogen pressure remained constant during all the experiments, the term $\frac{C_H}{\left(1+\sqrt{K_H \cdot C_H}\right)^2}$ was constant, and equation 4.13 can be simplified to

$$r_S = \frac{k''_s \cdot C_S}{(1+K_S \cdot C_S)} \tag{4.14}$$

If the reactions are presumed to follow the Arrhenius law, the temperature dependence of the merged parameter can be expressed as

$$k''_s = A'_S \cdot e^{-\frac{E_S}{R \cdot T}} \tag{4.15}$$

Finally, equation 4.14 can be written as

$$r_S = \frac{A'_S \cdot e^{-\frac{E_S}{R \cdot T}} \cdot C_S}{(1+K_S \cdot C_S)} \tag{4.16}$$

4.1.2. Parameter Estimation

The parameters were estimated by minimizing the sum of residual squares as defined in equation 4.17 using the Nelder-Mead optimization method, while the underlying ordinary differential equations (ODEs) were solved in Python through the LSODA solver.

$$Q=\sum_{i=1}^{n}\left(C_{Exp,i}-C_{Calc.i}\right)^2 \tag{4.17}$$

As the first approach, the parameters included in equation 4.14 were computed individually for the experimental temperatures (90˚C, 100˚C and 120˚C). The linearized Arrhenius plots for L-arabinose and D-galactose are shown in Figure 4.2.

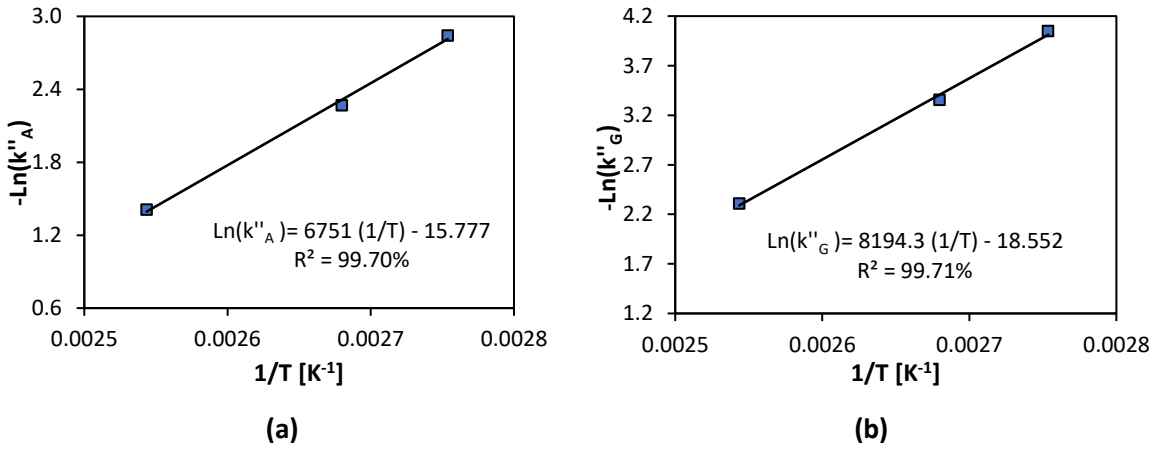

Figure 4.2. Arrhenius plot for the estimated k'_s parameters: (a) L-arabinose, (b) D-galactose

As expected, high coefficients of correlation for both sugars were obtained. Consequently, Arrhenius law can accurately describe the effect of the temperature on these reactions, as listed in Table 4.1.

Table 4.1. Arrhenius parameters determined by linear regression.

Sugar	A_S' [$L \cdot g_{Ru}^{-1} \cdot min^{-1}\ mol^{-1}$]	E_S [$J \cdot mol^{-1}$]
L-arabinose	7109908.9	56127.8
D-galactose	114033178.1	68127.6

The parameters obtained from the lineal regression analysis were used as initial values for the simultaneous optimization of the experimental data at different temperatures. The coefficient of correlation for the model was computed from equation 4.18, varying from 0-100%, considering that a good degree of explanation is achieved for values of R^2 in the range of 95-99%.

$$R^2=\left(1-\frac{\sum_{i=1}^{n}\left(C_{Exp,i}-C_{Calc.i}\right)^2}{\sum_{i=1}^{n}\left(C_{Exp,i}-C_{mean}\right)^2}\right)\cdot 100 \qquad (4.18)$$

The model-fitting results are displayed in Figure 4.3 and Figure 4.4, demonstrating how the proposed model very successfully described the experimental concentration profiles during the hydrogenation reaction on the prepared Ru/C foam catalyst at different temperatures.

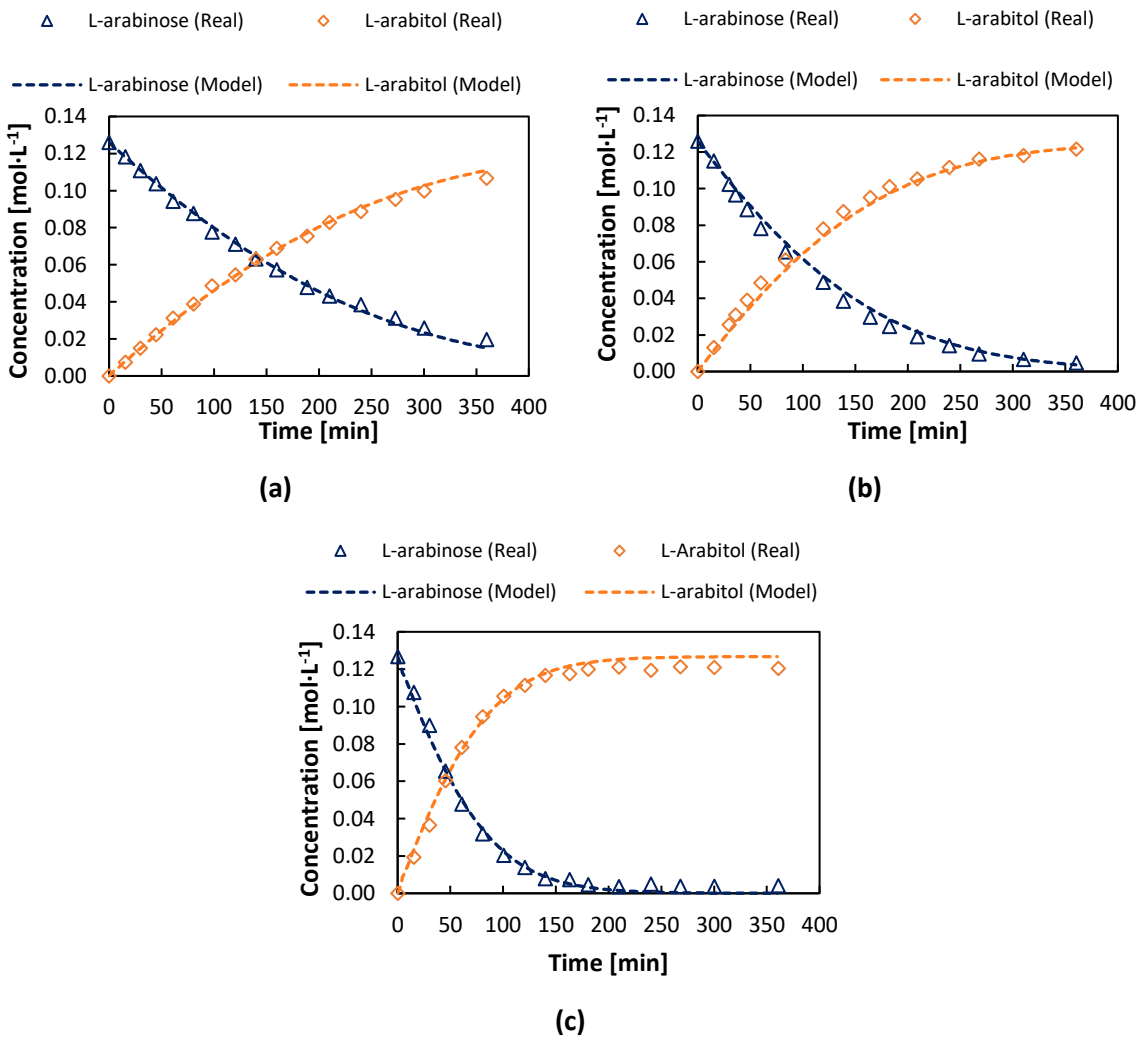

Figure 4.3. Modeling results for L-arabinose hydrogenation at 20 bar and different temperatures: (a) 90˚C, (b) 100˚C and (c) 120˚C.

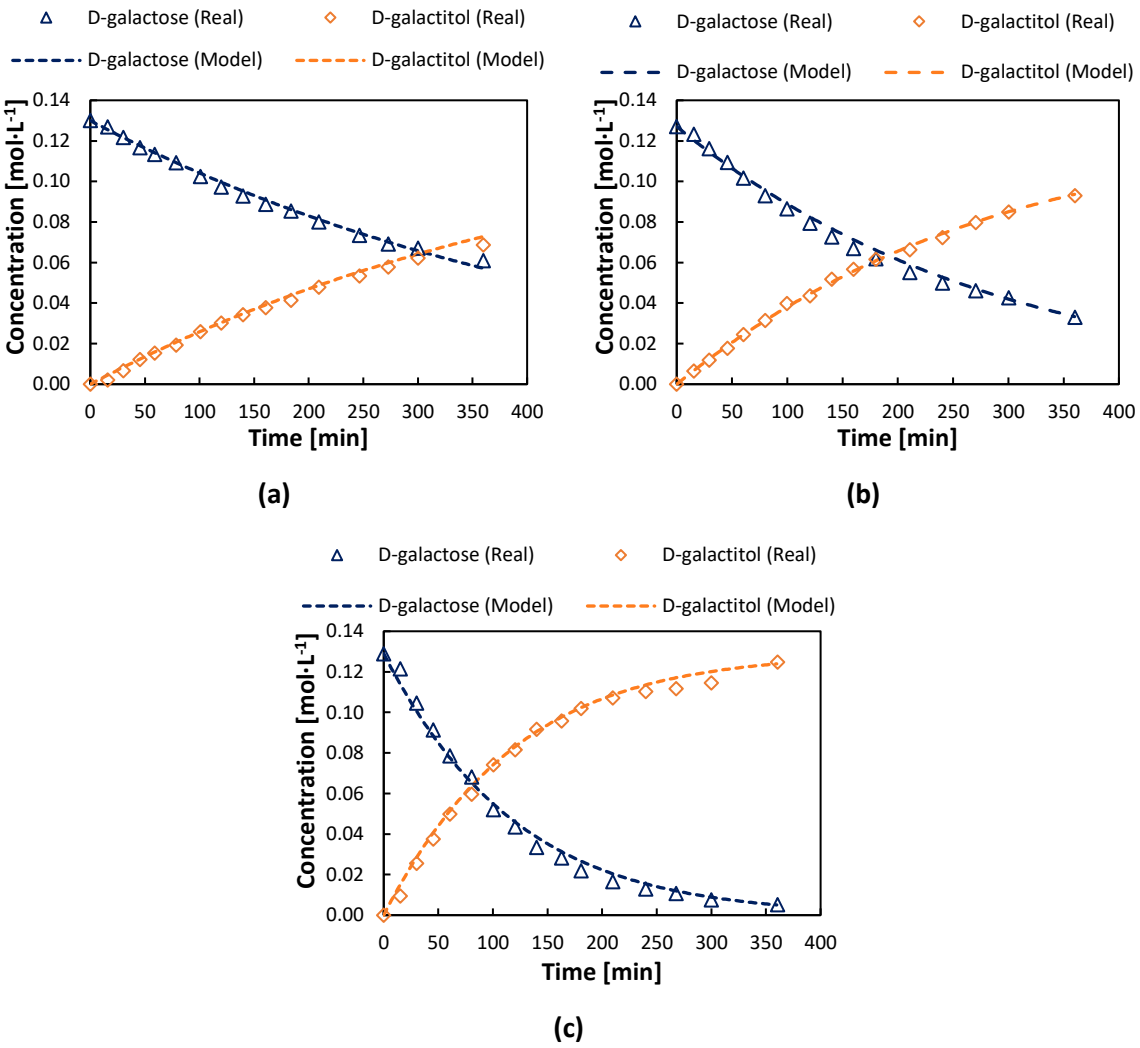

Figure 4.4. Modeling results for D-galactose hydrogenation at 20 bar and different temperatures: (a) 90˚C, (b) 100˚C and (c) 120˚C.

The parameters for the L-arabinose and D-galactose hydrogenation yielded by regression using the proposed model are listed in Table 4.2. High values of R^2 and small values of the objective function were obtained in both cases, which indicates the good performance of the model.

The apparent activation energies obtained in this work are in the order of magnitude of values reported in previous research [35, 36]. The adsorption parameter was higher for L-arabinose than for D-galactose, which was expected due to the smaller molecular size of L-arabinose compared to D-galactose.

Table 4.2. Kinetic parameters estimated for L-arabinose and D-galactose in individual hydrogenation experiments.

Sugar	A_s' [L·gRu^{-1}·min^{-1} mol^{-1}]	E_s [J·mol^{-1}]	K_s [L mol^{-1}]	R^2 [%]	SRS[1] [mol^2·L^{-2}]
L-arabinose	181393.97	44220.30	8.78	99.84	0.0008
D-galactose	663007.51	51738.46	1.56	99.89	0.0006

[1]Sum of the residual squares.

4.1.3. Sensitivity Analysis

The sensitivities of the estimated parameters were evaluated by plotting the parameter values against the corresponding objective function equation 4.17 while keeping the other values constant and equal to best-fitted from the model. The sensitivity plots of the objective function for the parameters A_S', E_S, and K_S are shown in Figure 4.5. The presence of sharp valleys in these graphs confirms that the parameters are well-defined, and all of them have an important contribution to the overall model.

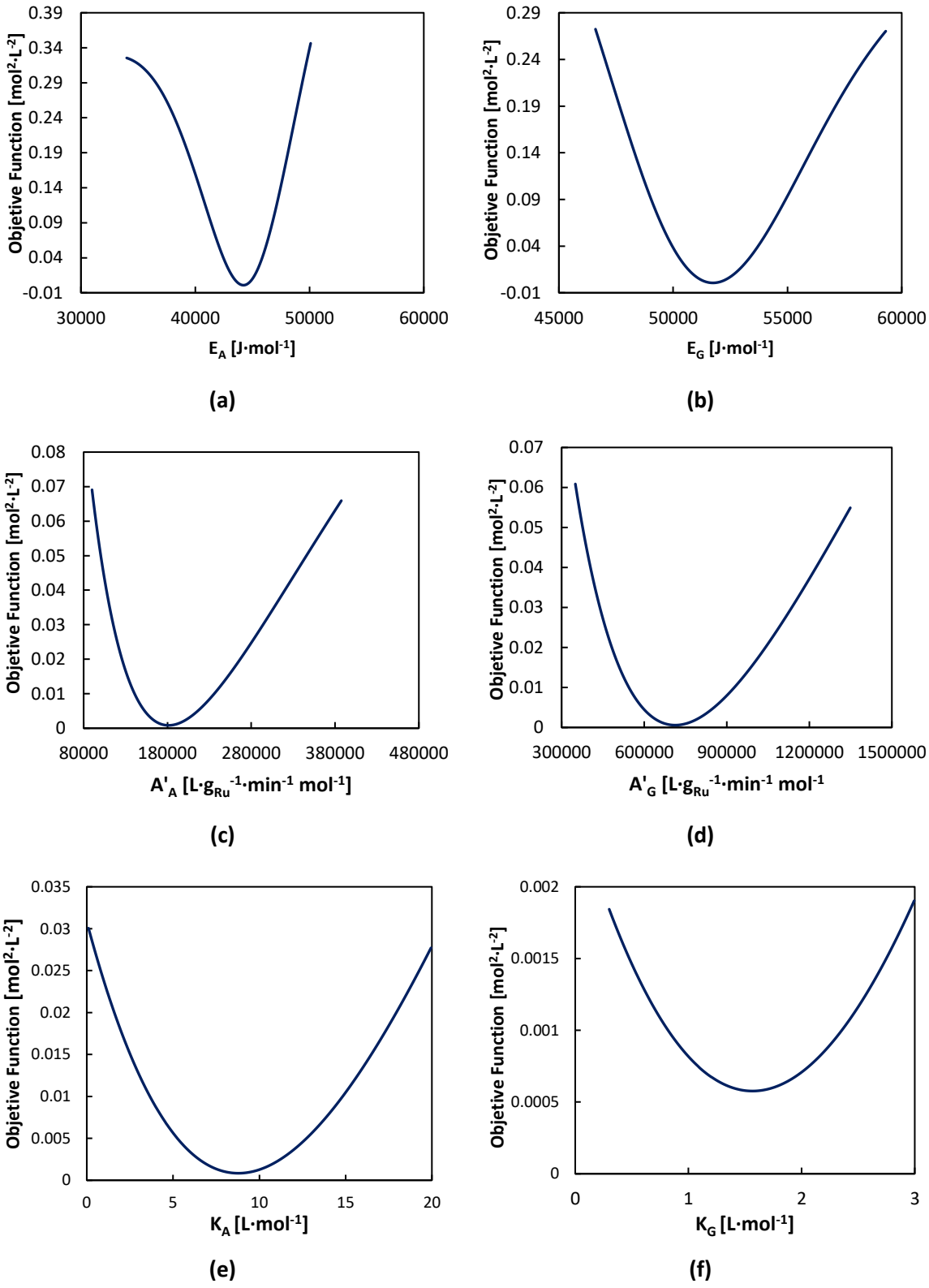

Figure 4.5. Sensitivity analysis of fitted parameters: (a) E_A, (b) E_G, (c) A_A', (d) A_G', (e)K_A, (f) K_G.

4.2. Modeling of Sugar Mixtures

4.2.1. Model Hypotheses

The hypotheses formulated in Section 4.1.1 regarding the reactor operation conditions are also valid to model the experimental data obtained from the sugar mixtures experiments: isothermal batch reactor, constant concentration of hydrogen during the reaction time, no mass transfer limitations, a constant volume of the reaction medium, and fixed catalyst mass are the main hypotheses for the quantitative modelling.

No by-products yields were considered, given the high selectivity observed in the experimental data (see Section 3.3.2.). Thus, the reactions were assumed to proceed towards the exclusive formation of sugar alcohols.

As in the case of individual sugar experiments, a non-competitive sugar-hydrogen adsorption mechanism was assumed, so the sugar molecules and hydrogen were adsorbed in different active sites. Moreover, the catalyst surface was supposed as ideal, so the Langmuir isotherm is sufficient to describe the adsorption processes. Hydrogen was presumed to be adsorbed in the dissociated form, and the adsorption of the products was discarded.

Additionally, it was assumed that the adsorption of L-arabinose was stronger than D-galactose, so the adsorption of the latter was neglected.

4.2.2. Derivation of Rate Expressions for the Kinetic Model

The liquid-phase mass balances for the batch reactor introducing the above-presented assumptions are given by equation 4.19-22, where A=L-arabinose, G=D-galactose, A_{OH}=L-arabitol, G_{OH}=D-galactitol, and the bulk density is defined as $\rho_B = \frac{m_{Cat}}{V_L}$.

$$\frac{dC_A}{dt} = -r_A \cdot \rho_B \quad (4.19)$$

$$\frac{dC_{A_{OH}}}{dt} = r_A \cdot \rho_B \quad (4.20)$$

$$\frac{dC_G}{dt} = -r_G \cdot \rho_B \quad (4.21)$$

$$\frac{dC_{G_{OH}}}{dt} = r_G \cdot \rho_B \quad (4.22)$$

The reaction mechanism based on the hypotheses presented in the previous section is shown in Figure 4.6, where * denotes an active site devoted to sugar adsorption (L-arabinose or D-galactose), whilst *' is a site for hydrogen adsorption.

$$A+* \overset{K_A}{\leftrightarrow} A*$$

$$G+* \overset{K_G}{\leftrightarrow} G*$$

$$H_2 + 2*' \overset{K_H}{\leftrightarrow} 2H*'$$

$$A* + 2H*' \overset{k_A}{\rightarrow} A_{OH} + * + *'$$

$$G* + 2H*' \overset{k_G}{\rightarrow} G_{OH} + * + *'$$

Figure 4.6 Reaction mechanism for the sugar mixtures hydrogenation.

Consequently, the adsorption quasi-equilibria for L-arabinose, D-galactose and hydrogen are defined by equations 4.23-25.

$$C_{*A} = K_A \cdot C_A \cdot C_* \quad (4.23)$$

$$C_{*G} = K_G \cdot C_G \cdot C_* \quad (4.24)$$

$$C_{*'H} = \sqrt{K_H \cdot C_H} \cdot C_{*'} \quad (4.25)$$

The site balances for sugar and hydrogen adsorption can be written as

$$C_{*A} + C_{*G} + C_* = C_0 \quad (4.26)$$

$$C_{*'H} + C_{*'} = C'_0 \quad (4.27)$$

Where C_0 and C'_0 denote the total concentration of the adsorption sites available for sugar and hydrogen, respectively. Substituting the quasi-equilibria expressions (equations 4.23-4.25) in the site balances (equations 4.26 and 4.27), the concentrations of vacant sites are

$$C_* = \frac{C_0}{1 + K_A \cdot C_A + K_G \cdot C_G} \quad (4.28)$$

$$C_{*'} = \frac{C'_0}{1 + \sqrt{K_H \cdot C_H}} \quad (4.29)$$

Considering that the surface reactions between the adsorbed sugar molecules and hydrogen are the rate-determining steps, the rate equations for L-arabinose, r_A and D-galactose, r_G becomes

$$r_A = k_A \cdot C_{*A} \cdot C_{*'H}^2 \quad (4.30)$$

$$r_G = k_G \cdot C_{*G} \cdot C_{*'H}^2 \quad (4.31)$$

The expressions for C_* and $C_{*'}$ are then inserted in the rate equations, which yields

$$r_A = \frac{k_A \cdot K_A \cdot K_H \cdot C_0 \cdot {C'_0}^2 \cdot C_A \cdot C_H}{(1 + K_A \cdot C_A + K_G \cdot C_G) \cdot \left(1 + \sqrt{K_H \cdot C_H}\right)^2} \quad (4.32)$$

$$r_G = \frac{k_A \cdot K_A \cdot K_H \cdot C_0 \cdot {C'_0}^2 \cdot C_G \cdot C_H}{(1 + K_A \cdot C_A + K_G \cdot C_G) \cdot \left(1 + \sqrt{K_H \cdot C_H}\right)^2} \quad (4.33)$$

The merged parameters are defined as

$$\kappa_A = k_A \cdot K_A \cdot K_H \cdot C_0 \cdot {C'_0}^2 \quad (4.34)$$

$$\kappa_G = k_G \cdot K_G \cdot K_H \cdot C_0 \cdot {C'_0}^2 \quad (4.35)$$

The reaction rate equations obtain the following forms

$$r_A = \frac{\kappa_A \cdot C_A \cdot C_H}{(1 + K_A \cdot C_A + K_G \cdot C_G) \cdot \left(1 + \sqrt{K_H \cdot C_H}\right)^2} \quad (4.36)$$

$$r_G = \frac{\kappa_G \cdot C_G \cdot C_H}{(1 + K_A \cdot C_A + K_G \cdot C_G) \cdot \left(1 + \sqrt{K_H \cdot C_H}\right)^2} \quad (4.37)$$

Furthermore, since the hydrogen pressure was kept constant during all the experiments, the term $\frac{C_H}{\left(1+\sqrt{K_H \cdot C_H}\right)^2}$ is constant, so equations 4.34 and 4.35 can be simplified to

$$r_A = \frac{\kappa'_A \cdot C_A}{(1 + K_A \cdot C_A + K_G \cdot C_G)} \quad (4.38)$$

$$r_G = \frac{\kappa'_G \cdot C_G}{(1 + K_A \cdot C_A + K_G \cdot C_G)} \quad (4.39)$$

Finally, including the hypothesis about the stronger adsorption of L-arabinose ($K_A >> K_G$)

$$r_A = \frac{\kappa'_A \cdot C_A}{(1 + K_A \cdot C_A)} \quad (4.40)$$

$$r_G = \frac{\kappa'_G \cdot C_G}{(1 + K_A \cdot C_A)} \tag{4.41}$$

4.2.3. Parameter Estimation

The parameters included in equations 4.38 and 4.39 were obtained by regression analysis, minimizing the sum of the residual squares (equation 4.17) using the Nelder-Mead optimization method, while the ordinary differential equations (ODEs) were solved through the LSODA solver in Python.

The coefficient of regression was computed as defined by equation 4.18. The estimated parameters are listed in Table 4.3. As can be observed from the table, a higher value was obtained for the objective function compared with the estimations conducted with individual sugars.

Table 4.3. Kinetic parameters estimated for L-arabinose and D-galactose in mixtures experiments.

Parameter	Value	R^2 [%]	SSE [$mol^2 \cdot L^{-2}$]
κ'_A	0.119		
κ'_G	0.090	99.45	0.0012
K_A	12.75		

Figure 4.7-9 display the concentration profiles of the reagents and products obtained from the model compared with the experimental data for the hydrogenation of mixtures of L-arabinose and D-galactose at 120˚C and 20 bar and different D-galactose to L-arabinose molar ratios. The results revealed that the model correctly follows the tendency of the experimental data. Nevertheless, some deviations are noticeable especially in case of L-arabinose and L-arabitol, which can be ascribed to systematic errors when determining the concentrations due to the overlapping of peaks in the chromatograms (see Appendix IV).

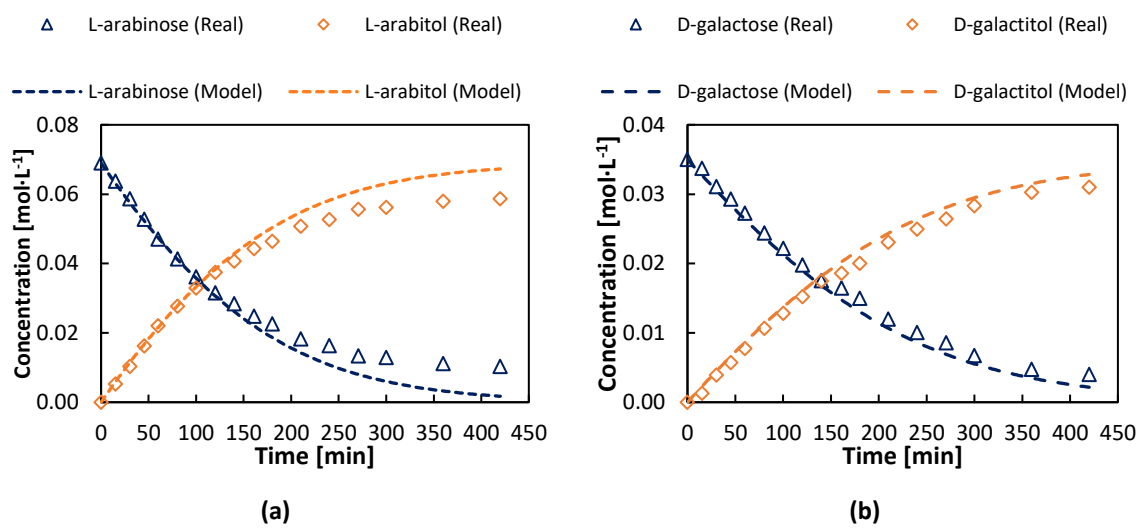

Figure 4.7. Modeling sugar mixtures hydrogenation results at 120˚C and 20 bar. Ratio=0.5: (a) L-arabinose, and (b) D-galactose.

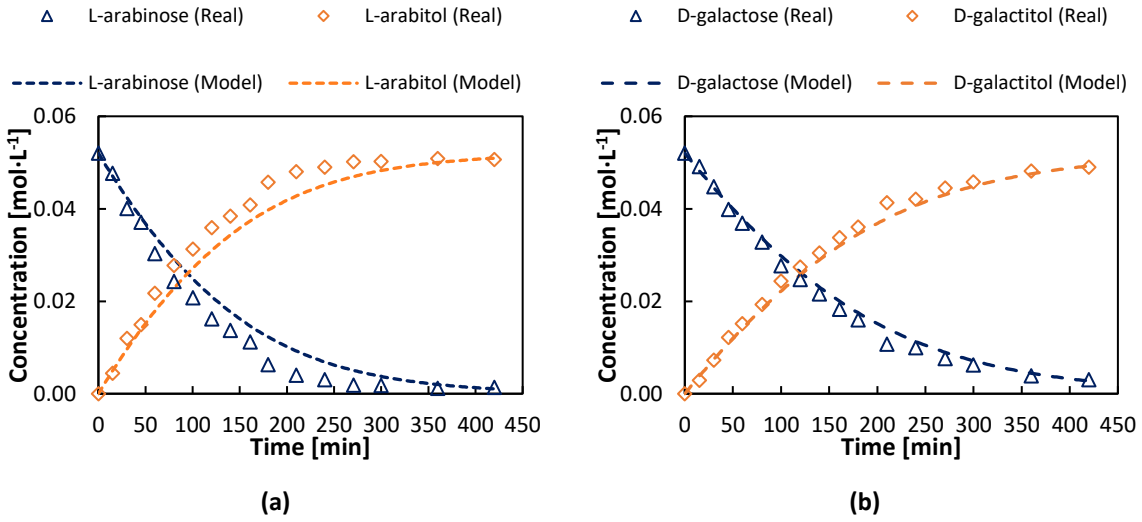

Figure 4.8. Modeling sugar mixtures hydrogenation results at 120˚C and 20 bar. Ratio=1: (a) L-arabinose, and (b) D-galactose.

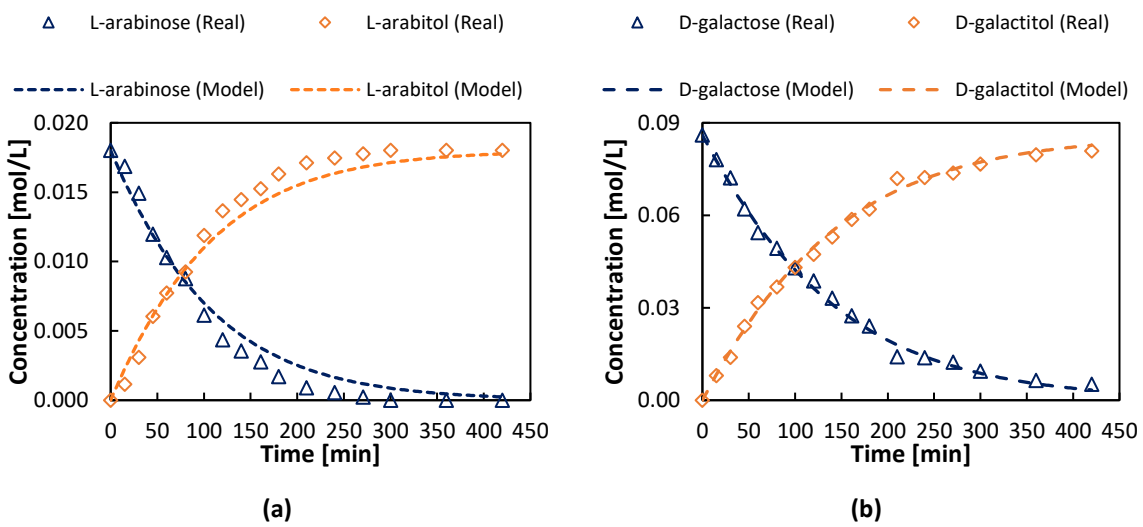

Figure 4.9. Modeling sugar mixtures hydrogenation results at 120˚C and 20 bar. Ratio=5: (a) L-arabinose, and (b) D-galactose.

The sensitivity plots of the objective function for the parameters κ'_A, κ'_G, and K_A are shown in Figure 4.10. The presence of sharp valleys in these graphs suggests that the parameters are well-defined, and all of them have an important contribution to the overall model.

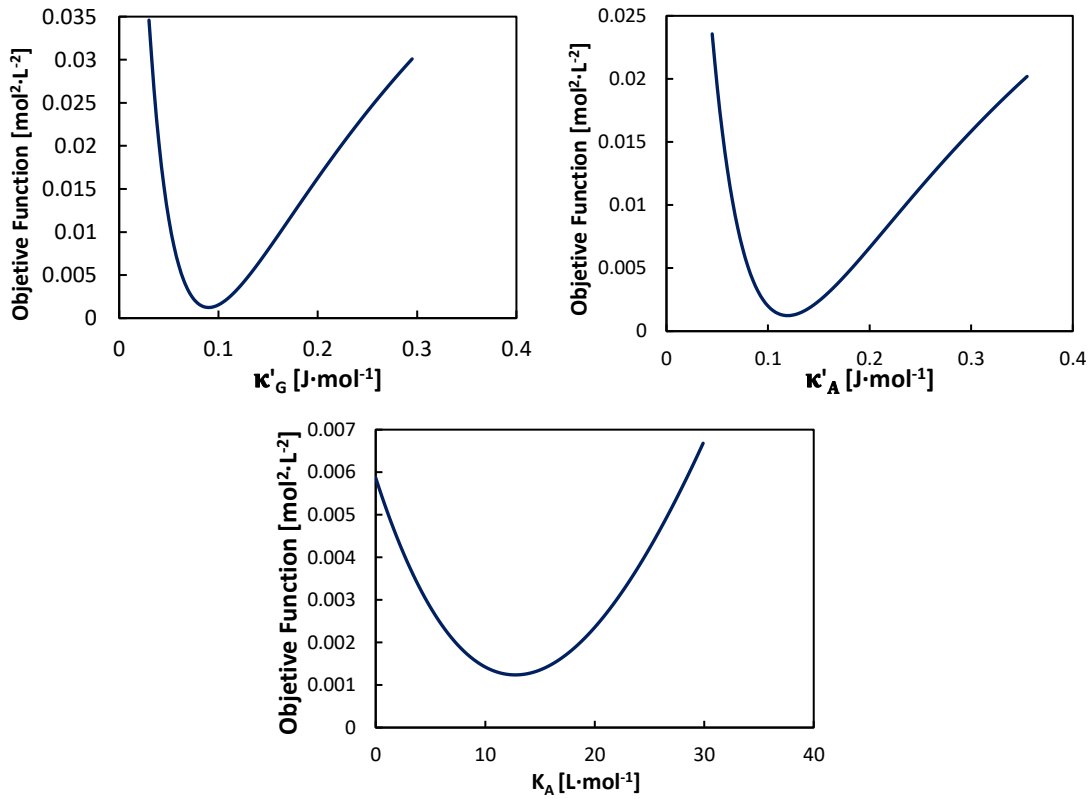

Figure 4.10. Sensitivity analysis of fitted parameters: (a) κ_A, (b) κ_G, (c) K_A.

4.2.4. Double Logarithmic Plots

Double logarithm plots have been used in the literature to confirm the correspondence of simultaneous reactions with a common mechanism [78, 80–82]. The idea is that the ratio of the reaction rates of the competing components is proportional to the ratio of their concentrations. Thus, if the mixture behavior obeys the supposed reaction mechanism, a double logarithm plot of the concentrations would result in a straight line [78].

In case of L-arabinose and D-galactose competing for hydrogen on the surface of the catalyst, dividing equations 4.38 and 4.39 yields

$$\frac{r_A}{r_G} = \frac{dC_A}{dC_G} = \frac{\kappa'_A \cdot C_A}{\kappa'_G \cdot C_G} \tag{4.42}$$

The relative reactivity of the components is denoted by the parameter α.

$$\alpha = \frac{\kappa_A}{\kappa_G} \tag{4.43}$$

Integrating equation 4.42, from the initial concentrations C_{A_0} and C_{G_0},

$$\int_{C_{A_0}}^{C_A} \frac{dC_A}{C_A} = \alpha \cdot \int_{C_{G_0}}^{C_G} \frac{dC_G}{C_G} \tag{4.44}$$

Solving the integrals and inserting the integration limits gives the logarithmic relationship,

$$-\ln\left(\frac{C_A}{C_{A_0}}\right) = -\alpha \cdot \ln\left(\frac{C_G}{C_{G_0}}\right) \tag{4.45}$$

Furthermore, $-\ln\left(\frac{C_A}{C_{A_0}}\right)$ was plotted against $\ln\left(\frac{C_G}{C_{G_0}}\right)$ for the data obtained from the mixture experiments. In case of ideal mixtures, the expression 4.45 predicts a linear relation, from which the relative reactivity α can be evaluated. The double logarithmic plots are shown in Figure 4.11, and the results suggest that both sugars follow the same kind of kinetics.

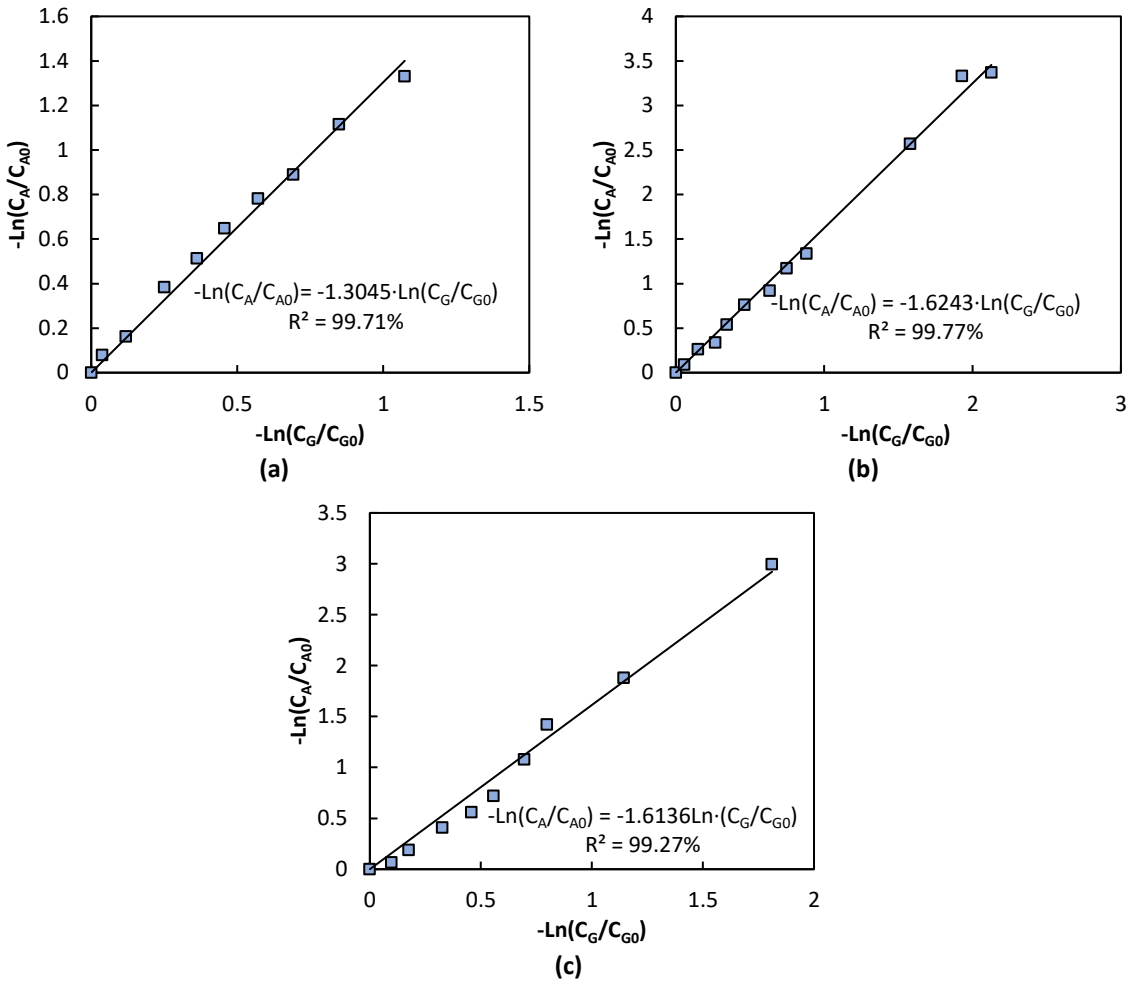

Figure 4.11. Double logarithmic plots of sugar mixtures at 120˚C and 20 bar: (a) D-galactose: L-arabinose=0.5, (b) D-galactose: L-arabinose=1, (a) D-galactose: L-arabinose=5.

As shown by in Table 4.4, the reactivity of L-arabinose is higher than that of D-galactose for all the ratios of the sugars. However, the relative reactivity varied with the initial molar ratio, indicating that the adsorption behavior of the system is not entirely ideal. Sifontes et al. [37] obtained similar results for binary sugar mixtures hydrogenation experiments in the presence of a Ru/C powder catalyst.

Table 4.4. Relative reactivities at different initial mole ratios of D-galactose to L-arabinose.

Molar Ratio (D-galactose to L-arabinose)	**Relative Reactivity (α)**
0.5	1.30
1	1.62
5	1.61

5. CONCLUSIONS AND FUTURE PERSPECTIVES

The aim of this work was to develop a novel open-cell solid foam catalyst to study the reaction kinetics of the selective hydrogenation of L-arabinose and D-galactose and their binary mixtures. The first part of the thesis was devoted to optimizing the catalyst preparation method through the implementation of different surface treatments, carbon coating conditions, and active metal incorporation techniques. The second part of this work was dedicated to obtain kinetic data for the individual sugars and mixtures of L-arabinose and D-galactose using the prepared foam catalyst in a batch reactor under typical hydrogenation conditions, temperatures within the range of 90-120˚C and 20-40 bar of hydrogen pressure to reveal the influence of temperature and pressure, and the interactions of the sugars during the experiments. Finally, the kinetic modeling and a series of confirmation calculations were performed with the experimental data to investigate the adequacy to plausible reaction mechanisms proposed to describe the hydrogenation of organic compounds.

A carbon coating method based on the polymerization of furfuryl alcohol (FA) was successfully applied to prepare the carbon-coated aluminum foams. The crosslinking of polyfurfuryl alcohol was identified as a relevant parameter to obtain a carbon layer with desired properties for a catalyst support, while the temperature control and water evaporation during the polymerization of FA were extremely important to generate a cross-linked foamy polymer as the base for an active carbon support. Additionally, surface roughness was induced on some aluminum foams prior to the carbon coating through anodic oxidation, which improved the cohesion and homogeneity of the carbon layer as revealed by SEM and EDX analysis.

Two ruthenium incorporation techniques were applied on the prepared carbon-coated foams: homogeneous deposition precipitation (HDP) and incipient wetness impregnation (IWI) using Ru (III) nitrosyl nitrate as the precursor solution in both cases. In the HPD method, the need for adequate urea-to-Ru molar ratio was evidenced to obtain an optimal pH evolution and a high carbon load for the deposition of the active Ru metal. Under the conditions studied in this work, a molar ratio of urea-to-Ru of 40 and a carbon loading exceeding 40% were required to obtain an active catalyst for the hydrogenation reactions. On the other hand, for the incipient wetness impregnation technique, the most important parameters were the carbon load and the concentration of the precursor solution.

The implementation of the two Ru incorporation methods resulted in distributions of small size Ru particles, with an average nanoparticle size of around 3 nm in both cases. However, the incipient wetness impregnation method allowed a superior load of ruthenium on the catalyst surface (~ 1.1%), hence a higher activity. Therefore, the catalysts prepared by IWI were used in the rotating foam batch reactor for the systematical kinetic studies.

The correct establishment of the *ex-situ* reduction conditions is essential to obtain a stable catalyst; this was evidenced for the catalysts prepared by IWI that presented induction periods and an increase in the activity in each consecutive experiment caused by an insufficient reduction time. Thus, TPR measurements were conducted, and the hydrogen exposure time was prolonged, establishing the new *ex-situ* reduction conditions at 300˚C and 5 h.

The hydrogenation of L-arabinose and D-galactose on the Ru/C foam catalyst yielded high selectivity towards sugar alcohols (≥98%) and conversions in the range of 60-98%, depending on the temperature. The influence of temperature on the reaction rate was strong, while the hydrogen pressure effect was rather minor, especially in case of D-galactose. Regarding the sugar mixtures, L-arabinose exhibited a higher rate, and an acceleration in the hydrogenation of both sugars was observed as the ratio of D-galactose to L-arabinose was increased, as a result of the competitive interactions of the sugars.

A kinetic model based on a non-competitive adsorption behavior between the sugar molecules and hydrogen was fitted to the experimental data. A very successful description of the concentration profiles and the effect of the temperature was achieved for the individual sugar data. As for the mixtures, a good fit with small deviations was observed, attributed to the difficulty of separating the compounds in the concentration analysis by HPLC. The sensitivity analysis of the estimated parameters revealed that all the parameters were well-defined, and they had a significant contribution to the model performance.

The experimental data of the hydrogenation of mixtures at 120˚C and 20 bar and different molar ratios of D-galactose to L-arabinose were evaluated through double logarithmic plots, which showed that both sugars follow a common reaction mechanism since the logarithmic plots resulted in

straight lines. Nevertheless, the relative reactivity varied with the initial molar ratio of the sugars, suggesting that the adsorption behavior of the system is not entirely ideal.

After about 100 h of use, some catalyst deactivation was observed. TEM micrographs of the spent catalyst showed that substantial agglomeration of particles took place, resulting in the increase of the average size from 3.6 nm to 5.2 nm, suggesting that this phenomenon is the main cause of deactivation. More research is needed to establish certainly the reasons for the deactivation of this kind of catalyst, which also would allow developing efficient regeneration methods. In general, the prepared catalyst exhibited a good selectivity, activity, and stability similar [74] and even superior to some other Ru/C catalysts described in the literature [72].

Many research opportunities can be derived from the results of this work, such as the improvement of the porosity of the carbon coating using a pore former such as poly (ethylene glycol), the scaling up of the carbon coating and anodic oxidation procedures, the optimization of the number of impregnation steps for the ruthenium incorporation method and evaluating the possibility of applying the HPD technique in consecutive steps in order to obtain a good particle dispersion characteristic of this method combined with an adequate Ru load.

From the viewpoint of industrial scaling up, the next step could be the use of the prepared foam catalyst in a continuous mode in a reactor configuration that allows taking advantage of the high mass and heat transfer rates, and low resistance to the diffusion associated with this kind of catalyst. In this sense, the use of a loop reactor could be a promising option. Furthermore, the reduction of other compounds containing carbonyl groups can be screened, whether they are individual sugars of high commercial importance such as xylose to produce xylitol, compounts from the hydrolysis of lignocellulosic materials such as sugar mixtures or levulinic acid to produce γ-valerolactone, which is also a potential chemical platform.

6. REFERENCES

1. Masson-Delmotte, V., P. Zhai, H.-O. Pörtner, D. Roberts, J. Skea, P.R. Shukla, A. Pirani, W. Moufouma-Okia, C. Péan, R. Pidcock, S. Connors, J.B.R. Matthews, Y. Chen, X. Zhou, M.I. Gomis, E. Lonnoy, T. Maycock, M. Tignor, & T. W. (eds.)]. (2019). *IPCC, 2018: Global Warming of 1.5°C. An IPCC special report on the impacts of global warming of 1.5 °C above pre-industrial levels and related global greenhouse gas emission pathways, in the context of strengthening the global response to the threat of climate change, sustainable development, and efforts to eradicate poverty*. *Intergovernmental Panel on Climate Change.* https://doi.org/10.1038/291285a0

2. Fritsche, U., Brunori, G., Chiaramonti, D., Galanakis, C.M., Hellweg, S, Matthews, R. & Panoutsou, C. (2020). *Future transitions for the Bioeconomy towards Sustainable Development and a Climate-Neutral Economy*. Luxembourg: © European Union. https://doi.org/10.2760/667966

3. United Nations. (2021). The Paris Agreement. Retrieved from https://www.un.org/en/climatechange/paris-agreement

4. Ruppert, A. M., Weinberg, K., & Palkovits, R. (2012). Hydrogenolysis goes bio: from carbohydrates and sugar alcohols to platform chemicals. *Angewandte Chemie International Edition*, *51*(11), 2564-2601. https://doi.org/10.1002/anie.201105125

5. Murzin, D. Y., Duque, A., Arve, K., Sifontes, V., Aho, A., Eränen, K., & Salmi, T. (2015). Catalytic hydrogenation of sugars. In *Biomass Sugars for Non-Fuel Applications* (pp. 89-133). Royal Society of Chemistry. https://doi.org/10.1039/9781782622079-00089

6. Ubando, A. T., Felix, C. B., & Chen, W. H. (2020). Biorefineries in circular bioeconomy: A comprehensive review. *Bioresource technology*, *299*, 122585. https://doi.org/10.1016/j.biortech.2019.122585

7. Ubando, A. T., Del Rosario, A. J. R., Chen, W. H., & Culaba, A. B. (2020). A state-of-the-art review of biowaste biorefinery. Environmental Pollution, 116149. https://doi.org/10.1016/j.envpol.2020.116149

8. AliAkbari, R., Ghasemi, M. H., Neekzad, N., Kowsari, E., Ramakrishna, S., Mehrali, M., & Marfavi, Y. (2021). High value add bio-based low-carbon materials: Conversion processes and circular economy. Journal of *Cleaner Production*, *293*, 126101. https://doi.org/10.1016/j.jclepro.2021.126101

9. Pinales-Márquez, C. D., Rodríguez-Jasso, R. M., Araújo, R. G., Loredo-Treviño, A., Nabarlatz, D., Gullón, B., & Ruiz, H. A. (2021). Circular bioeconomy and integrated biorefinery in the production of xylooligosaccharides from lignocellulosic biomass: A review. *Industrial Crops and Products*, *162*, 113274. https://doi.org/10.1016/j.indcrop.2021.113274

10. Werpy, T., & Petersen, G. (2004). *Top value added chemicals from biomass: volume I--results of screening for potential candidates from sugars and synthesis gas* (No. DOE/GO-102004-1992). National Renewable Energy Lab., Golden, CO (US). https://doi.org/10.2172/15008859

11. Zada, B., Chen, M., Chen, C., Yan, L., Xu, Q., Li, W., & Fu, Y. (2017). Recent advances in catalytic production of sugar alcohols and their applications. *Science China Chemistry*, *60*(7), 853-869. https://doi.org/10.1007/s11426-017-9067-1

12. McKendry, P. (2002). Energy production from biomass (part 1): overview of biomass. *Bioresource technology*, *83*(1), 37-46. https://doi.org/10.1016/S0960-8524(01)00118-3

13. Ruppert, A. M., Weinberg, K., & Palkovits, R. (2012). Hydrogenolysis goes bio: from carbohydrates and sugar alcohols to platform chemicals. *Angewandte Chemie International Edition*, *51*(11), 2564-2601.https://doi.org/10.1002/anie.201105125

14. Murzin, D. Y., Daigue, E., Slotte, R., Sladkovskiy, D. A., & Salmi, T. (2020). Techno-economic analysis for production of L-arabitol from L-arabinose. *Chemical Engineering & Technology*, *43*(7), 1260-1267. https://doi.org/10.1002/ceat.202000125

15. Fortune Bussiness Insights. (2020). Sugar Alchol Market Size, Share & COVID-19 Impact Analysis, By Type (Sorbito, Xyliyol, Maltitol, Erythritil and Isomalt), Application (Food and Beberages, Pharmaceuticals, and Cosmetics and Personal Care), and Reginal Forecast 2020-2027.

16. Ji, X. J., Huang, H., Nie, Z. K., Qu, L., Xu, Q., & Tsao, G. T. (2012). Fuels and chemicals from hemicellulose sugars. *Advances in Biochemical Engineering/Biotechnology*, *128*. https://doi.org/10.1007/10_2011_124

17. Mokhena, T. C., Mochane, M. J., Motaung, T. E., Linganiso, L. Z., Thekisoe, O. M., & Songca, S. P. (2018). Sugarcane Bagasse and Cellulose Polymer Composites. In *Sugarcane - Technology and Research*. https://doi.org/10.5772/intechopen.71497

18. Grembecka, M. (2015). Sugar alcohols—their role in the modern world of sweeteners: a review. *European Food Research and Technology*, *241*(1), 1-14. https://doi.org/10.1007/s00217-015-2437-7

19. Liao, Y., Liu, Q., Wang, T., Long, J., Zhang, Q., Ma, L., & Li, Y. (2014). Promoting hydrolytic hydrogenation of cellulose to sugar alcohols by mixed ball milling of cellulose and solid acid catalyst. *Energy & fuels*, *28*(9), 5778-5784. https://doi.org/10.1021/ef500717p

20. Liu, Q., Tan, J., Cai, C., Ma, L., & Wang, T. (2016). Enhanced Sugar Alcohol Production from Cellulose by Pretreatment with Mixed Ball-Milling and Solid Acids. *BioResources*, *11*(1). https://doi.org/10.15376/biores.11.1.1843-1854

21. Kobayashi, H., Ito, Y., Komanoya, T., Hosaka, Y., Dhepe, P. L., Kasai, K., Fukuoka, A. (2011). Synthesis of sugar alcohols by hydrolytic hydrogenation of cellulose over supported metal catalysts. *Green Chemistry*, *13*(2). https://doi.org/10.1039/c0gc00666a

22. Maki-Arvela, P., Salmi, T., Holmbom, B., Willfor, S., & Murzin, D. Y. (2011). Synthesis of sugars by hydrolysis of hemicelluloses-a review. *Chemical reviews*, *111*(9), 5638-5666. https://doi.org/10.1021/cr2000042

23. Ramos-Andrés, M., Aguilera-Torre, B., & García-Serna, J. (2021). Hydrothermal production of high-molecular weight hemicellulose-pectin, free sugars and residual cellulose pulp from discarded carrots. *Journal of Cleaner Production*, *290*, 125179. https://doi.org/10.1016/j.jclepro.2020.125179

24. Murzin, D. Y., Kusema, B., Murzina, E. V., Aho, A., Tokarev, A., Boymirzaev, A. S., ... & Salmi, T. (2015). Hemicellulose arabinogalactan hydrolytic hydrogenation over Ru-modified H-USY zeolites. *Journal of Catalysis*, *330*, 93-105. https://doi.org/10.1016/j.jcat.2015.06.022

25. Willför, S., Sjöholm, R., Laine, C., & Holmbom, B. (2002). Structural features of water-soluble arabinogalactans from Norway spruce and Scots pine heartwood. *Wood Science and Technology*, *36*(2). https://doi.org/10.1007/s00226-001-0137-x

26. Van Gorp, K., Boerman, E., Cavenaghi, C. V., & Berben, P. H. (1999). Catalytic hydrogenation of fine chemicals: sorbitol production. *Catalysis today*, *52*(2-3), 349-361. https://doi.org/10.1016/S0920-5861(99)00087-5

27. Chen, C. C., Chen, J. H., & Chao, C. G. (2005). Post-treatment method of producing ordered array of anodic aluminum oxide using general purity commercial (99.7%) aluminum. *Japanese Journal of Applied Physics, Part 1: Regular Papers and Short Notes and Review Papers*, *44*(3), 1529–1533. https://doi.org/10.1143/JJAP.44.1529

28. Kuusisto, J., Mikkola, J. P., Sparv, M., Wärnå, J., Karhu, H., & Salmi, T. (2008). Kinetics of the catalytic hydrogenation of d-lactose on a carbon supported ruthenium catalyst. *Chemical Engineering Journal*, *139*(1), 69–77. https://doi.org/10.1016/j.cej.2007.07.084

29. Simakova, I. L., Demidova, Y. S., Murzina, E. V., Aho, A., & Murzin, D. Y. (2016). Structure Sensitivity in Catalytic Hydrogenation of Galactose and Arabinose over Ru/C Catalysts. *Catalysis Letters*, *146*(7), 1291–1299. https://doi.org/10.1007/s10562-016-1752-3

30. Thakur, D. B., Tiggelaar, R. M., Hoang, T. M. C., Gardeniers, J. G. E., Lefferts, L., & Seshan, K. (2011). Ruthenium catalyst on carbon nanofiber support layers for use in silicon-based structured microreactors, Part I: Preparation and characterization. *Applied Catalysis B: Environmental*, *102*(1–2), 232–242. https://doi.org/10.1016/j.apcatb.2010.12.003

31. Wenmakers, P. W. A. M. (2009). Hairy Foam: Carbon nanofibers on solid foam as catalyst support. *Synthesis, mass transfer and reactor*. PhD Thesis. Eindhoven University of Technology.

32. Lali, F., Gärtner, S., Haase, S., & Lange, R. (2015). Preparation Method for Ruthenium Catalysts Supported by Carbon-Coated Aluminum Foams. *Chemical Engineering and Technology*, *38*(8), 1353–1361. https://doi.org/10.1002/ceat.201400676

33. Schimpf, S., Bron, M., & Claus, P. (2004). Carbon-coated microstructured reactors for heterogeneously catalyzed gas phase reactions: influence of coating procedure on catalytic activity and selectivity. *Chemical Engineering Journal*, *101*(1-3), 11-16. https://doi.org/10.1016/j.cej.2003.11.009

34. Najarnezhadmashhadi, A., Eränen, K., Engblom, S., Aho, A., Murzin, D., & Salmi, T. (2020). Continuous Hydrogenation of Monomeric Sugars and Binary Sugar Mixtures on a Ruthenium Catalyst Supported by Carbon-Coated Open-Cell Aluminum Foam. *Industrial and Engineering Chemistry Research*, *59*(30), 13450–13459. https://doi.org/10.1021/acs.iecr.0c01565

35. Sifontes Herrera, V. A., Oladele, O., Kordás, K., Eränen, K., Mikkola, J. P., Murzin, D. Y., & Salmi, T. (2011). Sugar hydrogenation over a Ru/C catalyst. *Journal of Chemical Technology and Biotechnology*, *86*(5), 658–668. https://doi.org/10.1002/jctb.2565

36. Sifontes Herrera, V. A., Saleem, F., Kusema, B., Eränen, K., & Salmi, T. (2012). Hydrogenation of L-Arabinose and D-Galactose Mixtures Over a Heterogeneous Ru/C Catalyst. *Topics in Catalysis*, *55*(7–10), 550–555. https://doi.org/10.1007/s11244-012-9833-z

37. Crezee, E., Hoffer, B. W., Berger, R. J., Makkee, M., Kapteijn, F., & Moulijn, J. A. (2003). Three-phase hydrogenation of D-glucose over a carbon supported ruthenium catalyst - Mass transfer and kinetics. *Applied Catalysis A: General*, *251*(1), 1–17. https://doi.org/10.1016/S0926-860X(03)00587-8

38. Salmi, T., Murzin, D. Y., Mikkola, J. P., Wärnå, J., Mäki-Arvela, P., Toukoniitty, E., & Toppinen, S. (2004). Advanced kinetic concepts and experimental methods for catalytic three-phase processes. *Industrial & engineering chemistry research*, *43*(16), 4540-4550. https://doi.org/10.1021/ie0307481

39. Najarnezhadmashhadi, A., Wärnå, J., Eränen, K., Trajano, H. L., Murzin, D., & Salmi, T. (2021). Modelling of kinetics, mass transfer and flow pattern on open foam structures in tubular reactors: Hydrogenation of arabinose and galactose on ruthenium catalyst. *Chemical Engineering Science*, *233*, 116385–116395. https://doi.org/10.1016/j.ces.2020.116385

40. Mikkola, J.-P., Salmi, T., & Sjöholm, R. (1999). Modelling of kinetics and mass transfer in the hydrogenation of xylose over Raney nickel catalyst. *Journal of Chemical Technology & Biotechnology: International Research in Process*, *74*(7), 655–662. https://doi.org/10.1002/(SICI)1097-4660(199907)74:7%3C655::AID-JCTB96%3E3.0.CO;2-G

41. Ho, P. H., Ambrosetti, M., Groppi, G., Tronconi, E., Palkovits, R., Fornasari, G., Benito, P. (2019). Structured Catalysts-Based on Open-Cell Metallic Foams for Energy and Environmental Applications. In *Studies in Surface Science and Catalysis* (pp. 303–327). https://doi.org/10.1016/B978-0-444-64127-4.00015-X

42. Cybulski, A., & Moulijn, J. A. (2005). The present and the future of structured catalysts: An overview. In *Structured Catalysts and Reactors*. CRC Press. https://doi.org/10.1201/9781420028003

43. Montebelli, A., Visconti, C. G., Groppi, G., Tronconi, E., Cristiani, C., Ferreira, C., & Kohler, S. (2014). Methods for the catalytic activation of metallic structured substrates. *Catalysis Science & Technology*, *4*(9), 2846-2870. https://doi.org/10.1039/c4cy00179f

44. Tronconi, E., Groppi, G., & Visconti, C. G. (2014). Structured catalysts for non-adiabatic applications. *Current Opinion in Chemical Engineering*, *5*, 55-67. https://doi.org/10.1016/j.coche.2014.04.003

45. Pangarkar, K., Schildhauer, T. J., van Ommen, J. R., Nijenhuis, J., Kapteijn, F., & Moulijn, J. A. (2008). Structured packings for multiphase catalytic reactors. *Industrial & engineering chemistry research*, *47*(10), 3720-3751. https://doi.org/10.1021/ie800067r

46. Gancarczyk, A., Sindera, K., Iwaniszyn, M., Piątek, M., Macek, W., Jodłowski, P. J., & Kołodziej, A. (2019). Metal foams as novel catalyst support in environmental processes. *Catalysts*, *9*(7), 587. https://doi.org/10.3390/catal9070587

47. Ho, P. H., Ambrosetti, M., Groppi, G., Tronconi, E., Jaroszewicz, J., Ospitali, F., … Benito, P. (2018). One-step electrodeposition of Pd-CeO2 on high pore density foams for environmental catalytic processes. *Catalysis Science and Technology*, *8*(18). https://doi.org/10.1039/c8cy01388h

48. Wenmakers, P. W., van der Schaaf, J., Kuster, B. F., & Schouten, J. C. (2010). Comparative modeling study on the performance of solid foam as a structured catalyst support in multiphase reactors. *Industrial & Engineering Chemistry Research*, *49*(11), 5353-5366. https://doi.org/10.1021/ie900644e

49. Nijhuis, T. A., Beers, A. E., Vergunst, T., Hoek, I., Kapteijn, F., & Moulijn, J. A. (2001). Preparation of monolithic catalysts. *Catalysis Reviews*, *43*(4), 345-380. https://doi.org/10.1081/CR-120001807

50. Moreno-Castilla, C., Mahajan, O. P., Walker Jr, P. L., Jung, H. J., & Vannice, M. A. (1980). Carbon as a support for catalysts—III glassy carbon as a support for iron. *Carbon*, *18*(4), 271-276. https://doi.org/10.1016/0008-6223(80)90050-0

51. Vergunst, T., Kapteijn, F., & Moulijn, J. A. (2002). Preparation of carbon-coated monolithic supports. *Carbon*, *40*(11), 1891-1902. https://doi.org/10.1016/S0008-6223(02)00034-9

52. Iroegbu, A. O., & Hlangothi, S. P. (2019). Furfuryl alcohol a versatile, eco-sustainable compound in perspective. *Chemistry Africa*, *2*(2), 223-239. https://doi.org/10.1007/s42250-018-00036-9

53. Hucke, E. E. (1975). *U.S. Patent No. 3,859,421*. Washington, DC: U.S. Patent and Trademark Office.

54. Tondi, G., Cefarin, N., Sepperer, T., D'Amico, F., Berger, R. J. F., Musso, M., Vaccari, L. (2019). Understanding the polymerization of polyfurfuryl alcohol: Ring opening and diels-alder reactions. *Polymers*, *11*(12), 2126–2141. https://doi.org/10.3390/polym11122126

55. Munnik, P., de Jongh, P. E., & de Jong, K. P. (2015). Recent developments in the synthesis of supported catalysts. *Chemical reviews*, *115*(14), 6687-6718. https://doi.org/10.1021/cr500486u

56. Thakur, D. B., Tiggelaar, R. M., Weber, Y., Gardeniers, J. G. E., Lefferts, L., & Seshan, K. (2011). Ruthenium catalyst on carbon nanofiber support layers for use in silicon-based structured microreactors. Part II: Catalytic reduction of bromate contaminants in aqueous phase. *Applied Catalysis B: Environmental*, *101*(1–2), 243–250. https://doi.org/10.1016/j.apcatb.2010.12.004

57. Toebes, M. L., Van Der Lee, M. K., Tang, L. M., Huis In 't Veld, M. H., Bitter, J. H., Jos Van Dillen, A., & De Jong, K. P. (2004). Preparation of Carbon Nanofiber Supported Platinum and Ruthenium Catalysts: Comparison of Ion Adsorption and Homogeneous Deposition Precipitation. *The Journal of Physical Chemistry B*, *108*(31), 11611–11619. https://doi.org/10.1021/jp0313472

58. Manyar, H. G., Weber, D., Daly, H., Thompson, J. M., Rooney, D. W., Gladden, L. F., … Hardacre, C. (2009). Deactivation and regeneration of ruthenium on silica in the liquid-phase hydrogenation of butan-2-one. *Journal of Catalysis*, *265*(1), 80–88. https://doi.org/10.1016/j.jcat.2009.04.013

59. Rodríguez-Reinoso, F., & Sepúlveda-Escribano, A. (2001). Porous carbons in adsorption and catalysis. In *Handbook of surfaces and interfaces of materials* (pp. 309-355). Academic Press. https://doi.org/10.1016/b978-012513910-6/50066-9

60. Mason, R. B. (1956). Effect of Aluminum Sulfate in the Sulfuric Acid Electrolyte on Anodic Polarization. *Journal of The Electrochemical Society*, *103*(8), 425–429. https://doi.org/10.1149/1.2430373

61. Lali, F., Böttcher, G., Schöneich, P. M., Haase, S., Hempel, S., Lange, R. (2015). Preparation and characterization of Pd/Al2O3 catalysts on aluminum foam supports for multiphase hydrogenation reactions in rotating foam reactors. *Chemical Engineering Research and Design*, *94*, 365–374. https://doi.org/10.1016/j.cherd.2014.08.012

62. Sanz, O., Almeida, L. C., Zamaro, J. M., Ulla, M. A., Miró, E. E., Montes, M. (2008). Washcoating of Pt-ZSM5 onto aluminium foams. *Applied Catalysis B: Environmental*, *78*(1–2), 166–175. https://doi.org/10.1016/j.apcatb.2007.09.024

63. Burgos, N., Paulis, M., Montes, M. (2003). Preparation of Al2O3/Al monoliths by anodisation of aluminium as structured catalytic supports. *Journal of Materials Chemistry*, *13*(6). https://doi.org/10.1039/b212242a

64. Masuda, H., Hasegwa, F., Ono, S. (1997). Self-Ordering of Cell Arrangement of Anodic Porous Alumina Formed in Sulfuric Acid Solution. *Journal of The Electrochemical Society*, *144*(5), L127–L130. https://doi.org/10.1149/1.1837634

65. Kozhukhova, A. E., du Preez, S. P., Bessarabov, D. G. (2020). The effects of pore widening and calcination on anodized aluminum oxide prepared from Al6082. *Surface and Coatings Technology*, *383*, 125234–125246. https://doi.org/10.1016/j.surfcoat.2019.125234

66. Choura, M., Belgacem, N. M., Gandini, A. (1996). Acid-catalyzed polycondensation of furfuryl alcohol: Mechanisms of chromophore formation and cross-linking. *Macromolecules*, *29*(11), 3839-3850. https://doi.org/10.1021/ma951522f

67. Constant, K. P., Lee, J. R., Chiang, Y. M. (1996). Microstructure development in furfuryl resin-derived microporous glassy carbons. *Journal of Materials Research*, *11*(9), 2338–2345. https://doi.org/10.1557/JMR.1996.0297

68. Cepollaro, E. M., Caputo, D., Cimino, S., Gargiulo, N., Lisi, L. (2020). Synthesis and Characterization of Activated Carbon Foam from Polymerization of Furfuryl Alcohol Activated by Zinc and Copper Chlorides. *C — Journal of Carbon Research*, *6*(3), 45–60. https://doi.org/10.3390/c6030045

69. Koopman, P. O. J., Kieboom, A. P. G., Van Bekkum, H. (1981). Induction effects in liquid phase hydrogenation catalyzed by ruthenium on carbon. *Colloids and Surfaces*, *3*(1), 1–12. https://doi.org/10.1016/0166-6622(81)80030-3

70. Koopman, P. G. J., Buurmans, H. M. A., Kieboom, A. P. G., van Bekkum, H. (1981). Solvent-Reactant-Support interactions in liquid phase hydrogenation. *Recueil des Travaux Chimiques des Pays-Bas*, *100*(4), 129–136. https://doi.org/10.1002/recl.19811000407

71. Maximov, A. L., Zolotukhina, A. V., Mamedli, A. A., Kulikov, L. A., Karakhanov, E. A. (2018). Selective Levulinic Acid Hydrogenation in the Presence of Hybrid Dendrimer-Based Catalysts. Part I: Monometallic. *ChemCatChem*, *10*(1), 222–233. https://doi.org/10.1002/cctc.201700691

72. Wang, X., Lan, G., Liu, H., Zhu, Y., Li, Y. (2018). Effect of acidity and ruthenium species on catalytic performance of ruthenium catalysts for acetylene hydrochlorination. *Catalysis Science and Technology*, *8*(23), 6143–6149. https://doi.org/10.1039/c8cy01677a

73. Koopman, P. G. J., Kieboom, A. P. G., van Bekkum, H. (1981). Characterization of ruthenium catalysts as studied by temperature programmed reduction. *Journal of Catalysis*, *69*(1), 172–179. https://doi.org/10.1016/0021-9517(81)90139-1

74. Rio, S., Peru, G., Léger, B., Kerdi, F., Besson, M., Pinel, C., … Ponchel, A. (2020). Supported ruthenium nanoparticles on ordered mesoporous carbons using a cyclodextrin-assisted hard-template approach and their applications as hydrogenation catalysts. *Journal of Catalysis*, *383*, 343–356. https://doi.org/10.1016/j.jcat.2019.10.021

75. Tourvieille, J.-N. (2010). *Ultrasound effect on hydrogenation of sugars : catalyst deactivation and modelling*. Master's Thesis. Åbo Akademi and Université de Lyon.

76. Arena, B. J. (1992). Deactivation of ruthenium catalysts in continuous glucose hydrogenation. *Applied Catalysis A, General*, *87*(2), 219–229. https://doi.org/10.1016/0926-860X(92)80057-J

77. Aho, A., Roggan, S., Eränen, K., Salmi, T., Murzin, D. Y. (2015). Continuous hydrogenation of glucose with ruthenium on carbon nanotube catalysts. *Catalysis Science and Technology*, *5*(2), 953–959. https://doi.org/10.1039/c4cy01088d

78. Pyatnitsky, Y. I. (1994). Some new approaches to the competitive catalytic reaction kinetics. *Applied Catalysis A, General*, *113*(1). https://doi.org/10.1016/0926-860X(94)80238-6

79. Kusema, B. T., Hilpmann, G., Mäki-Arvela, P., Willför, S., Holmbom, B., Salmi, T., Murzin, D. Y. (2011). Selective hydrolysis of arabinogalactan into arabinose and galactose over heterogeneous catalysts. *Catalysis Letters*, *141*(3), 408–412. https://doi.org/10.1007/s10562-010-0530-x

80. Hussey, A. S., Baker, R. H., Keulks, G. W. (1968). Competitive hydrogenations on platinum. *Journal of Catalysis*, *10*(3). https://doi.org/10.1016/S0021-9517(68)80007-7

81. Cerveny, L., Ruzicka, V. (1982). Competitive Catalytic Hydrogenation in the Liquid Phase on Solid Catalysts. *Catalysis Reviews*, *24*(4). https://doi.org/10.1080/03602458208079662

82. Rader, C. P., Smith, H. A. (1962). Competitive Catalytic Hydrogenation of Benzene, Toluene and the Polymethylbenzenes on Platinum. *Journal of the American Chemical Society*, *84*(8). https://doi.org/10.1021/ja00867a021

APPENDIX I: HPLC CALIBRATION DATA

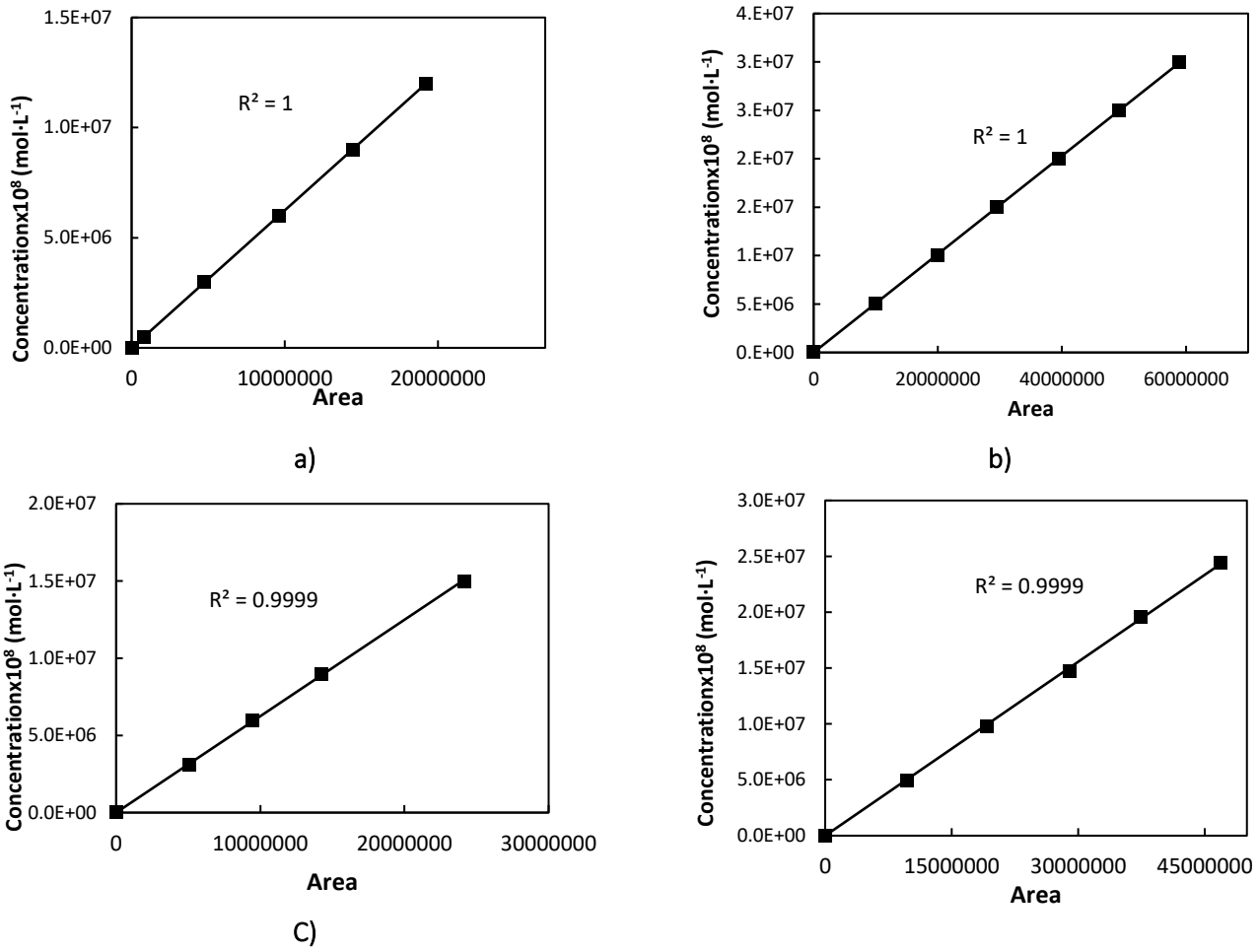

Figure I-1. HPLC calibration curves for sugars and sugar alcohols: (a) L-arabinose, (b) D-galactose, (c) L-arabitol, (d) D-galactitol.

$$C_{Sample}=a\cdot A_{HPLC}\cdot 10^{-8} \quad (A1)$$

Table I-1. HPLC calibration factor and retention times for sugars and sugar alcohols.

Component	a	Retention Time [min]
L-arabinose	0.6244	16.557
D-galactose	0.5077	14.387
L-arabitol	0.6245	22.193
D-galactitol	0.5188	26.123

APPENDIX II: HPLC CURVE OF SUGAR MIXTURES (EXAMPLE)

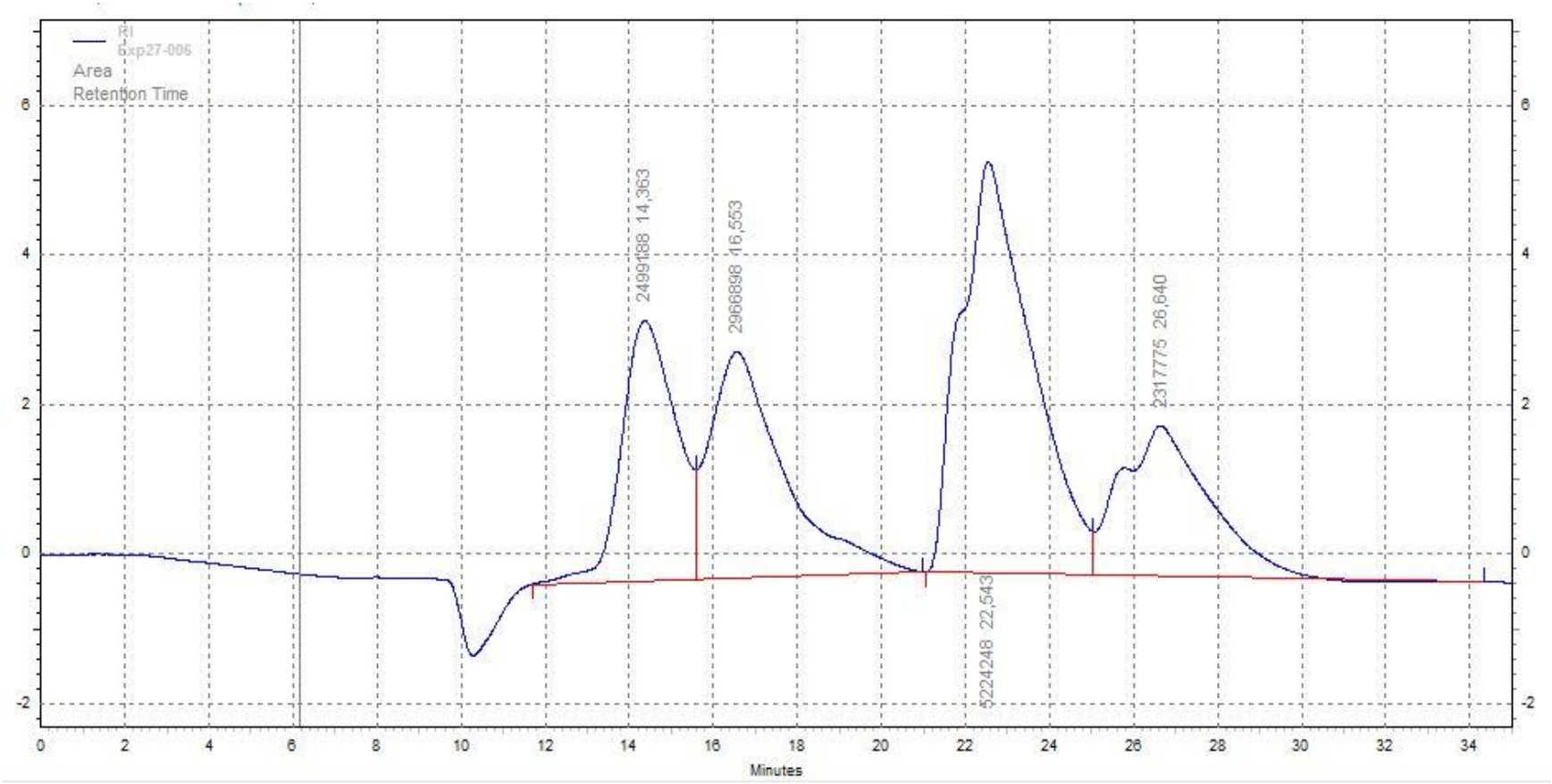

Figure II-1. Chromatogram displaying overlapping of reagents and products during sugar mixtures hydrogenation experiments.

APPENDIX III: KINETICS RESULTS

Individual Sugar Experiments

Results from hydrogenation experiments of L-arabinose and D-galactose at 20 bar and different temperatures (120˚C, 100˚C and 90˚C).

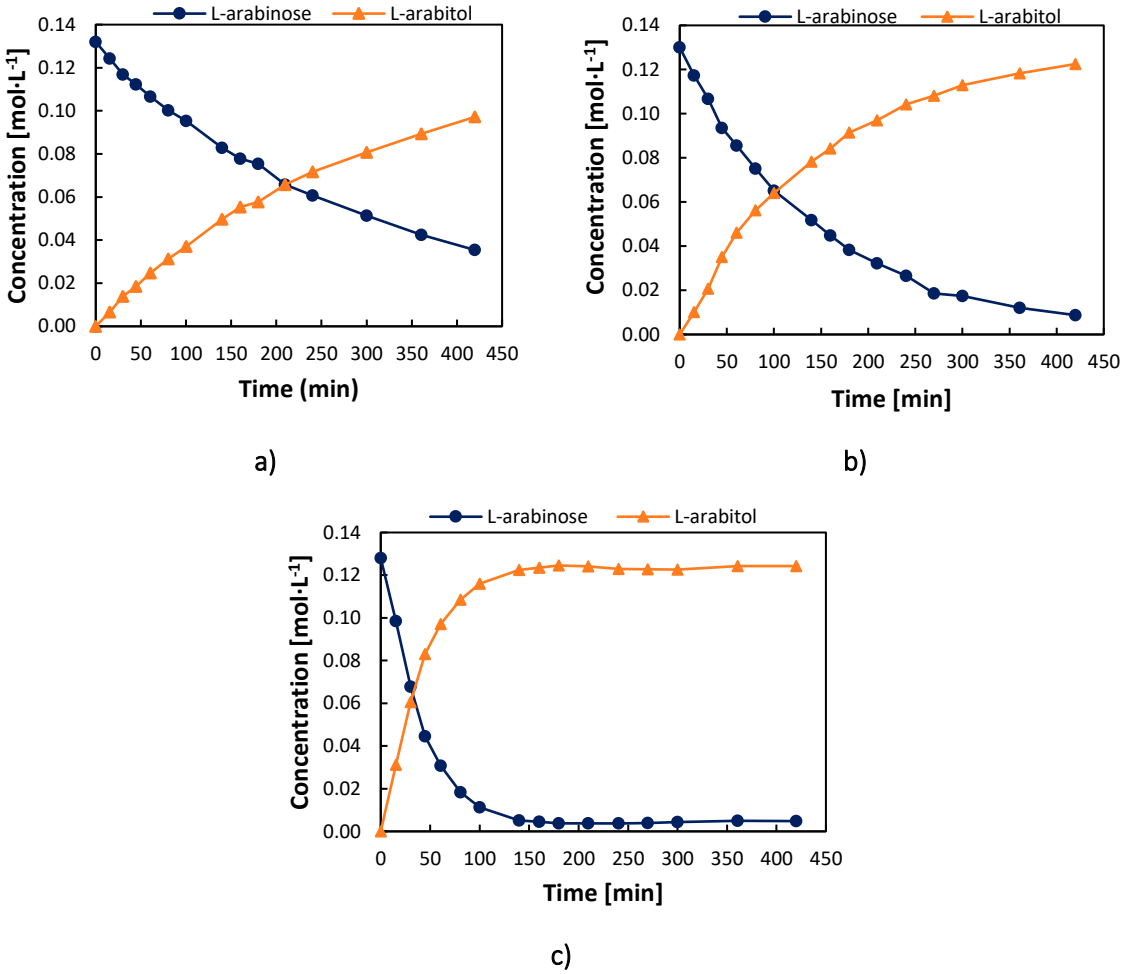

Figure III-1. Hydrogenation of L-arabinose—0.13M at 20 bar varying temperature a)90˚C, b)100˚C and c) 120˚C

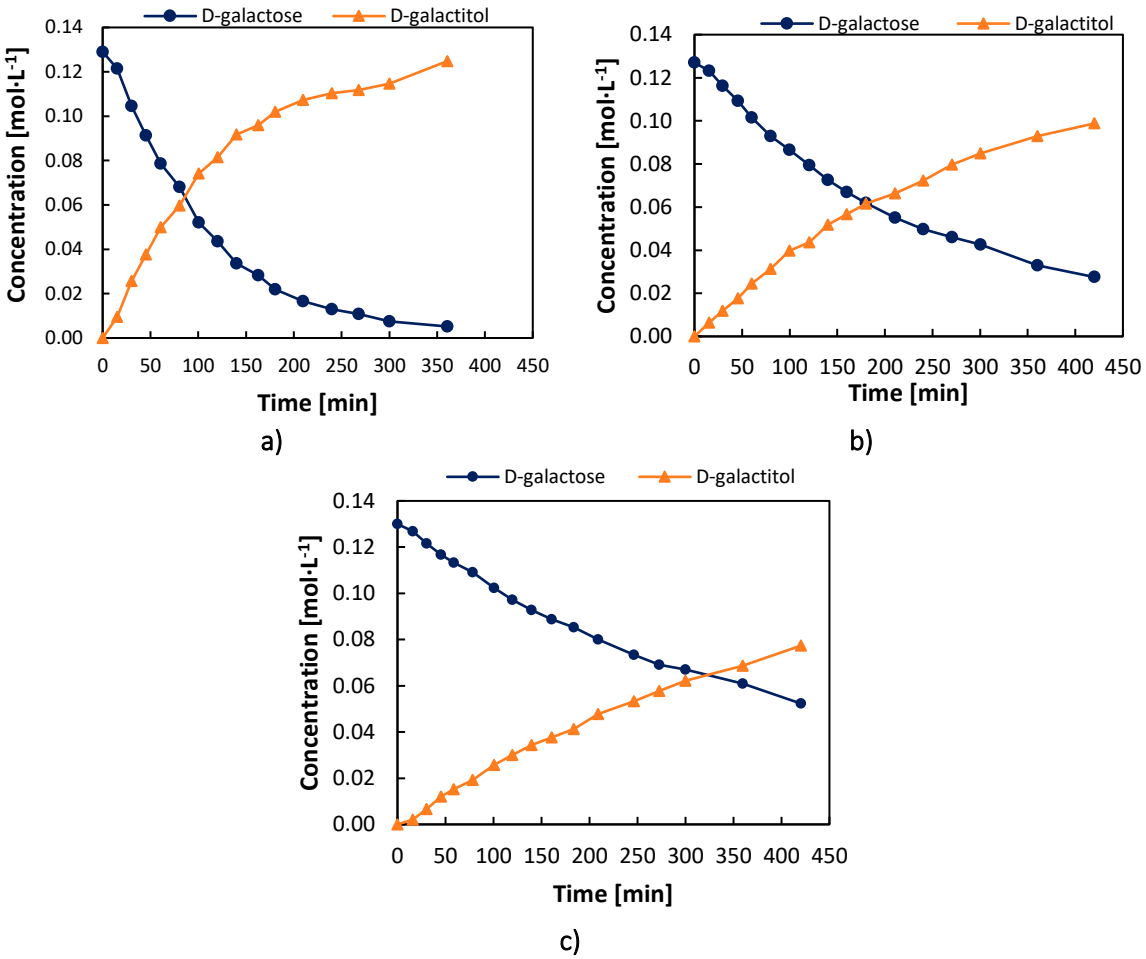

Figure III-2. Hydrogenation of D-galactose—0.13M at 20 bar varying temperature a)120˚C, b)100˚C and c) 90˚C

Mixture Experiments

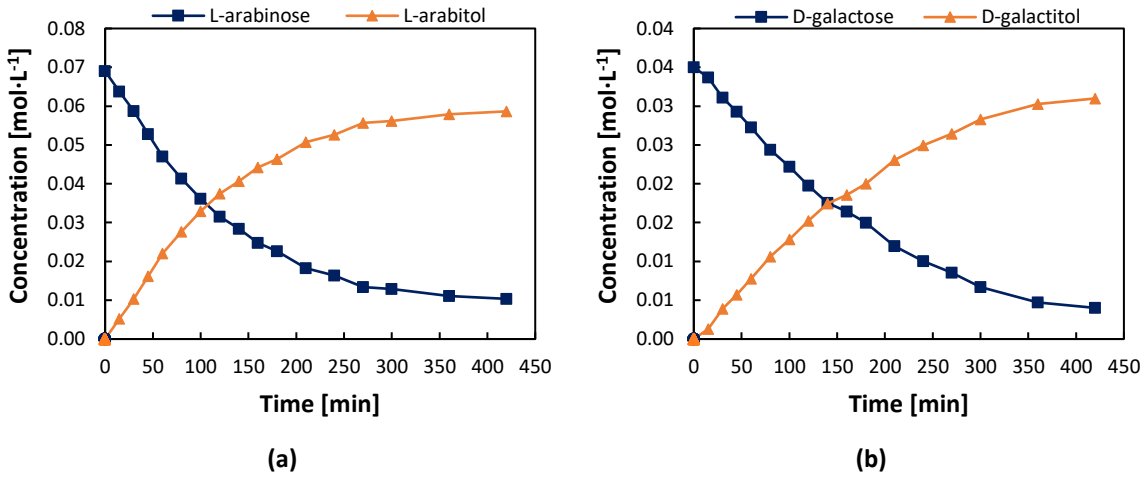

Figure III-3. Hydrogenation of sugar mixtures hydrogenation results at 120˚C and 20 bar. Ratio=0.5: (a) L-arabinose, and (b) D-galactose.

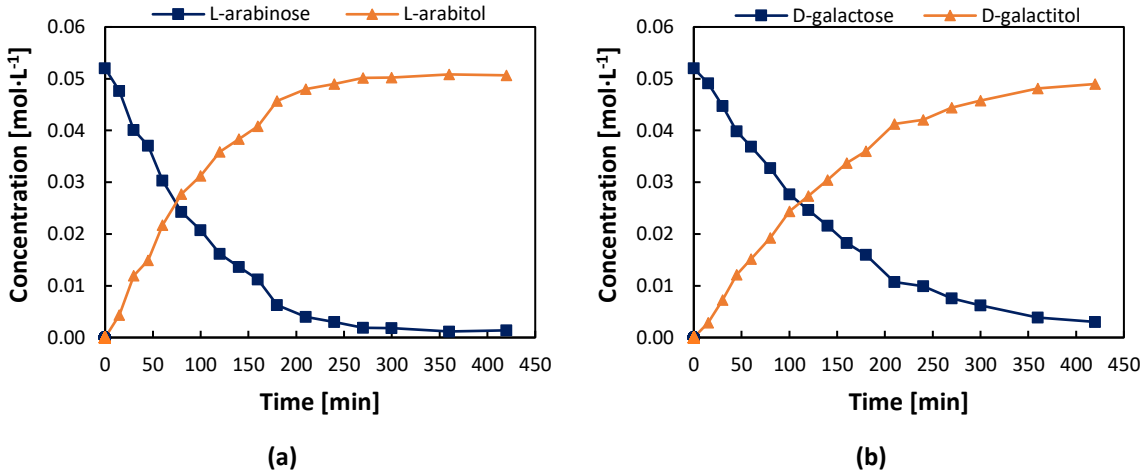

Figure III-4. Hydrogenation of sugar mixtures hydrogenation results at 120˚C and 20 bar. Ratio=1: (a) L-arabinose, and (b) D-galactose.

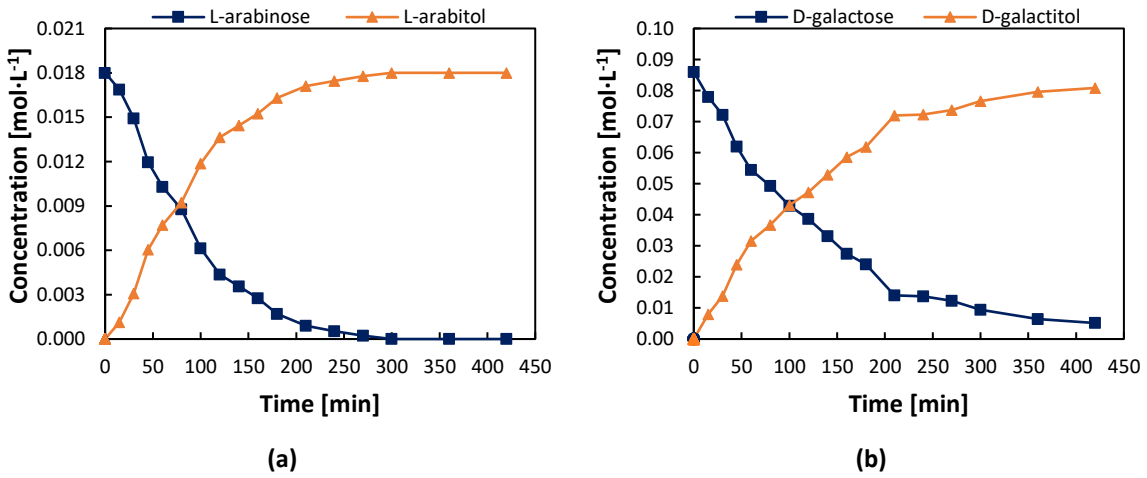

Figure III-5. Hydrogenation of sugar mixtures hydrogenation results at 120˚C and 20 bar. Ratio=5: (a) L-arabinose, and (b) D-galactose.

APPENDIX IV: MODELING SINGLE SUGAR HYDROGENATION (PYTHON CODE)

```
import os
import numpy as np
import pandas as pd
from scipy.integrate import solve_ivp
import matplotlib.pyplot as plt
from scipy.optimize import minimize

print("\n---Sugar Hydrogenation---\n")
#CONSTANTS
ncomp = 2                                   #Number of components-- Arabinose, Arabitol or Galactose, Galactitol
nre =3                                      #Number of reactions
mC = 0.01418816                             #Mass of Ru      [g]
VL = 130/1000                               #Reaction Volume [L]
rho = mC/VL                                 #Bulk density    [g/L]
T= [90+273.15, 100+273.15,120+273.15]       #Temperatures    [K]
R= 8.314                                    #Gas constant    [J/mol]

#2. READING DATA
dirpath = os.getcwd() + "\\"
trainname = "KINETIC_DATA .xlsx"
data=np.array(pd.read_excel (dirpath + trainname,"Comb_Galactose"))          #Choose "Comb_Galactose" or "Comb_Arabinose"
nserie=int(data.shape[1]/2)
ndata=data.shape[0]
nser=ncomp*nre
t_span=np.zeros((nserie,ndata-1))
t_train=np.zeros((ndata))                   #Experimental Time Vector
C_train=np.zeros((ndata,nser))              #Experimental Concentration Matrix

t_train=data[:,0]
C_train[:,0]=data[:,1]
C_train[:,1]=data[:,2]
C_train[:,2]=data[:,4]
C_train[:,3]=data[:,5]
C_train[:,4]=data[:,7]
C_train[:,5]=data[:,8]

#  KINETIC MODEL
dC=np.zeros(ncomp*3)                        #Initializing Derivatives Vector
r=np.zeros(3)                               #Initializing Reaction Rates Vector
k=[814434, 55956, 0.7]                      #Initial Values for the Parameters A=k[0], E=k[1] and kS=k[2]
```

```
def model (t, C, k):                                    #Differential equations function.
   for i in range (0,3):
      r[i]=((k[0]*np.exp(-k[1]/(T[i]*R)))*C[2*i])/((1+k[2]*C[2*i]))        #Reaction rates
      dC[2*i]=-r[i]*rho                                  #Mole balances for the sugar
      dC[2*i+1]=r[i]*rho                                  #Mole balances for the sugar alcohol
   return dC

C0 = C_train[0,:]                                       #Stablishing initial conditions at t=0 min
tspan= [0, t_train[-1]]                                  #Defining integration range
C_int=np.zeros((len(t_train),ncomp*3))                              # interpolation
t_train=t_train.flatten()

#OPTIMIZATION
def of(k): #Objetive Function
   sol = solve_ivp(lambda t,C: model(t,C,k), t_span=tspan,
           y0=C0, method='LSODA',t_eval=t_train)
   C_int = sol.y.T

   error=abs(C_int-C_train)**2                                  #Objective function
   errorval=sum(sum(error))
   return errorval

def R2(k):                                              #Determination Coefficient
   sol = solve_ivp(lambda t,C: model(t,C,k), t_span=tspan,
           y0=C0, method='LSODA',t_eval=t_train)
   C_int = sol.y.T
   Cmean=sum(C_train)/ndata

   R2=(1-((sum((C_train-C_int)**2))/(sum((C_train-Cmean)**2))))*100
   R2=sum(R2)/nser
   return R2

#SOLUTION
#Calling optimization solver
res = minimize(of, k, method='nelder-mead',
          options={'xatol': 1e-8, 'disp': True})
k=res.x                                                 #Obtained parameters
R2v=R2(k)                                                #Computing coefficient of correlation for the model
t = np.linspace(0,tspan[1], num=200) # time points

#Solving with optimal parameters
sol = solve_ivp(lambda t,C: model(t,C,k), t_span=tspan,
          y0=C0, method='LSODA', t_eval=t.flatten())
C = sol.y.T
t=sol.t
#Showing Estimated Paramaters
print("A=" + str(k[0])+" L/gRu*min*mol")
print("EA=" + str(k[1])+" J/mol")
print("k'=" + str(k[2])+" L/mol")
print("R2="+ str(R2v)+ " %")
```

APPENDIX V: MODELING SUGAR MIXTURES HYDROGENATION (PYTHON CODE)

```
import os
import numpy as np
import pandas as pd
from scipy.integrate import solve_ivp
import matplotlib.pyplot as plt
from scipy.optimize import minimize

print("\n---Sugar Mixtures Hydrogenation---\n")

#CONSTANTS
ncomp = 2                                          #Number of components-- Arabinose, Arabitol
nre =1                                             #Number of reactions
mC = 0.01179148318                                 #Mass of Ru      [g]
VL = 130/1000                                      #Reaction Volume [L]
rho = mC/VL                                        #Bulk density    [g/L]
T= [90+273.15, 100+273.15, 120+273.15]             #Temperatures    [K]
R= 8.314                                           #Gas constant    [J/mol]

#2. READING DATA
dirpath = os.getcwd() + "\\"
trainname = "MIXTURES.xlsx"
data=np.array(pd.read_excel (dirpath + trainname,"Hoja1"))
nserie=int(data.shape[1]/2)
ndata=data.shape[0]
nser=ncomp*nre
t_span=np.zeros((ndata))
##t_train=np.zeros((ndata))                        #Experimental Time Vector
C_train=np.zeros((ndata,nser))                     #Experimental Concentration Matrix
##
t_train=data[:,0]
for i in range (0, nser):
   C_train[:,i]=data[:,i+1]

###  KINETIC MODEL
dC=np.zeros(nser)                                  #Initilazing Derivatives Vector
r=np.zeros(6)                                      #Initilazing Reaction Rates Vector
k=[0.2, 0.1, 7.99400900e+00]    #Arabinose initial constants                    #Initial Values for
the Parameters A=k[0], E=k[1] and kS=k[2]

def model (t, C, k):

   r[0]=k[0]*C[0]/(1+k[2]*C[0])
   r[1]=k[1]*C[1]/(1+k[2]*C[0])
```

```
    r[2]=k[0]*C[4]/(1+k[2]*C[4])
    r[3]=k[1]*C[5]/(1+k[2]*C[4])

    r[4]=k[0]*C[8]/(1+k[2]*C[8])
    r[5]=k[1]*C[9]/(1+k[2]*C[8])

    dC[0]=-r[0]*rho
    dC[1]=-r[1]*rho
    dC[2]=r[0]*rho
    dC[3]=r[1]*rho
    dC[4]=-r[2]*rho
    dC[5]=-r[3]*rho
    dC[6]=r[2]*rho
    dC[7]=r[3]*rho
    dC[8]=-r[4]*rho
    dC[9]=-r[5]*rho
    dC[10]=r[4]*rho
    dC[11]=r[5]*rho

    return dC

C0 = C_train[0,:]
tspan= [0, t_train[-1]]                                  #Defining integration range
C_int=np.zeros((len(t_train),ncomp*3))                          # interpolation
t_train=t_train.flatten()


#OPTIMIZATION
def of(k): #Objetive Function
    sol = solve_ivp(lambda t,C: model(t,C,k), t_span=tspan,
            y0=C0, method='Radau',t_eval=t_train)
    C_int = sol.y.T

    error=abs(C_int-C_train)**2                          #Objective function
    errorval=sum(sum(error))
    return errorval

def error (k):
    sol = solve_ivp(lambda t,C: model(t,C,k), t_span=tspan,
            y0=C0, method='LSODA',t_eval=t_train)
    C_int = sol.y.T
    error=abs(C_int-C_train)**2                          #Objective function
    SE=((sum(sum(error))/(ndata-1))**0.5)

    return SE

def R2(k):                                          #Determination Coefficient
    sol = solve_ivp(lambda t,C: model(t,C,k), t_span=tspan,
            y0=C0, method='LSODA',t_eval=t_train)
```

```
    C_int = sol.y.T
    Cmean=sum(sum(C_train))/(ndata*6)

    R2=(1-((sum(sum((C_train-C_int)**2)))/(sum(sum((C_train-Cmean)**2)))))*100


    return R2

###SOLUTION
#Calling optimization solver
res = minimize(of, k, method='nelder-mead',
            options={'xatol': 1e-8, 'disp': True})
k=res.x                                          #Obtained parameters
R2v=R2(k)                                          #Computing coefficient of determination for the model
t = np.linspace(0,tspan[1], num=200) # time points

###Solving with optimal parameters
sol = solve_ivp(lambda t,C: model(t,C,k), t_span=tspan,
            y0=C0, method='Radau', t_eval=t.flatten())
C = sol.y.T
t=sol.t

###Showing Estimated Paramaters
print("k'1=" + str(k[0])+" L/gRu*min*mol")
print("k'2=" + str(k[1])+" J/mol")
print("kA=" + str(k[2])+" L/mol")
print("R2="+ str(R2v)+ " %")
```